NASA CONTRACTOR REPORT

NASA CR-1139

VAPOR-CHAMBER FIN STUDIES

OPERATING CHARACTERISTICS OF FIN MODELS

by H. R. Kunz, S. S. Wyde, G. H. Nashick, and J. F. Barnes

Prepared by
UNITED AIRCRAFT CORPORATION
East Hartford, Conn.
for Lewis Research Center

NATIONAL AERONAUTICS AND SPACE ADMINISTRATION • WASHINGTON, D. C. • AUGUST 1968

NASA CR-1139

VAPOR-CHAMBER FIN STUDIES

OPERATING CHARACTERISTICS OF FIN MODELS

By H. R. Kunz, S. S. Wyde, G. H. Nashick, and J. F. Barnes

R.R. PWAC-3154

Prepared under Contract No. NAS 3-7622 by
PRATT & WHITNEY AIRCRAFT
Division of United Aircraft Corporation
East Hartford, Conn.

for Lewis Research Center

NATIONAL AERONAUTICS AND SPACE ADMINISTRATION

For sale by the Clearinghouse for Federal Scientific and Technical Information
Springfield, Virginia 22151 – CFSTI price $3.00

FOREWORD

This report describes work conducted by Pratt & Whitney Aircraft Division of United Aircraft Corporation under NASA Contract 3-7622. It was originally issued as Pratt & Whitney Report PWA-3154, July 1967. Martin Gutstein of the Space Power Systems Division, NASA-Lewis Research Center, was the Project Manager.

ABSTRACT

This report presents the test results from experiments on two vapor-chamber fin (heat pipe) geometries and compares these results with a theory developed and presented in a prior report. Typical temperature distributions were obtained for heat pipe operation plus limiting heat flux data which was compared to the theory. This comparison indicated that the theory showed the correct trends at low levels of heat flux. An effect of working fluid inventory was found which was not included in the present theory. Tests with a noncondensable gas present in the chamber were found to result in complete mixing of this gas with the working fluid vapor.

TABLE OF CONTENTS

LIST OF FIGURES

I. SUMMARY

This report summarizes the work performed to investigate the operating characteristics and limits of vapor-chamber fins or heat pipes.

Two different vapor-chamber fin configurations were fabricated. On one type, the planar-fin model, both the condenser and evaporator sections were in the same plane. The other type, the box-fin model, consisted of a box-shaped chamber with the evaporator and condenser sections perpendicular to each other. The latter type was constructed in two identical halves so that it could be tested either as a full-box configuration where one condenser section was above and the other below the chamber or as a half-box configuration. The half-box configuration was only tested with the condenser section below the chamber.

Three different types of wicks were fabricated for the planar model, two of which were tested. The third type failed structurally before testing. Nevertheless, this same type was successfully tested with the box-fin model.

The design of the test configurations and the test program were based on a simplified analysis of heat-pipe operation and a preliminary study of wick characteristics pertinent to heat-pipe operation. The above analysis and study represent the first part of the program. This report summarizes the final part of the program on the operating characteristics of vapor-chamber fins.

Tests with the planar-fin model yielded a typical temperature distribution within the wick backup plate and one limiting heat flux. The one limiting heat flux value obtained was in good agreement with the theoretical prediction.

Tests with the box-fin model yielded typical temperature distributions, nine capillary pumping failure points, and operating characteristics of a fin with a noncondensable gas in the chamber. The capillary failure points obtained were all lower than the theoretical predictions. At heat fluxes below about 32,000 Btu/hr ft^2, however, the trend of the capillary failure point data agreed with the theoretical predictions, which suggested that the tests used to determine the minimum effective pore radius of the wick may have been inadequate. At heat fluxes above 32,000 Btu/hr ft^2, both the trend and the limiting heat flux values disagreed with the predictions. This disagreement could be attributed to the above-indicated cause, plus an interaction between boiling and capillary pumping. An effect of liquid inventory on the capillary pumping limits was measured but was not included in the present theory. Differences between full-box and half-box operation indicated that an interaction existed between top and bottom box halves.

The tests with a noncondensable gas indicated that the gas completely mixed with the working-fluid vapor. This mixing was attributed to the large cross-sectional area for vapor flow in the full-box configuration, plus the relatively large difference between the molecular weights of the condensable and noncondensable fluids.

II. INTRODUCTION

The work of Grover, et al[1], and other investigators [2, 3] has shown that the vapor-chamber fin or heat pipe is a heat transfer device that can exhibit an extremely high effective thermal conductivity, much greater in fact than any known homogeneous material. The heat pipe consists of a long closed container in which vaporization and condensation of a fluid take place. Heat added at one end of the container causes evaporation of liquid into vapor. Condensation of the vapor along the length of the container maintains the surface at a nearly constant temperature. The resulting condensate is returned to the heated end of the container by the action of capillary forces in the liquid layer which is contained in a wick lining the inside of the cavity.

A parametric study done by Haller, Lieblein, and Lindow[4] indicated that the heat pipe might be used as a vapor-chamber fin in reducing the weight of a radiator for a Rankine-cycle space powerplant. An investigation was therefore begun under Contract NAS3-7622 to explore and define the mechanisms of fluid transport and heat transport in vapor-chamber fins or heat pipes, to provide design information for space radiators and other applications. The investigation was divided into three tasks, 1) wicking studies, 2) boiling studies, and 3) operating fin studies.

The detailed results of the first two tasks of the program were reported in report NASA CR-812[5]. In that report the basic theory was developed and the characteristics of the wicking materials that are needed to predict the operating limits of a heat pipe were measured experimentally. These characteristics are the maximum height to which the heat pipe liquid will rise in a vertical wick, the wicking material friction factor (reciprocal of the permeability) and the evaporative heat transfer characteristics of a liquid-saturated wick.

This report discusses the experiments which were conducted on operating vapor-chamber fins in the third task, and relates the results obtained under the first two tasks. Two types of fin models using three different wick structures that were studied in the first two tasks were tested. Section III of this report describes the test equipment and procedure used in the experimental studies of operating vapor-chamber fins. The theoretical predictions of the different configurations used in this study are presented in Section IV. The test results and discussion of these results are presented in Section V.

---

[1] See Page 63 for numbered list of references

III. DESCRIPTION OF TEST EQUIPMENT AND PROCEDURE

Two types of fin models were tested. One was a planar-fin model; that is, both the heated and cooled sections of the fin wick were in the same plane. Although three different types of wicks were fabricated for this model, successful tests were run on only two types. The other fin model tested was the box-geometry type, in which the wicks were ell-shaped, the heat entering the short leg of the ell and extracted from the long leg. Each of the ell-shaped wicks was bonded to a half box. This model could be tested by either bolting two half boxes together or by bolting a cover to either half box to form a sealed vapor chamber. Only one type of wick was tested in the box-fin model.

The following sections describe the two fin models, the test facility, wick preparation, and the test procedure used in the program.

A. Description of Planar Fin

1. General Description

The planar fin was constructed of six basic parts, 1) a capillary pump (wick), 2) wick backup plate, 3) cooling channel section, 4) heater section, 5) top cover plate, and 6) tilting-table assembly. These parts were assembled as shown by the cross-sectional view in Figure 1 to form a cavity with a wick on its bottom surface. This cavity was heated on one end of the bottom side and cooled on the other end. The tilting table added a variable angle test capability to the assembly. Silicone rubber sheet gasket material was used to seal the vapor chamber against external leaks and to seal the cooling channel section from both cross-channel and external leakage. After the six above-mentioned items were assembled, the entire fin was wrapped with a layer of Fiberfrax insulation blanket to reduce heat losses.

2. Detailed Description

The wick backup plate was made of AMS 5512 stainless steel, 0.050 inch thick in the evaporator region and 0.225 inch thick in the condenser region. The wick was brazed or epoxy-bonded to the upper plane of the backup plate surface. The under surface of the plate fitted against the heater section on the 0.050 inch thick end and the condenser section on the 0.225 inch thick end. Grooves were machined in the condenser section on the cooling-channel side of the backup plate to receive the chromel-alumel thermocouples. These were 0.020 inch in diameter, stainless-steel sheathed, and had welded junctions. Forty-two such thermocouples were installed in the grooves. The junction of each thermocouple was covered with low-temperature silver braze material on the H13 and M12 planar-fin, and resistance-welded chromel wire on the H6 planar model, to make the surface smooth. The evaporator region had twenty-five 0.020 inch diameter, stainless steel sheathed, bare wire junction, chromel-alumel thermocouples installed between the ten strip heaters. The thermocouples were held in place by small stainless steel wire straps across the thermocouple sheath, and resistance welded to the under side of the backup plate. The leads of these thermocouples

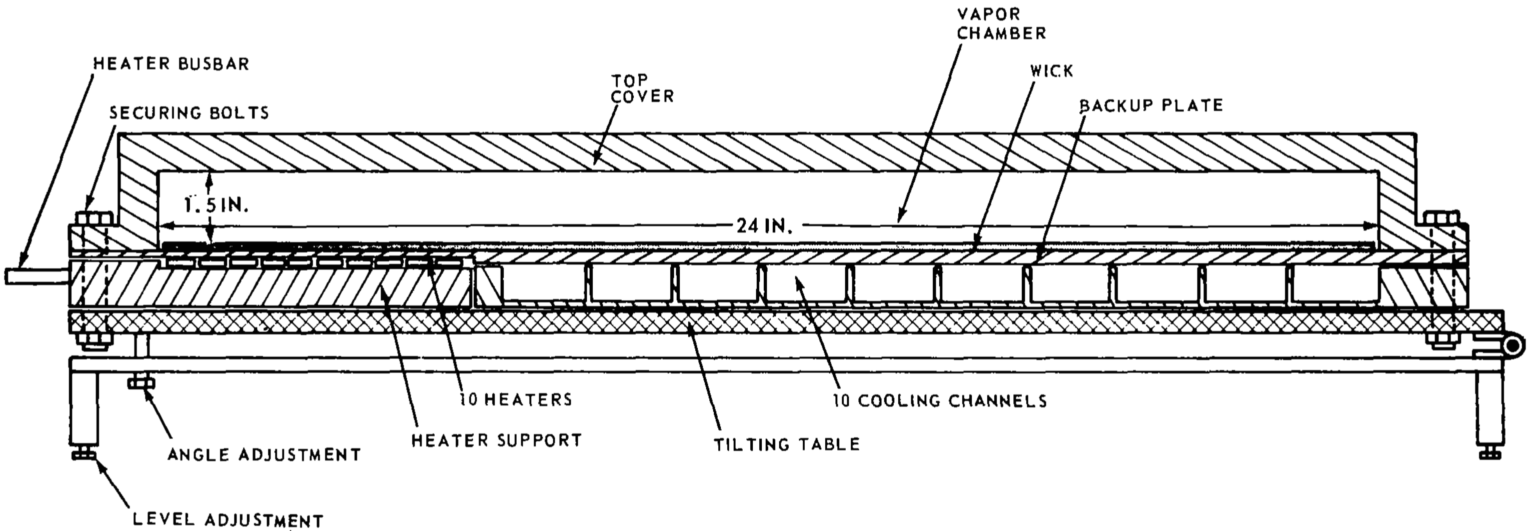

Figure 1 Cross-Section of Planar-Fin Model

extended out from each side of the fin and were supported by a structure fastened to the edge of the backup plate.

The wicks were of two basic types, sintered fibers and sintered powders, and all three wicks fabricated were nominally 24 x 6 x 0.1 inch in dimensions. Figure 2 shows a photograph of the sintered powder wick M2. Other pertinent details of the wicks are presented in the table below.

Wick	Material	Porosity, %*	Type	Mean Fiber or Powder Diameter**
H6	nickel	88.0	sintered fiber	0.0006 inch
H13	AISI 430 SS	82.2	sintered fiber	0.0030 inch
M2	AISI 316 SS	65.8	sintered powder	150-297 microns

* based on previous tests (see report NASA CR-812, June 1967) and manufacturers' specifications

** based on manufacturers' specifications

The sintered fiber wick H13 was directly attached to the backup plate by a high temperature nickel-base braze material, GE 8104. The sintered fiber wick H6 was first sintered to a nickel foil 24 x 6 x 0.010 inch and then oven-brazed to the backup plate with GE 8104 braze material. The foil was used in this case to prevent the braze material from flowing into the wick, since this wick had very fine pores. The methods of application were recommended and performed by the wick manufacturer, Huyck Metals Company. The sintered powder wick was epoxy-bonded to the backup plate which originally had the H13 wick bonded to it after the latter wick failed structurally. Epoxy bonding was necessary since brazing would have destroyed the thermocouples attached to the backup plate. The epoxy used was Epoxylite 5524 which has a useful temperature limit of about 660°F. Tests on small samples made at Pratt and Whitney Aircraft verified this limit.

The first cooling channel section used in testing was fabricated from Mycalex 400, a glass-bonded mica material which exhibits high compressive strength and relatively low thermal and electrical conductivity characteristics. This material would reduce axial conduction. However, Mycalex 400 could withstand very little bending and subsequently cracked after a few hours of testing. Cooling channel sections were then fabricated from a single slab of laminated Fiberglas. The Fiberglas cooling sections were flexible enough to withstand the small flexing which resulted from vapor-chamber pressures during the testing of the planar fin. Each cooling channel had a flow-straightening device consisting of a baffle and 50-mesh screen assembly inserted in the inlet of the channel. Immersion-type thermocouples were installed in each inlet and exit fitting of the cooling channels.

The heater section consisted of strip heaters, a support section, and the busbars. The heater support section was fabricated of Mycalex 400 and supported ten 0.020 inch thick Inconel strip heaters with an effective heater surface of 6 x 3/8 inch each,

Figure 2 M2 Wick Installed on Backup Plate XP-75600

or a total of 22.5 square inches when all ten heaters were used. The strip heaters had a 0.010 inch thick flame spray coating of aluminum oxide in order to isolate the heaters electrically from the backup plate. The heaters were arranged in parallel and clamped at the ends to two copper busbars. The busbars ran parallel to the fin axis and protruded outward from one end, where large terminals from the power source were attached. Figure 3 shows a photograph of the assembled heater section.

The number of heaters used could vary from 1 to 10 in order to vary the heated length (area) of the evaporator region. The Mycalex 400 proved satisfactory for the heater support material.

The top cover plate was constructed of AMS 5512 stainless steel. This plate was designed to safely withstand internal chamber pressures up to 150 psia. The cover had fittings for installing two Statham 0–200 psia pressure transducers to measure the chamber pressure, one located at the evaporator end and the other located at the condenser end of the fin. Six chromel-alumel welded-junction type thermocouples were installed protruding through the wall into the chamber to measure the vapor temperature. Nine chromel-alumel bare wire junction type thermocouples were resistance-welded to the outside surface of the top cover plate to aid in heat loss calculations. A 1/4-inch AMS 5524 stainless-steel tube was welded to each end of the cover plate to facilitate evacuating and filling the chamber with the working fluid. Two Bourdon type pressure gages were attached to these tubes to check the pressure indicated by the pressure transducers. The pressure transducer readout was a Honeywell Brown strip chart recorder.

The tilting table was used primarily to vary the angle of elevation of the fin model with respect to the horizon. It also helped to support the pressure forces applied to the wick backup plate assembly. The tilting table was constructed of two flat sheets of cold-rolled steel 1/2 inch thick. The two plates of steel were fastened together at the condenser end of the fin by two flat hinges. The bottom plate had four legs welded to it, one at each corner. The legs were internally threaded at the base to receive the level-adjusting screws. Opposite the hinged end of the table (i.e. the evaporator end) were two angle-adjusting screws threaded into the bottom stationary plate and pressing on the under side of top plate. The top plate of the tilting table had clearance holes about its periphery to receive the bolts which pass through the top cover plate, backup plate, and cooling or heating section. Nuts tightened on these bolts on the under side of the movable top plate held the heating and cooling sections firmly to the under side of the backup plate. The installation and tightening of these nuts completed the planar-fin assembly.

During an actual test the reference surface for the angle measurement was the top surface of the top cover plate. This surface was leveled with a protractor-type level before starting a test.

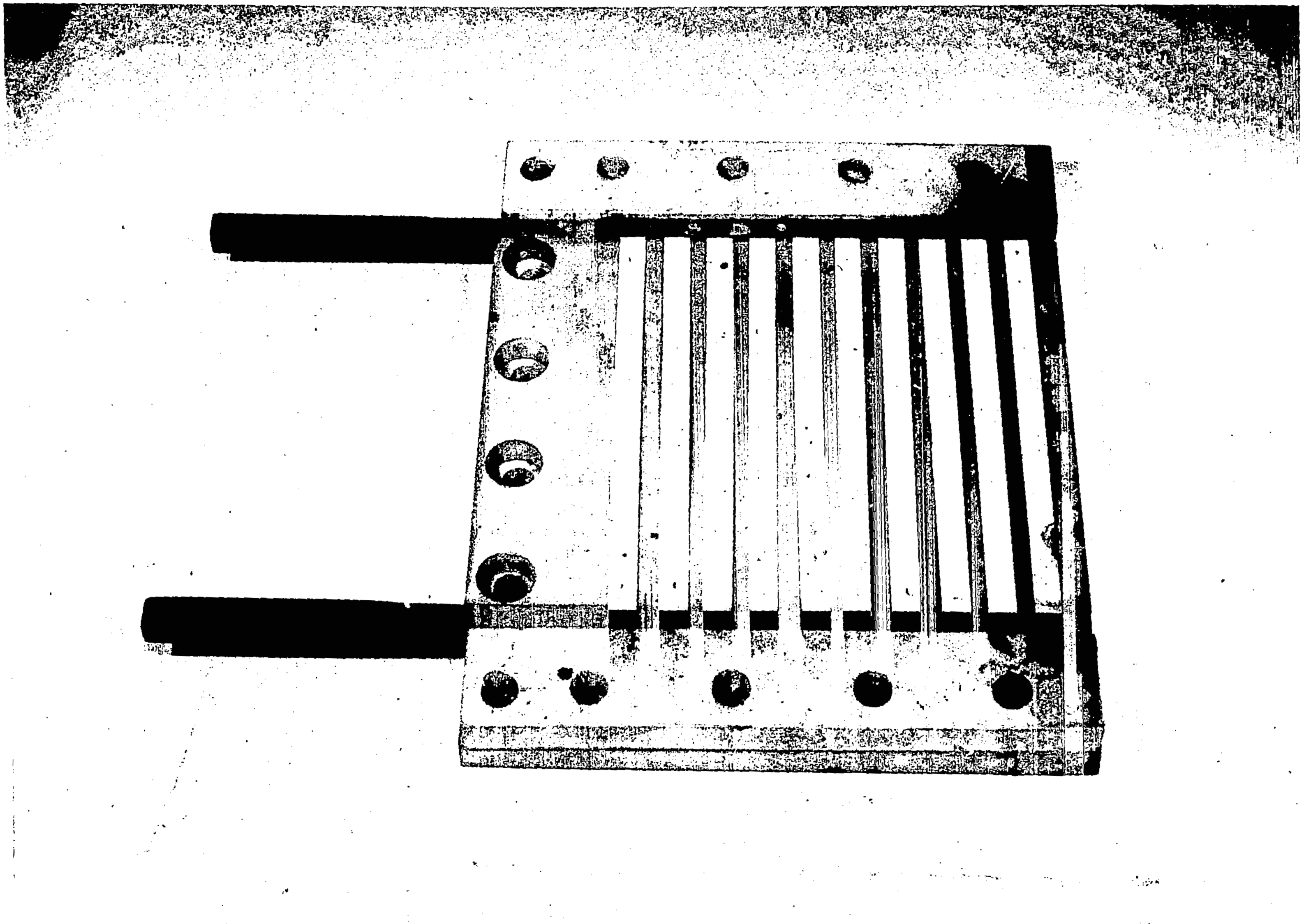

Figure 3 Planar Fin Heater Assembly XP-74171

3. Detailed Description of Modified H6 Planar Fin

After the first few tests with the H6 planar fin, the wick became detached from the backup plate in the evaporator region. To facilitate further testing with the H6 planar fin, the assembly was modified to make use of the remaining bonded wick-backup plate region (approximately 18 inches). A new cooling-channel assembly was fabricated with six channels to cover about 60 percent of the original condenser length. The remainder of the original condenser length was used for a new evaporator section. The original evaporator region was therefore considered an adiabatic region. The area previously used as the heater region was supported by a large spacer. The power supply attachments, the top cover plate, and the tilting table did not require alterations. Also, additional instrumentation was not needed. This modification resulted in imbedded-type thermocouples in the new evaporator section of the backup plate instead of skin-type thermocouples as in the original heater region. Figure 4 shows a photograph of the assembled modified H6 planar-fin model without the tilting table, and Figure 5 after its disassembly. Figure 6 is a sketch of the backup plate with wick attached and indicates the condenser and evaporator sections in both the original and modified fin configurations. The locations of all of the thermocouples for the modified planar-fin configuration are shown in Figure 7.

B. Description of Box Fin

1. General Description

The box-fin model consisted of two box halves with wicks installed, two sets of cooling channels with five cooling channels in each set, four sets of coolant manifolds, two strip heaters, a heater support assembly, and a tilting table. Figure 8 is a photograph of the assembled box fin and Figure 9 a cross-sectional view. Assembly of the box-fin model consisted of bolting the two box halves together, sandwiching this subassembly between the cooling channels and cooling-channel manifolds with bars and tierods, and bolting the heater section to the box end where the short leg of the wick is located. Gaskets were used between the mating surfaces of the two box halves, the box halves and the cooling channels, and the cooling channels and their manifolds.

2. Detailed Description

The two box halves were made of AMS 5512 stainless steel and were identical in construction. Each box half had a sintered fiber wick of AISI 430 stainless steel bonded to it. Figure 10 shows the box fin halves with the wick applied. The wick, designated H13, was 82.2 percent porous with a mean fiber diameter of 0.003 inch. It was manufactured and installed in the box halves by Huyck Metals Company. The wick was made in one continuous strip nominally 25.5 x 5 x 0.10 inch in dimensions and bonded with a nickel-base braze material GE 8104.

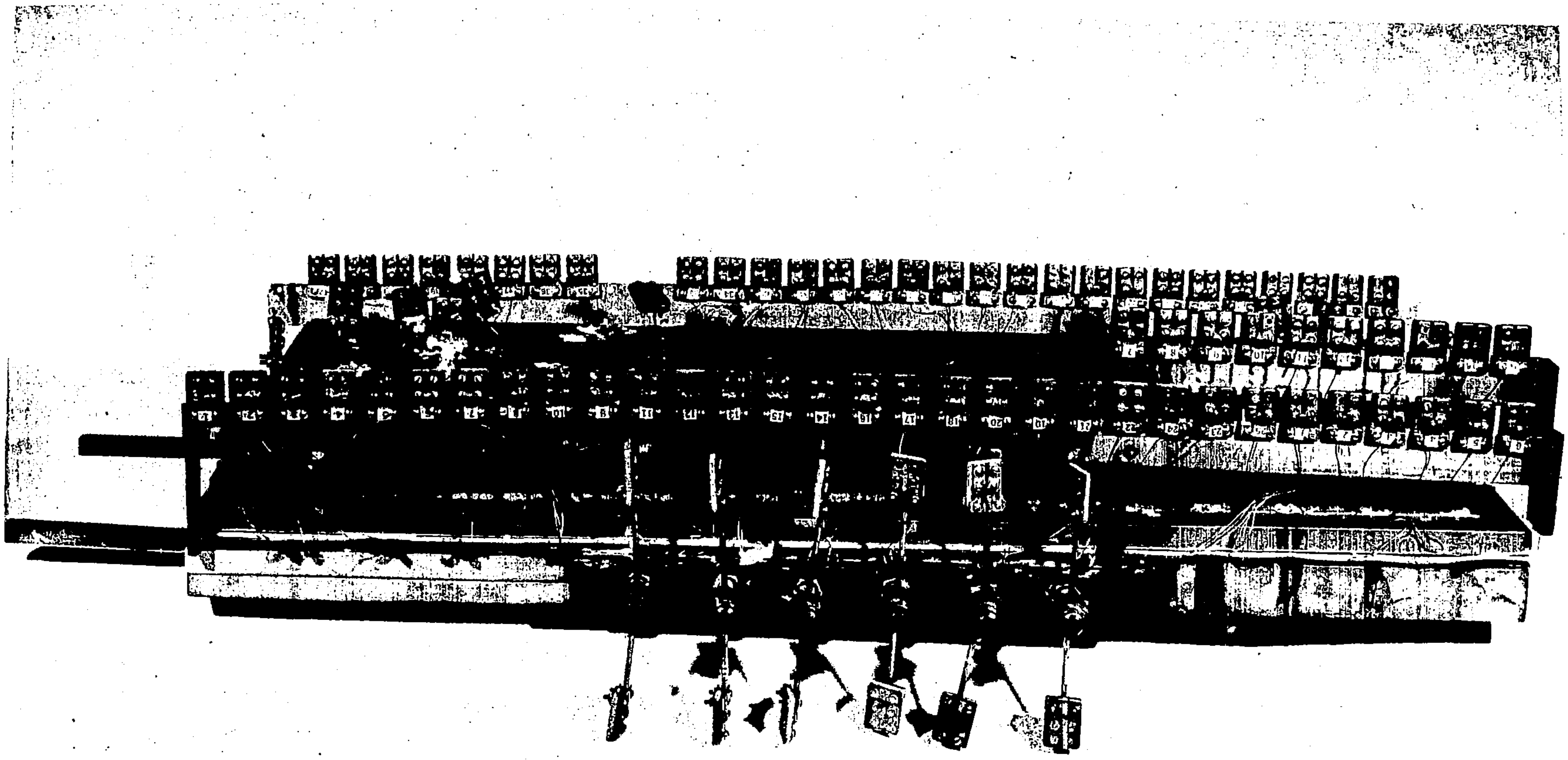

Figure 4 Assembly of Modified H6 Planar Fin XP-74167

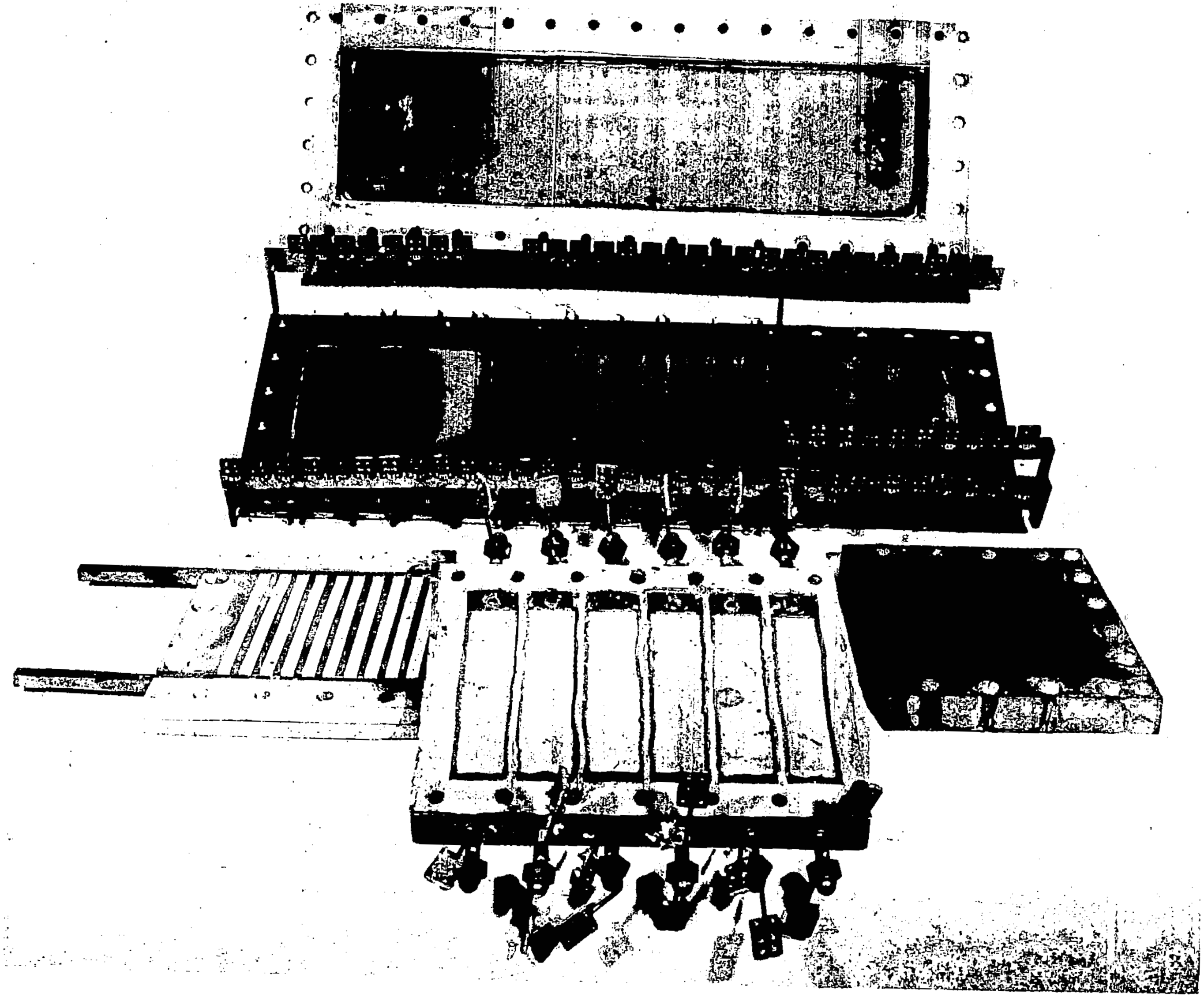

Figure 5 Modified H6 Planar Fin Disassembled XP-74168

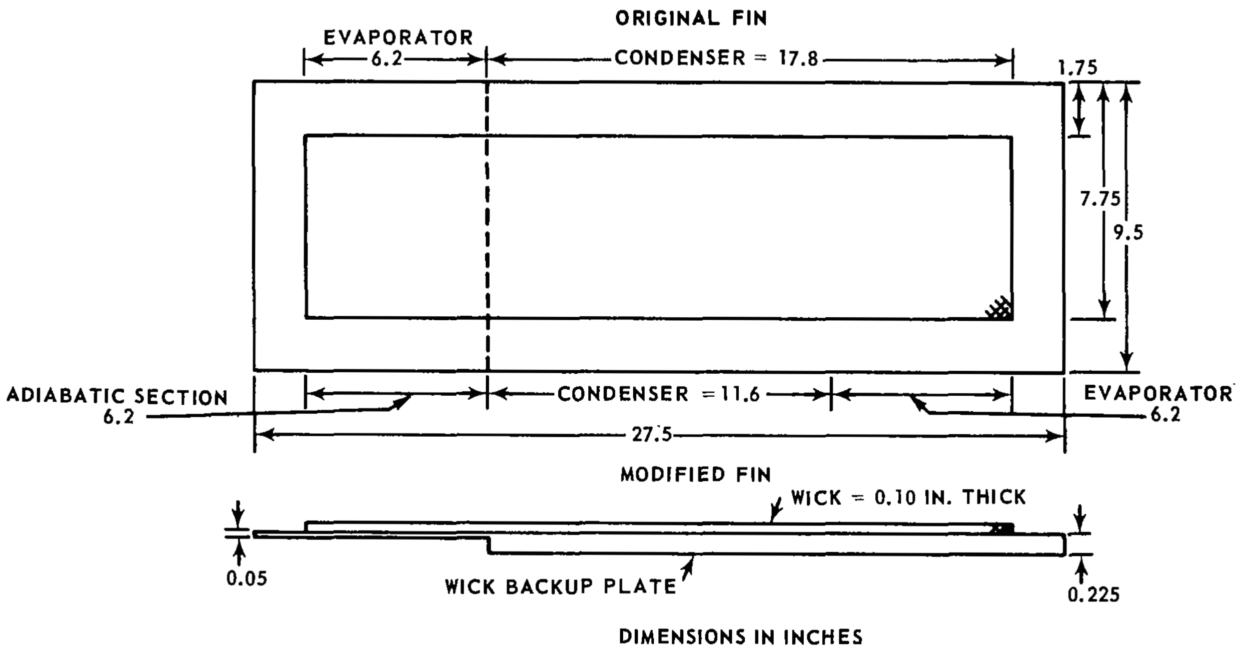

Figure 6 Original and Modified Versions of Wick Backup Plate Assembly for Planar Fin

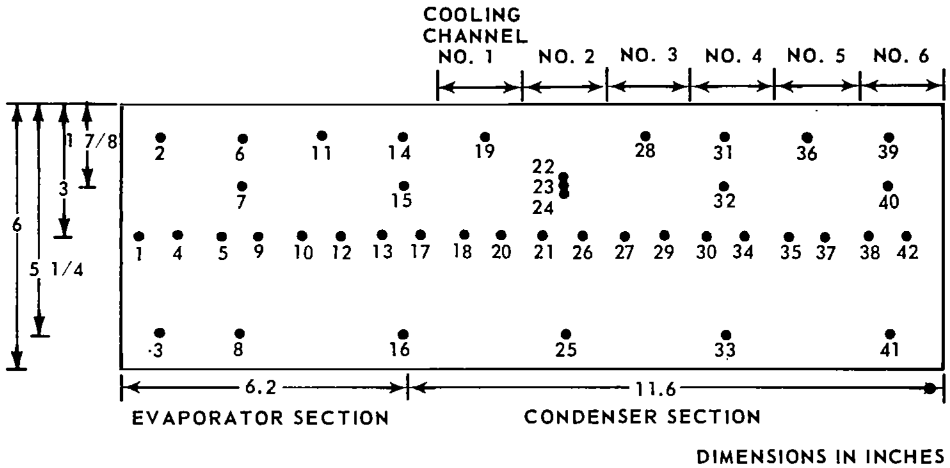

Figure 7 Thermocouple Locations for Modified Planar Fin

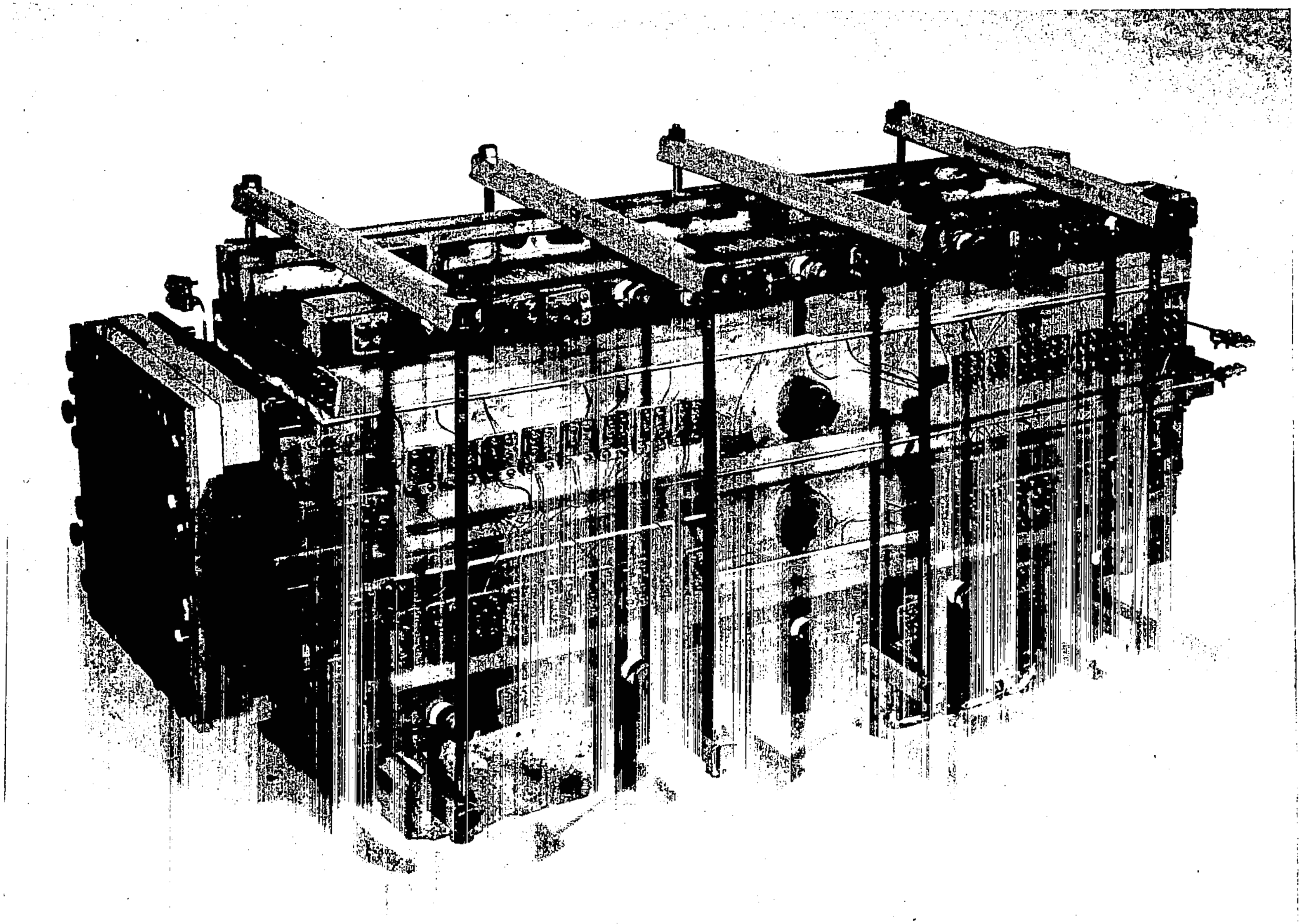

Figure 8 Assembled Box-Geometry Fin Model XP-74166

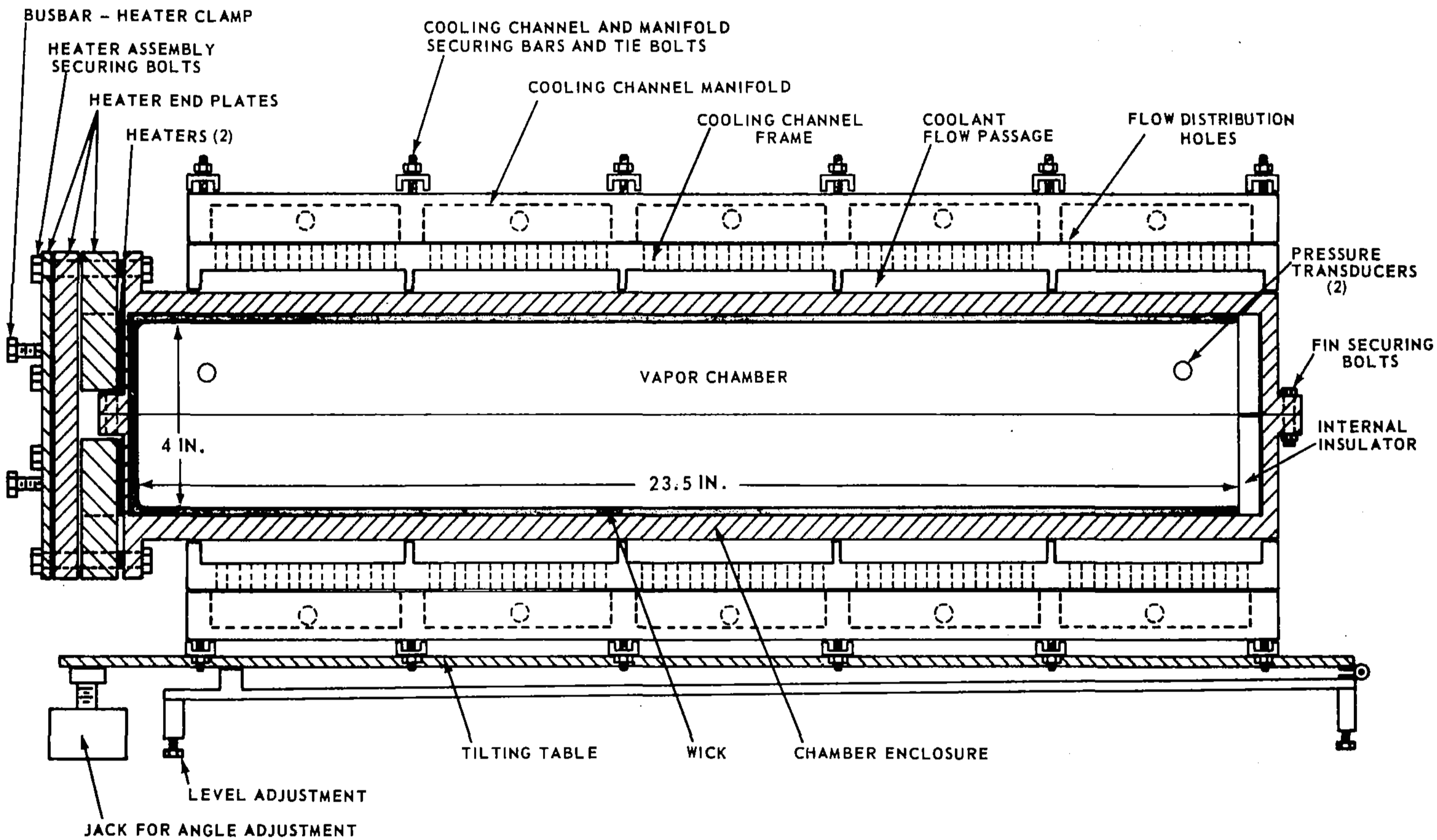

Figure 9 Cross-Section of Box-Geometry Fin Model

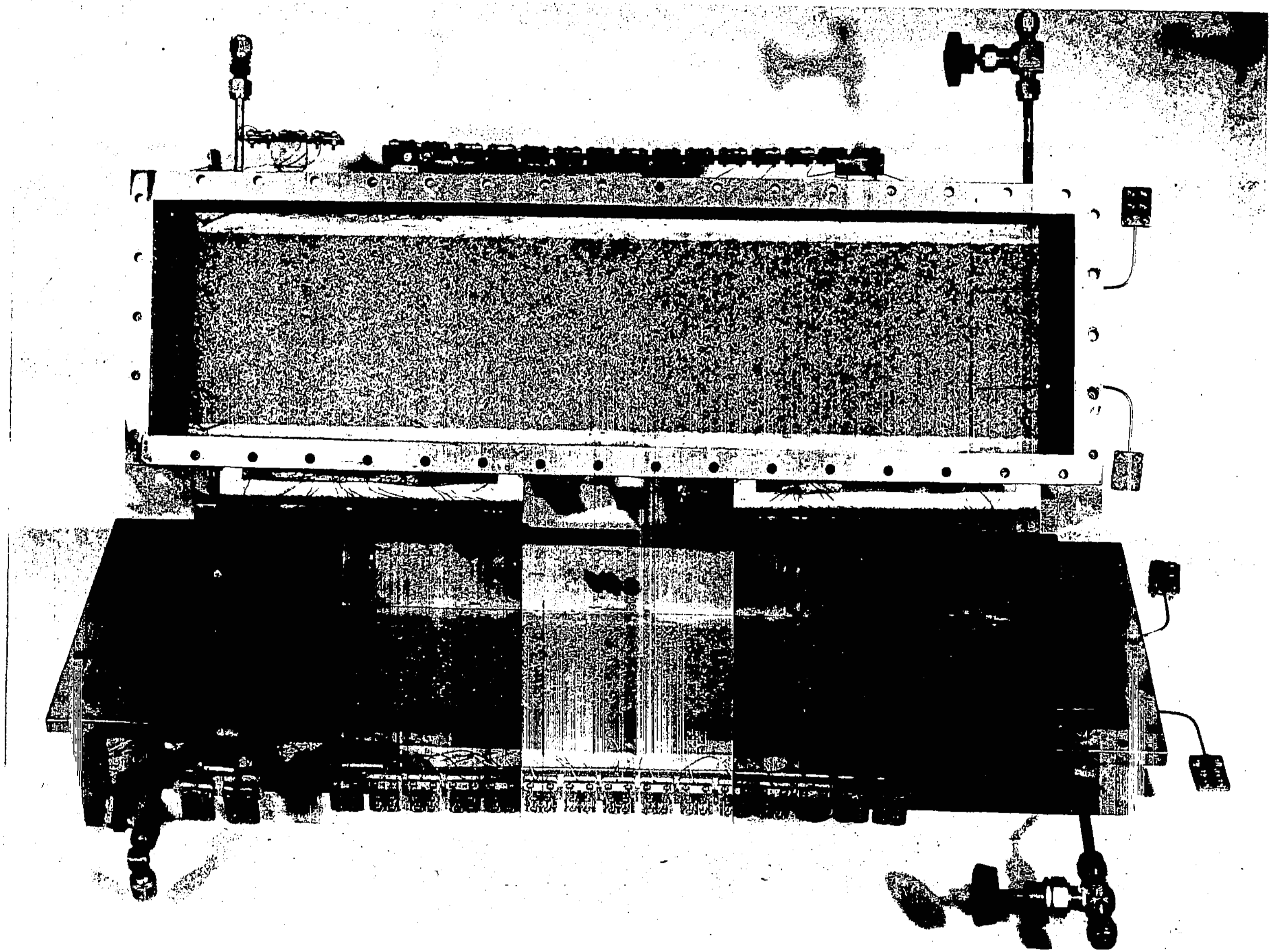

Figure 10 Box Halves with H13 Wicks Installed XP-74174

It had a 90-degree 1/4-inch radius bend which provided a continuous path for the working fluid to pass from the condenser to the evaporator region. The small void left by the bend when the wick was fitted to the corner of the box half was filled with GE 8104 braze material at the same time that the wick was being bonded to the box-fin half. The portion of the wick bonded to the 1/8-inch thick evaporator end was nominally 2 x 5 x 0.10 inch thick. The portion of the wick bonded to the 0.40-inch thick condenser region was nominally 23.5 x 5 x 0.10 inch.

Each box half had four 1/16-inch diameter, stainless-steel-sheathed, welded-junction, chromel-alumel thermocouples protruding through the chamber wall to measure the vapor temperature. Thirty 0.020-inch diameter, stainless-steel-sheathed, welded-junction, chromel-alumel thermocouples were imbedded in grooves on the outside surface of the condenser section of each box half. Chromel wire resistance-welded in place was used to cover the thermocouple junctions and the outer edge of the groove where the coolant channel was sealed against the box. The evaporator end plate had five 0.020-inch diameter, stainless-steel-sheathed, welded-junction, chromel-alumel thermocouples imbedded in grooves. The entire length of the groove was filled with resistance-welded chromel wire after the thermocouple was installed. The chromel wire was applied in excess and smoothed off to enable the strip heaters to fit in intimate contact with the heater end plate. The locations of all thermocouples attached to the box-fin half are shown in Figure 11.

The box fin was water-cooled by means of two sets of cooling channels. Each set had five separate channels with individual flow control valves. Each channel was 5.5 x 4.4 x 0.5 inch with eight 1/4-inch diameter flow distribution holes at the inlet and exit (see Figure 9). The ten cooling channels received and expelled water through four manifolds instrumented with immersion type thermocouples. The manifolds and the cooling channels were secured to the box fin by large clamps which encompassed the fin and pressed the top and bottom cooling assemblies to the box fin. The first cooling channel sets were made of Mycalex 400 which cracked after a few hours of testing. New manifolds and cooling channels were then fabricated from a single slab of laminated Fiberglas. The Fiberglas cooling channels and manifolds proved satisfactory under all further test conditions.

Silicone rubber was used for gasket material between the cooling channels and the box surface. Cork was used as the gasket material between the cooling manifolds and cooling channels. The two strip heaters were made of Nichrome V heater ribbon and were 5 x 1.625 x 0.0089 inch in dimensions. The heaters were covered by a 0.010-inch thick layer of aluminum oxide to prevent electrical short circuits through the box fin. Power was supplied to the heaters from the rectified power supply by means of copper busbars pressed to the heater strips by clamping devices in the heater support assembly. Each heater strip had an effective heater surface area of 8.125 square inches.

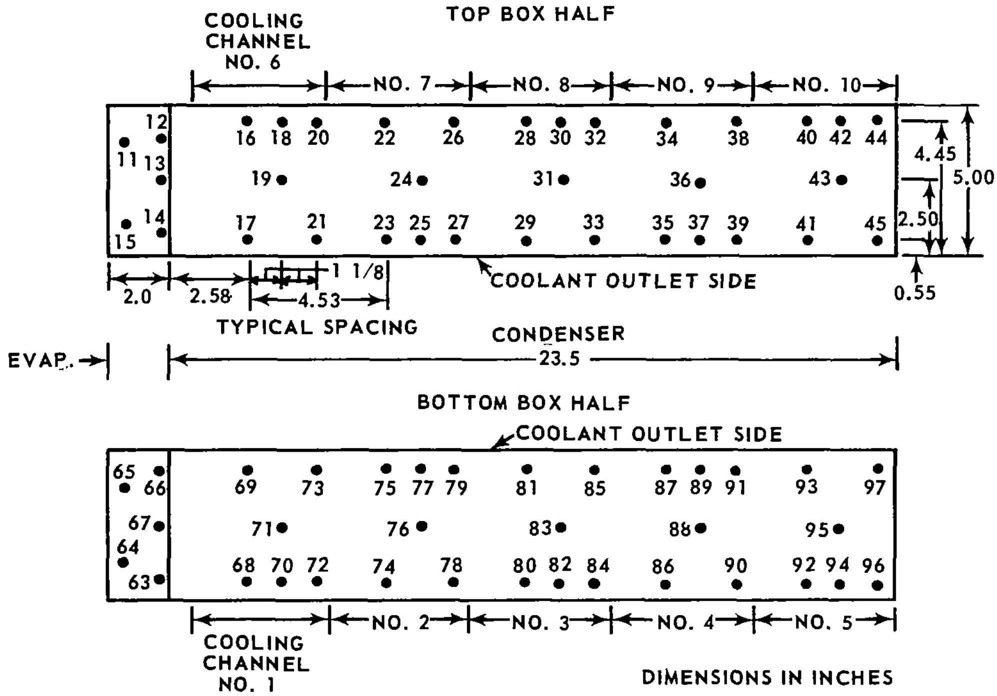

Figure 11 Thermocouple Locations Relative to Wicks for Box Fin

The heater support assembly consisted of three Mycalex 400 insulators and one outer stainless-steel plate (see Figures 8 and 9). The assembly served to press the heaters against the evaporator end of the box fins.

The tilting table used in the box-fin assembly was the same as that used in the planar fin. The reference surface for leveling and angle tests was taken as the top of the top cooling channel set for the tests with both box-fin halves. The reference surface for the half-box fin tests was taken as the top of the cover plate.

When both box-fin halves were tested simultaneously, they were bolted together with a silicone rubber gasket between the two parting flanges. When one box-fin half was tested, the half box was bolted to a smooth flat cover plate with a silicone rubber gasket between the parting flange and the plate. The cover plate was made of AMS 5524 stainless steel, and was 30 x 7.5 x 0.5 inch in dimensions.

C. <u>Description of Test Facility</u>

A sketch of the facility for testing the vapor-chamber fin models is shown in Figure 12. The essential facilities needed to operate such a device are a heating source for one section and a cooling source for the other. An electrical heat source and a recirculating cooling system were used for this program. Additional facilities included the vacuum pump system for evacuating the chamber and the instrumentation devices.

The heating system rectified 440-volt alternating current to direct current. The power level was controlled by a powerstat.

The cooling water was heated in a closed tank pressurized from a high-pressure nitrogen bottle. The water was pumped through a filter and then fed in separately controlled parallel lines into the flowmeters and the separate cooling channels of the fin model. After leaving the cooling channels the water was collected into a single line, passed through an intercooler, then returned to the tank. This enclosed recirculating system made possible a higher coolant temperature level than a non-recirculating system. Also, to some extent, dissolved gases in the water could be expelled with the circulating system.

The major components and measuring devices of the facility are listed and described in Table 1. Temperatures were read out on a 0-800°F Honeywell-Brown potentiometer with an accuracy of ±1.6°F. Pressures indicated by the chamber pressure transducers were recorded on a Honeywell-Brown strip chart recorder.

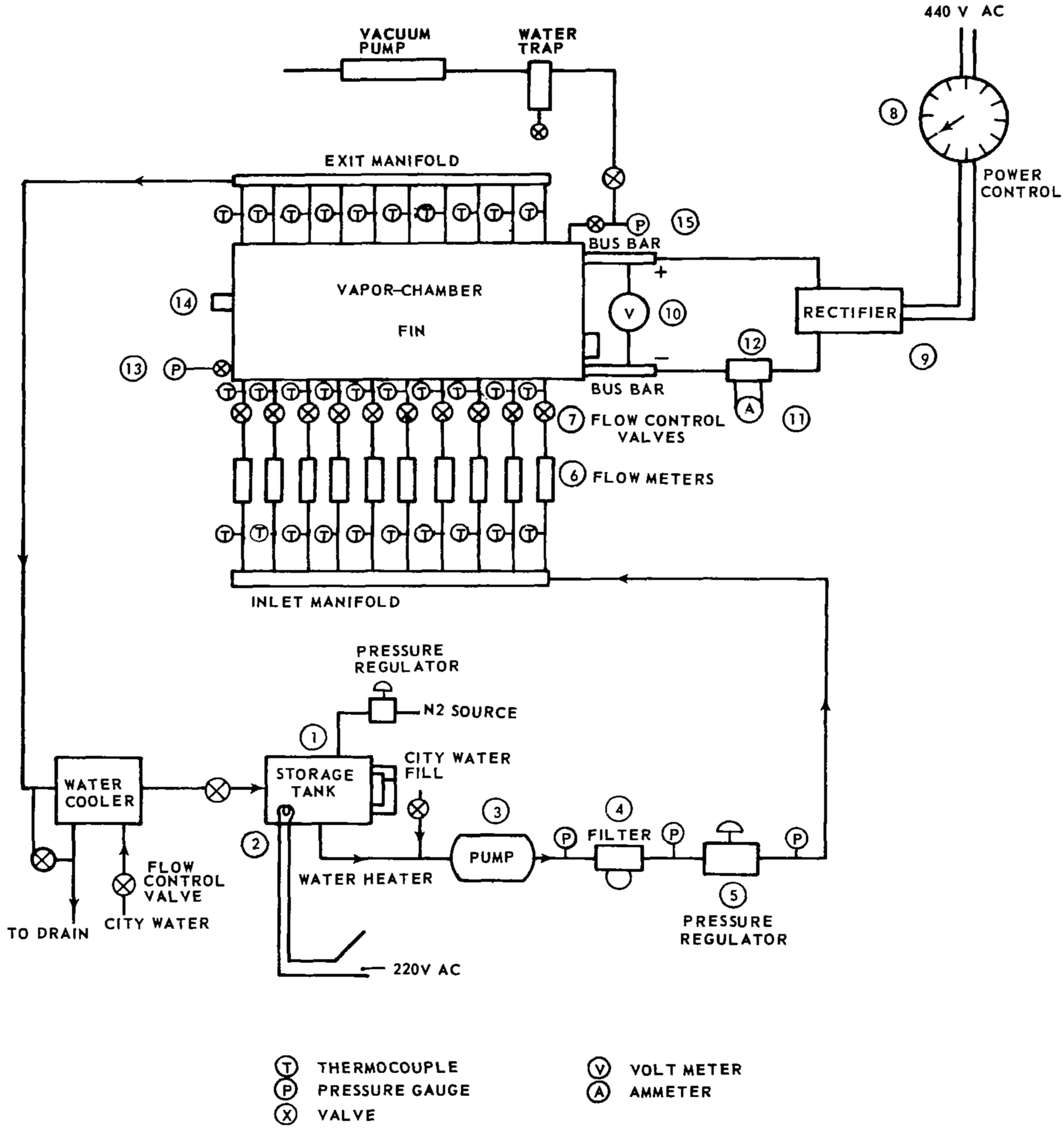

Figure 12 Schematic Diagram of Vapor-Chamber Fin Test Facility

TABLE 1

Item	Name	Manufacturer	Description
1.	storage tank	P&WA	stainless steel, 10-gallon capacity
2.	cooling water heater	General Electric	5000 watt, 220v AC, Calrod heater
3.	circulator pump	Allis Chalmers	centrifugal type, 0-60 gpm capacity, type SSHH, 55 psi rise
4.	filter	Norgren	5μ sintered element
5.	pressure regulator	Norgren	Type 11-009, 0-125 psig range
6.	flowmeter	Fischer-Porter	1.52 gpm water, Model 10A3565A, 10-inch scale, Buna-N packing
7.	flow control valve	Hoke	Model 4RB286-4Y280-13, brass body, angle type
8.	power control	Superior Electric	6-stack, 3-phase, Powerstat, 50 KVA capacity, Model 30M1256CL-6y
9.	rectifier	Utilyte	12 KVA 750 amp at 12 v DC or 1500 amp at 6v DC Model UV610
10.	voltmeter	Weston	1970 series ±1% accuracy 0-10 v DC
11.	ammeter	Weston	1970 series ±1% accuracy 0-50 mv, 0-1000 amp
12.	shunt	Weston	0-1000 amp. 0-50 mv
13.	pressure gage	Helicoid	0-160 psig range, bronze Bourdon tube type
14.	pressure transducer	Statham	Model PA288 TC, Serial No. 37314, 37315, 0-200 psig, flush mounted
15.	vacuum gage	Helicoid	Type 410 - bronze Bourdon tube type, 30 inch Hg to 30 psig range, 0.5 inch and 0.2 lb subdivisions

D. Fin Preparation

Both the box and planar fins were prepared for testing after being installed on the backup plates by the procedure listed below:

1) cleaning,
2) assembly,
3) pressure and vacuum leak check, and
4) evacuation and fill.

The cleaning procedure used on both the box and planar fin was similar to that used on the wick materials of Tasks I and II, the only deviations being in the baking time and temperature. The cleaning procedure used is listed below:

1) The wick was washed in a vapor degreaser and immediately rinsed in distilled water before the condensed vapor re-evaporated.
2) It was rinsed in a bath of reagent-grade acetone.
3) The wick was immediately rinsed in distilled water followed by two distilled-water baths.
4) It was air-dried in a clean oven as shown in the table below:

Wick	Temp., °F	Time, Hours	Oven Atmosphere
Planar H13	600	5.0	air
Planar H6	600-700	3.0	air
Planar M2	275	2.0	air
Box H13	275	2.0	air

After the wicks were oven dried, they were stored in clean air-tight plastic bags filled with a nitrogen atmosphere until needed for assembly. The assembly of the planar and box fin is described in Sections IIIA and IIIB. When assembly of the fin was complete, the chamber was pressure-checked for external leaks with nitrogen gas. The fin was charged with a pressure approximately 10 percent above the expected fin test pressure. At this point, the nitrogen source was removed and the rate of pressure decay was noted on a Bourdon-tube pressure gage. When all detectable leaks were eliminated, the chamber was evacuated with a vacuum roughing pump to a pressure of approximately 2 inches of mercury or less measured on a Bourdon-tube pressure gage. As an additional leak check the pressure change was noted. When no rise in chamber pressure was seen in half an hour, the fin cavity was considered to be leaktight and the filling procedure was started.

The fin cavity was filled with distilled water or Freon 113, using a 0-100 milliliter buret as a measuring device. See sketch below.

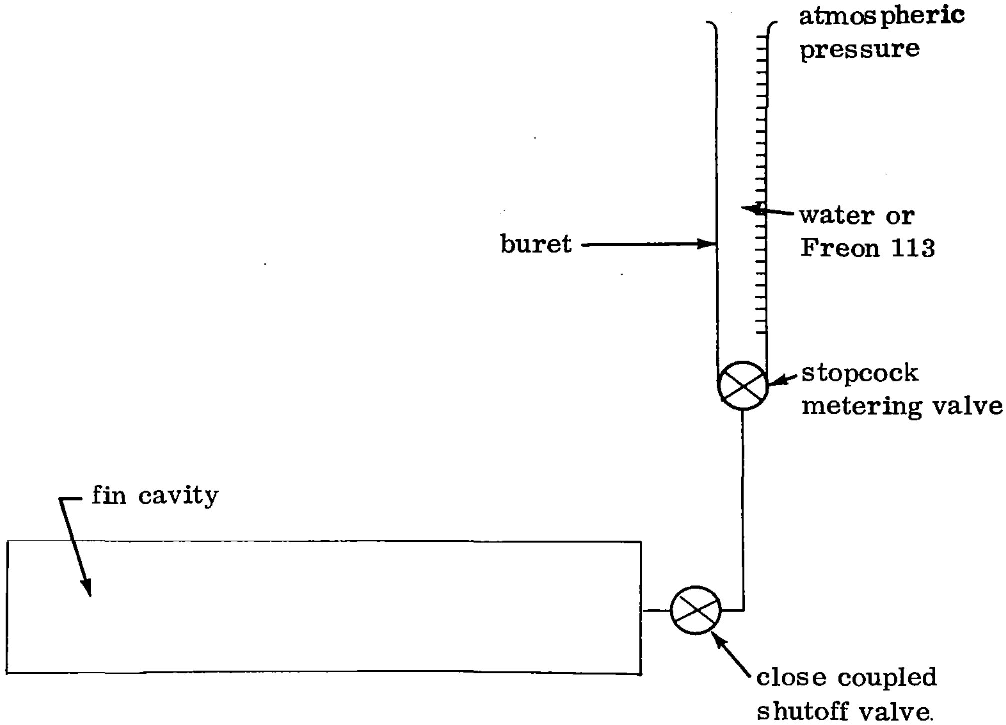

The fluid was forced into the chamber by the pressure difference between the atmosphere and the internal pressure of the chamber. The amount of fluid was metered by the stopcock at the base of the buret. The quantity of fluid added could be measured to ±1 milliliter with the buret. This represents less than 0.6 percent of the wick void volume of any configuration tested. The percent of liquid inventory of the wick was based on the total volume of liquid that the wick would absorb, which was calculated from the porosity and wick overall dimensions. This volume of liquid was added at room temperature. When the desired amount of distilled water or Freon 113 was added, the valve which was close-coupled to the fin cavity was closed and the buret assembly was removed. The valve was then capped off to prevent any minute leakage of air or working fluid (depending on the chamber pressure). At this point in the filling process the chamber pressure was subatmospheric. In the tests where noncondensable gas was desired, the gas was then forced in under pressure. The amount of noncondensable gas present could be determined from knowledge of the chamber dimensions and the chamber pressure at the time of fill.

E. Test Procedure

At the start of a test, water at 225°F was circulated through the cooling channels to preheat the fin assembly. When a pressure of approximately 15 psia or more was reached in the fin chamber, power was applied to the heaters. The power was started at a low value and increased to the desired evaporator heat flux in discrete increments to prevent the wick from prematurely drying out in the evaporator region. If the wick inadvertently became dried out during a startup, the heater was shut off and the fin assembly allowed to cool until the temperature in the evaporator end of the wick was lower than the saturation temperature for one-half hour. At this lower temperature the fin could be restarted. When the desired power was reached, the cooling-water flow and temperature were adjusted to obtain the desired chamber pressure.

Pressure in the fin cavity was read on both the pressure transducers and the Bourdon tube pressure gages. The Bourdon pressure gages were read by opening the valves close-coupled to the fin. When the reading was complete the valves were reclosed to minimize heat loss through the pressure gages.

Pressure, temperature, cooling flow, and heater power were recorded for each test point. In most of the test series, orientation, number of heaters operating (evaporator length), and number of cooling channels operating (condenser length), were held fixed, while heat flux was raised from a low value to higher values in increments, with adjustments of coolant flow and temperature level to maintain the approximate desired chamber pressure. In some tests the heat flux was fixed and angle of orientation varied.

IV. OBJECTIVES AND THEORETICAL PREDICTIONS

A. Introduction

Unlike a conventional fin, a vapor-chamber fin ideally operates isothermally. Heat transfer in a vapor-chamber fin is accomplished by evaporation at one section of a wick-lined enclosure and condensation at another section. For ordinary operation below the maximum heat-flux level, the working fluid flows through the wick from the condenser section to the evaporator section, as a result of capillary forces. The maximum heat flux at which a vapor-chamber fin will operate is that value at which a liquid deficiency first results in the evaporator. This can occur when forces opposing liquid flow in the wick, such as frictional and gravitational forces, exceed the capillary forces (i.e., capillary pumping limit), when film-type boiling conditions occur in the evaporator, or by a combination of these effects.

An analytical model was proposed and equations were derived in Report NASA CR-812 for predicting the limiting heat flux in a vapor-chamber fin due to capillary pumping only. A major assumption made in the analysis was that the wick is completely filled with liquid prior to the limiting heat flux. The model used in the analysis should be suitable at low heat flux levels where heat is conducted through the wick-liquid composite to the liquid-vapor interface where evaporation takes place. At higher heat-flux levels where the boiling process occurs in the wick structure, this simplified model may not apply. The details of the analysis are discussed in detail in NASA CR-812.

B. Theoretical Equation

On the basis of the analysis, two fin configurations, a planar-fin model and a box-fin model, were designed and fabricated. In the planar design the evaporator and condenser are in the same plane. In the box fin, which is made of two identical halves, the evaporator and condenser are perpendicular.

The final equation defined in NASA CR-812 can be applied directly to the planar-fin model when the condensing and evaporative section comprise the total wick length and $0 \leq \theta \leq 180°$. This equation is presented below:

$$Q/A_{\substack{\text{cond.}\\ \text{max.}}} = \left[\left(\frac{2\rho_L h_{VL}\sigma}{\mu_L}\right)\left(\frac{\delta}{x_C x_T}\right)\left(\frac{g}{g_o}\frac{\rho_L}{\sigma}\right)_{WR} - \frac{2\rho_L^2\, h_{VL}}{\mu_L}\;\frac{g}{g_o}\left(\frac{\delta}{\ell_m x_C}\right)\sin\theta\right]\frac{\ell_m}{K_1} \tag{1}$$

In order to account for any adiabatic section in the planar fin model, the equation can be modified slightly for two special cases as shown below, depending upon the position of the adiabatic section. It should be noted that in the following equations the maximum evaporator heat flux is the dependent variable, whereas in the preceding equation the maximum condenser heat flux was dependent.

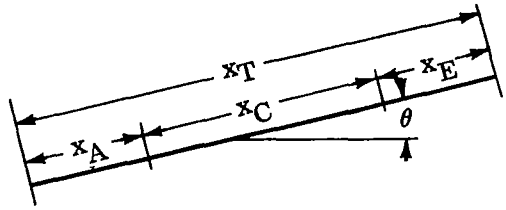

Case 1. Adiabatic Section Located at End Farthest from Evaporator and $0° \leq \theta \leq 180°$

$$Q/A_{\substack{\text{evap.}\\ \text{max.}}} = \left[\left(\frac{2\rho_L h_{VL}\sigma}{\mu_L}\right)\left(\frac{\delta}{x_E(x_E+x_C)}\right)\left(\frac{g}{g_o}\ \frac{\rho_L}{\sigma}\right)_{WR} - \frac{2\rho_L^2 h_{VL}}{\mu_L}\ \frac{g}{g_o}\ \frac{1}{\ell_m}\left(\frac{\delta x_T}{x_E(x_E+x_C)}\right)\sin\theta\right]\frac{\ell_m}{K_1}$$

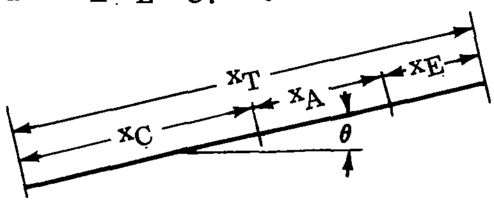

Case 2. Adiabatic Section Located Between Evaporator and Condenser and $0° \leq \theta \leq 180°$

$$Q/A_{\substack{\text{evap.}\\ \text{max.}}} = \left[\left(\frac{2\rho_L h_{VL}\sigma}{\mu_L}\right)\left(\frac{\delta}{x_E(x_E+x_C)+2x_E x_A}\right)\left(\frac{g}{g_o}\ \frac{\rho_L}{\sigma}\right)_{WR} - \frac{2\rho_L^2 h_{VL}}{\mu_L}\ \frac{g}{g_o}\ \frac{1}{\ell_m}\left(\frac{\delta x_T}{x_E(x_E+x_C)+2x_E x_A}\right)\sin\theta\right]\frac{\ell_m}{K_1} \qquad (3)$$

For the box-fin model further modifications were necessary to account for the fact that the evaporator section was perpendicular to the condenser section. The resultant equations depending on the position of adiabatic section, are shown below.

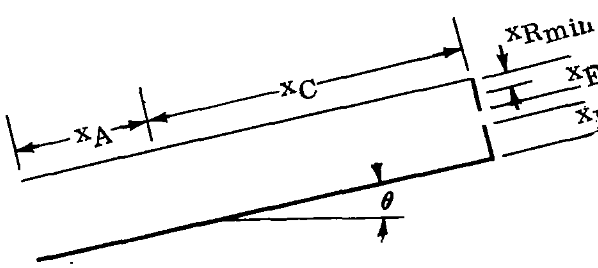

Case 1. Adiabatic Section Located at End Farthest from Evaporator and $0° \leq \theta \leq 90°$

$$Q/A_{\substack{\text{evap.}\\ \text{max.}}} = \left[\left(\frac{2\rho_L h_{VL}\sigma}{\mu_L}\right)\left(\frac{\delta}{x_E\,(x_C + 2x_{R\,min}) - x_{R\,min}^2}\right)\left(\frac{g}{g_o}\;\frac{\rho_L}{\sigma}\right)_{WR} - \frac{2\rho_L^2 h_{VL}}{\mu_L}\;\frac{g}{g_o}\;\frac{1}{\ell_m}\left(\frac{-(x_C + x_A)\sin\theta \pm x_{R\,min}\cos\theta}{x_E\,(x_C + 2x_{R\,min}) - x_{R\,min}^2}\right)\right]\frac{\ell_m}{K_1} \qquad (4)$$

The upper sign in Equation (4) applies to the top box half while the lower sign applies to the bottom box half. $x_{R\,min}$ is defined as the distance from the condenser-evaporator junction to the point in the evaporator where the radius of curvature of the liquid-vapor interface is a minimum.

For the bottom box half $\qquad x_{R\,min} = x_E \qquad (5)$

and for the top box half $\qquad x_{R\,min} = x_E - \dfrac{g\,h_{VL}\,\delta\,\rho_L^2\cos\theta}{g_o\,K_1\,\mu_L\,(Q/A)_{evap.\,max.}} \quad \text{for } x_{Rmin} > 0 \qquad (6)$

Equation (6) is derived from the momentum,continuity, and energy equations, noting that the change in pressure with length due to capillary forces is zero at R min. If the solution of Equations (4) and (6) yields a negative value of $x_{R\,min}$, the minimum interfacialradius of curvature is located at the condenser-evaporator junction, and $x_{R\,min} = 0$.

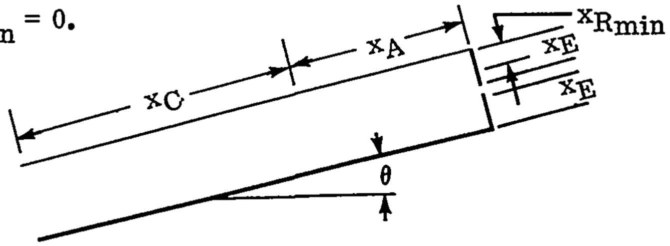

Case 2. Adiabatic Section Located Between Evaporator and Condenser and $0° \leq \theta \leq 90°$

$$Q/A_{\substack{\text{evap.}\\ \text{max.}}} = \left[\left(\frac{2\rho_L h_{VL}\sigma}{\mu_L}\right)\left(\frac{\delta}{x_E\,(x_C + 2x_A + 2x_{R\,min}) - x_{R\,min}^2}\right)\left(\frac{g}{g_o}\;\frac{\rho_L}{\sigma}\right)_{WR} - \frac{2\rho_L^2 h_{VL}}{\mu_L}\;\frac{g}{g_o}\;\frac{1}{\ell_m}\left(\frac{-(x_C + x_A)\sin\theta \pm x_{R\,min}\cos\theta}{x_E\,(x_C + 2x_A + 2x_{R\,min}) - x_{R\,min}^2}\right)\right]\frac{\ell_m}{K_1} \qquad (7)$$

The upper sign applies to the top box half while the lower sign applies to the bottom box half. Further modifications of the above equations for both the planar and box-fin models would be necessary if θ is outside the prescribed range, since the locations of the maximum and minimum radii of curvature become functions of angle[6].

C. Criteria for Selection of Wick Material and Dimensions

It is apparent from Equations (1) and (5) that ℓ_m/K_1 is the important wick characteristic in a zero-gravity force field while the additional parameter ℓ_m becomes important for an inclined fin in one "g". Since the fins may ultimately be used for one "g" operation and in zero gravity fields, it is desirable to test with wicks of both high capillary forces (indicated by large ℓ_m) and high capillary pump capacity (indicated by ℓ_m/K_1).

Another important characteristic of the wick which does not appear as a parammeter in Equations (1) through (5) is the boiling heat transfer characteristic of the wick. The wick material must be such that a high heat flux is possible before film boiling occurs. Preliminary boiling characteristic tests were run in Task 2 of the contract and results of these tests were reported in NASA CR-812.

For the above-stated reasons, the following wicks were selected for fin tests:

1. Sintered nickel fiber wick H6-selected for high ℓ_m with good ℓ_m/k_1, and desirable boiling characteristics.

2. Sintered stainless steel fiber wick H13-selected for high ℓ_m/K_1 with good ℓ_m, and desirable boiling characteristics.

3. Sintered stainless steel powder wick M2-selected for having properties between those of H6 and H13 wicks, as well as being representative of a different type of construction.

Values of ℓ_m, K_1 and the boiling heat flux characteristics were determined in Tasks 1 and 2 and reported in Reference 5. The value of ℓ_m for the H6 wick was greater than the height of the sample used in Task 1. Thus, a wicking rise test was performed on the actual H6 wick used in the fin tests. A wicking rise test was also performed on the H13 planar fin. These resulting important wick characteristics are shown in the table below:

Wick Type	ℓ_m, ft	$\ell_m/K_1 \times 10^9$, ft^3	Limiting Heat Flux due to Film Boiling, Btu/hr ft^2
H6	1.57	0.52	>100,000
H13	0.53	6.57	>130,000
M2	0.81	2.38	90,000

The overall fin length was based upon practical fabrication limits for the sintered porous wicks mentioned above. A vendor who fabricated the wicks was limited to wicks 24 inches in length due to the size of the sintering ovens. A maximum condenser length of 17.8 inches, and an evaporator length of 6.2 inches were chosen for the planar-fin design in order to obtain data from each of the selected wicks at reasonable values of heat flux. For the box fin the condenser length was chosen to be 23.5 inches and the evaporator length to be 2 inches.

D. Predicted Performance of Various Configurations

The three different wicks H6, M2 and H13 were fabricated for use in the planar fin and H13 was fabricated for use in the box fin. Performance predictions were made for all of the fabricated configurations. These predictions are presented in Figures 13 through 16.

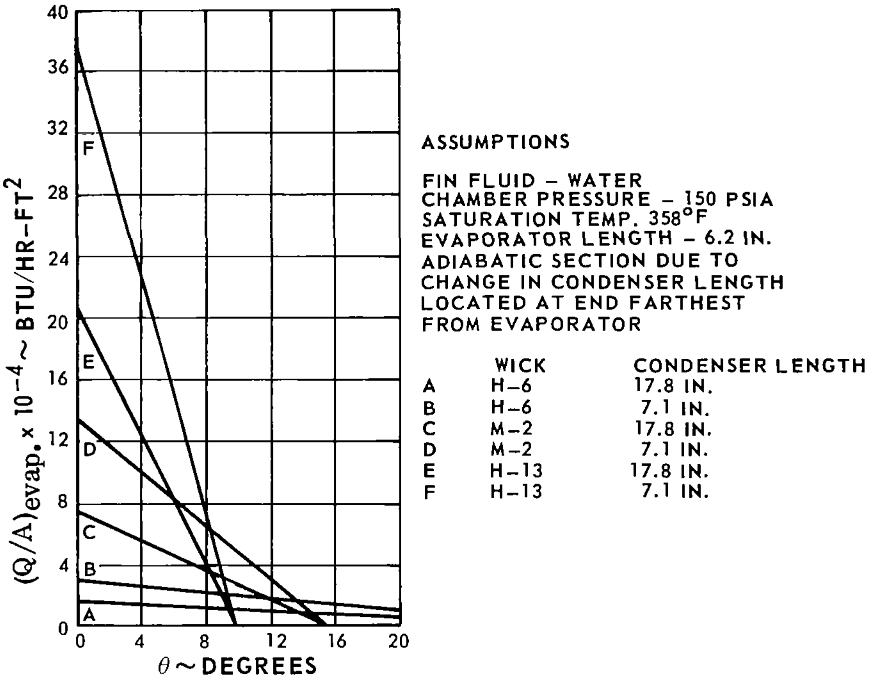

Figure 13 Predicted Maximum Evaporator Heat Flux as Function of Angle of Inclination and Condenser Length for Three Different Wicks in Planar-Fin Model

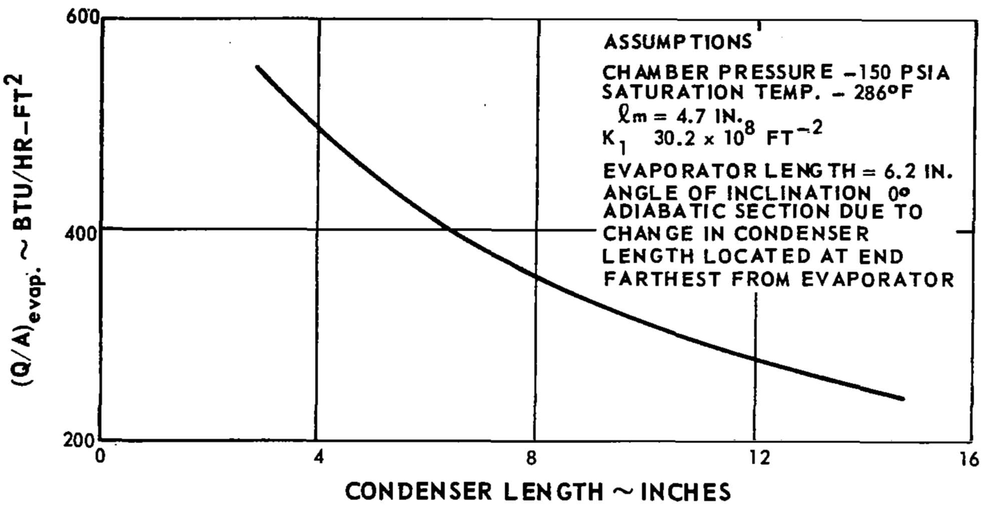

Figure 14 Predicted Maximum Evaporator Heat Flux vs Condenser Length for H6 Planar-Fin Model with Freon 113 as Working Fluid

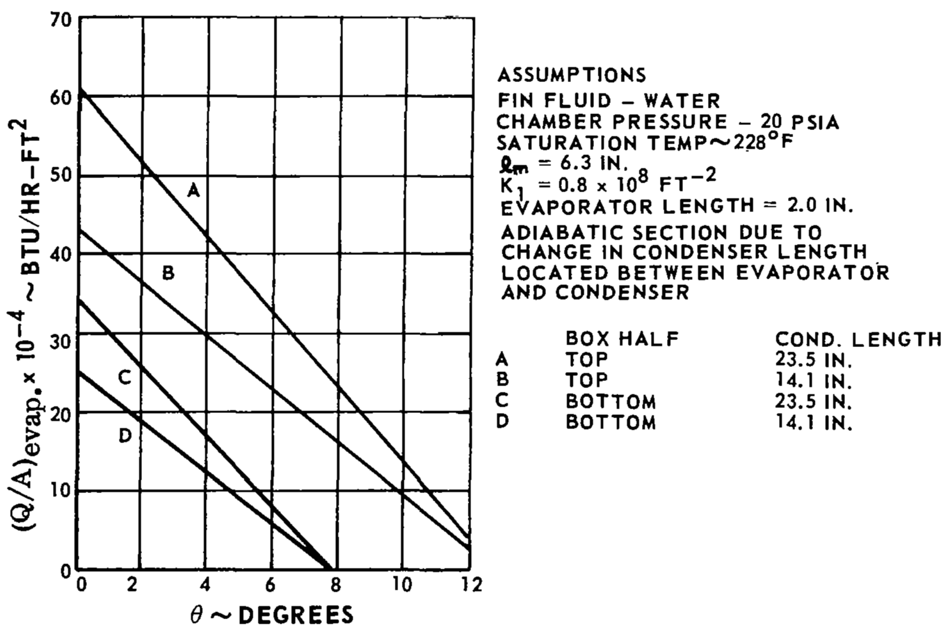

Figure 15 Predicted Maximum Evaporator Heat Flux vs Angle of Inclination for H13 Box-Fin Model

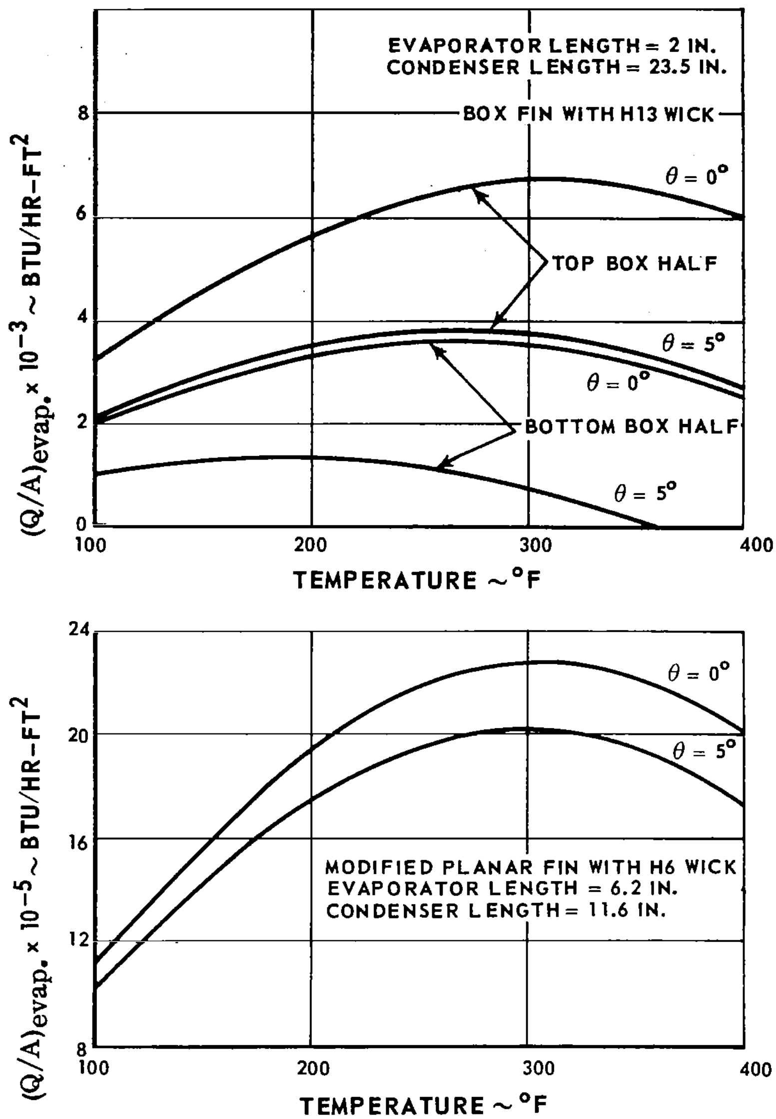

Figure 16 Predicted Maximum Evaporator Heat Flux as Function of Saturation Temperature with Water as Test Fluid

Figure 13 shows, for the maximum planar-fin condenser length of 17.8 inches, that the fin with wick material H13 should not fail in the horizontal position due to the capillary pump limitation of the wick at an evaporator heat flux less than 207,000 Btu/hr ft^2. This high value might exceed the limiting heat flux due to film boiling. However, the analysis indicates that a limiting heat flux should occur over a wide range of evaporator heat flux as angle of inclination is varied. As can also be seen in Figure 13, the value of limiting heat flux was predicted to be strongly dependent on condenser length.

The limiting heat flux for the planar fin with wick material H6 in the horizontal position is predicted to occur for all condenser lengths at a value below the expected film boiling limit. The graph also indicates that the value of limiting heat flux is strongly dependent on condenser length. For example with the fin horizontal the limit increases from 16,000 to 30,000 Btu/hr ft^2 with a reduction in condenser length from 17.8 inches to 7.1 inches.

The fact that ℓ_m, in addition to ℓ_m/K_1, becomes an important parameter for a fin in a gravity field can be seen in Figure 13, where it is shown that for a condenser length of 17.8 inches a planar fin with wick H13 (high ℓ_m/K_1 and good ℓ_m) should perform better at angles less than 9.2 degrees while the fin wick H-6 (high ℓ_m and good ℓ_m/K_1) should perform better at angles greater than 9.2 degrees.

The limiting heat flux predictions for the third planar-fin wick, M2, are shown in Figure 13 to be between those for H6 and H13 in the horizontal position. Also, the slope of the Q/A limit versus angle of inclination is between that of the other two wicks. The highest predicted value of limiting heat flux for M2 was not below that of the expected film boiling limit. In other words with the maximum length of 17.8 inches and the horizontal orientation, this wick should be limited by film boiling rather than capillary pump limits.

In order to determine the effects of fluid properties on limiting heat flux, Freon 113 was chosen as a test fluid in addition to water. Figure 14 shows the predicted limiting heat flux vs condenser length for a horizontal H6 planar fin with Freon 113 as the working fluid. A comparison of Figures 13 and 14 shows that fin performance was predicted to be significantly poorer with Freon 113 as the working fluid than with water. With Freon 113 as the test fluid, the external heat losses of the planar fin were predicted to be the same order of magnitude as the evaporator heat load. Thus, it would be expected that any data obtained with Freon 113 as the test fluid would be more qualitative in nature than quantitative.

The predicted limiting heat flux for the box fin is shown in Figure 15. The variation of evaporator maximum heat flux with fin orientation and condenser length for both the top and bottom box halves is shown. Since gravity aids the flow of liquid in the evaporator section of the top box half and opposes the flow of liquid in the bottom box half, separate curves for each box half are presented, assuming that the halves act independently. These curves indicate that the bottom box half should fail at a significantly lower heat flux than the top box half and that operation is not possible when the angle the condenser section makes with the horizontal is greater than eight degrees.

In addition to variables of condenser length and fin orientation presented above, fluid property variations with temperature affect the predicted limiting heat flux. These predicted effects are presented in Figure 16 for two fin configurations at two angles of inclination. This figure shows that in the temperature range considered, a maximum value occurs for each curve. The fluid properties which show greatest change with temperature are the fluid surface tension and liquid viscosity.

For several reasons, prediction of the performance of a vapor-chamber fin with noncondensable gases present is of interest. First, it is conceivable that a noncondensable gas might not be completely purged from a fin before the working fluid is added. Secondly, it might be desirable to add a noncondensable gas so that the heat flux-operating temperature level characteristics are altered. This can be accomplished under proper design conditions if the noncondensable gas and working vapor do not mix appreciably. It is possible, depending on fin design and operating conditions, for there to be no mixing, partial mixing or complete mixing of condensable and noncondensable gases. An analysis presented in Appendix 3 predicts the fin operating conditions considering uniform mixing and no mixing, conditions that should bracket the operating conditions.

V. TEST RESULTS AND DISCUSSION

One hundred thirty-six tests were run on the two vapor-chamber fin models. Table 2 contains a list of each series of tests and the main variables associated with each series. Comments are also noted in this table. Table 3 contains a list of the significant data obtained for each test.

The following sections contain a presentation and discussion of the test results. Test numbers referred to in this section correspond to those denoted in Tables 2 and 3.

A. Planar-Fin Tests

Three different wicks were fabricated for the planar fin. These were a large-pore sintered stainless steel fiber wick (H13), a small-pore sintered nickel fiber wick (H6), and a small-pore stainless steel powder wick (M2). All three wicks eventually evidenced deterioration in the bond between the wick and backup plate. No data was obtained for the H13 wick since this 430 stainless steel wick corroded in a manner which is not typical for this material. Also very little useful data was obtained for the M2 wick because of the bond failure between the wick and backup plate. The bond failure of the H6 wick became apparent during preliminary tests and this model was subsequently modified. Several tests on this modified version produced usable data before bond failure became so excessive that the data could not be analyzed adequately.

The following sections contain discussions of the results from the tests on H6 and M2 wicks.

1. Sintered Nickel Fiber Wick H6

Tests numbers 1 to 20 were run on the modified planar model with the H6 wick. A temperature distribution for one of the tests (Test No. 3) is shown in Figure 17. In this figure as well as in all others presented in this report, the actual measured wall temperatures are plotted. Also, all heat flux values presented have been modified to account for heat losses. This temperature distribution is considered typical for the planar-fin model under normal conditions (i.e., before limiting heat flux is reached). End conduction losses account for the lower temperatures at the ends of the evaporator section than at the center. The rise in temperature at the end of the condenser is due to conduction from the adiabatic section (evaporator section in the original design).

Tests Nos. 3-8 resulted in a probable limiting heat flux occurring during Tests Nos.7 and 8 at a heat flux between 23,500 and 26,700 Btu/hr ft^2. Figure 18 shows the rise in temperature with time of thermocouples located in the backup plate in the evaporator section. The temperatures at the end rose more rapidly

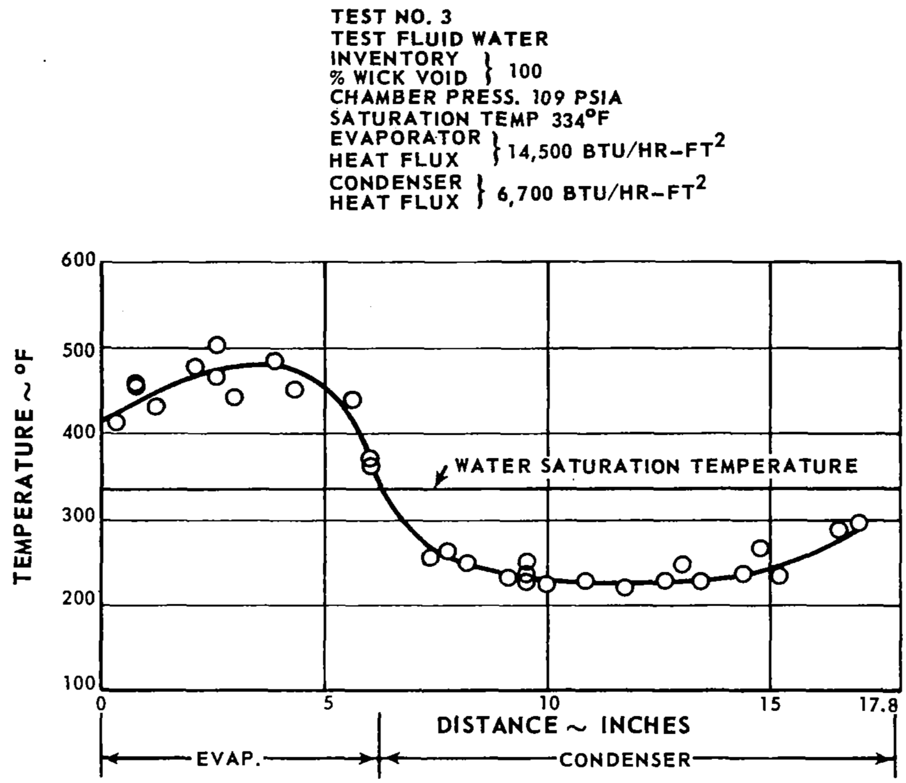

Figure 17 Typical Temperature Distribution for Planar Fin with H6 Wick

than those in the midsection of the evaporator, indicating that liquid water was not being pumped the full length of the evaporator. Test No. 7 showed a normal temperature distribution similar to that shown in Figure 17, as did Test No. 9. This fact eliminated the possibility that the rise in evaporator end temperatures occurred due to wick-to-backup plate bond failure.

The separation of the wick from the backup plate manifests itself by a deterioration of the heat transfer performance in the evaporator section. Figure 19 shows how the average wall superheat (ΔT_{sat}) corrected for temperature drop through the backup plate varies with evaporator heat flux corrected for heat losses. The results of five different series of tests numbered chronologically are shown with the wick in the horizontal orientation. As can be seen in this figure, there are noticeable changes between Tests Nos. 7 and 9, and between Tests Nos. 15 and 17. These changes indicate major separations in the bond between the wick and backup plate.

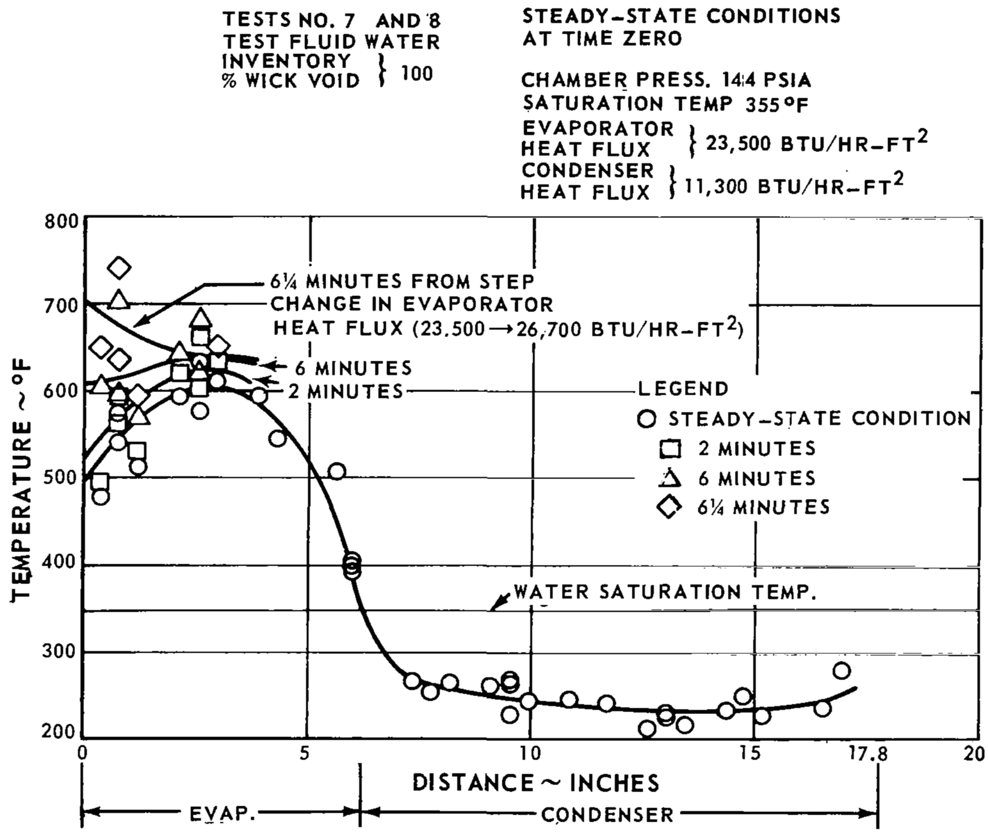

Figure 18 Temperature Distribution for Planar Fin with H6 Wick Indicating Limiting Heat Flux

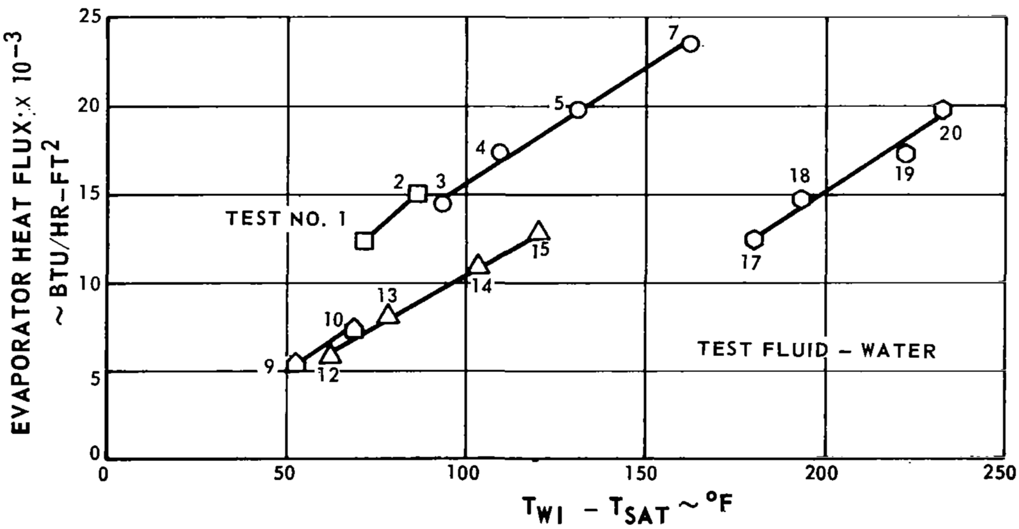

Figure 19 Evaporator Heat Flux vs Average Wall Superheat for Planar Fin with H6 Wick in Horizontal Position

Tests Nos. 11 and 16 were performed with the wick inclined at 15 and 5 degrees respectively to the horizontal. In Test No. 11 the measured wall temperatures in the evaporator section were much higher than those measured in a subsequent horizontal test (No. 12) at approximately the same heat flux (see Figure 20). However, steady-state conditions were not reached in Test No. 11 because the test was terminated due to the occurrence of excessively high wall temperatures during the transient period. Similar results occurred in Test No. 16 conducted at a 5-degree angle.

Shown in the table below are the experimental and predicted values of the limiting heat flux obtained in Tests No. 7 and 8. The predicted values are based on the analysis discussed in the previous section. As can be seen, good agreement was found.

Angle Measured From Horizontal, Deg.	Limiting Evaporator Heat Flux - Btu/hr ft^2 Predicted	Measured
0	22,200	23,500-26,700 (corrected for heat loss)

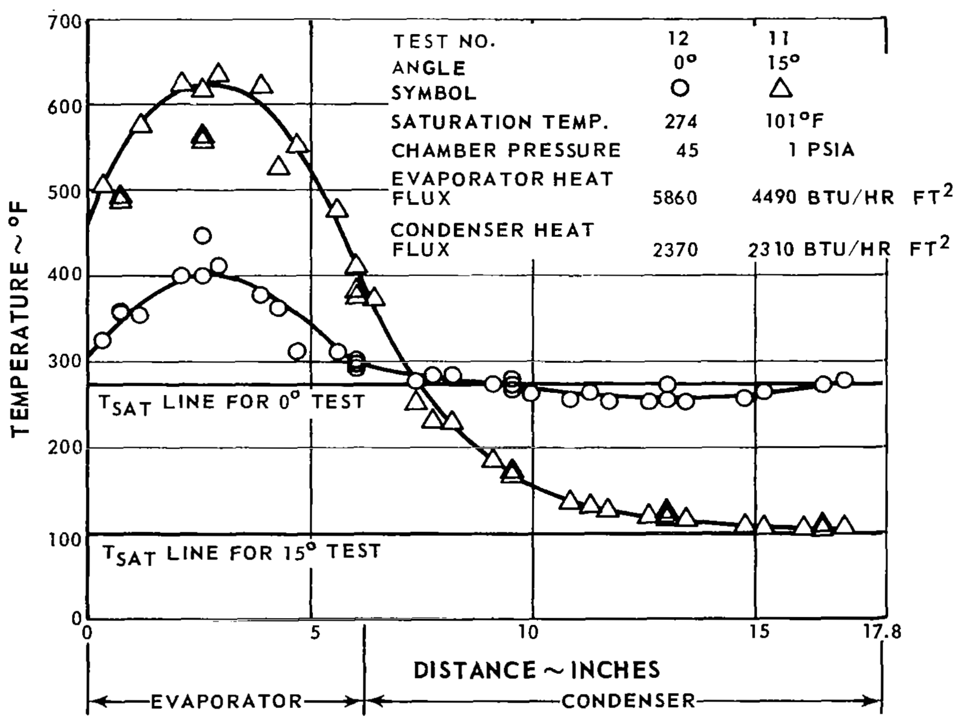

Figure 20 Temperature Distribution for Planar Fin with H6 Wick at Zero and Fifteen Degrees. 100% Inventory with Water as Test Fluid

A possible explanation of the higher-than-predicted capillary-failure heat flux is that excess liquid flowed by gravity from the condenser section over the wick into the evaporator section. This explanation is plausible since the void volume of the wick is a calculated value based on overall dimensions and an approximate wick porosity, and the liquid was filled at room temperature. Because of liquid expansion with temperature, the latter fact alone would account for true liquid inventory being about 109 percent when the designated fill inventory is 100 percent. Unfortunately the structural failure of the wick prevented further experiments which could have provided additional data to compare with the theory.

Overall heat transfer coefficients were calculated for both the condenser and evaporator sections for all horizontal tests. It was thus determined that the separation between wick and backup plate was the controlling resistance. Therefore, the information obtained on heat transfer coefficient was not typical and not useful for design purposes. The test series run at different chamber pressures did not produce any definite conclusions since wick separation also clouded this picture.

2. Sintered Stainless-Steel Powder Wick M2

Tests Nos. 132-136 were run with an M2 wick in the planar-fin model. At the end of the series it was apparent that the wick had separated from the backup plate. No apparent limiting heat flux points were obtained. The data is of little use since the extent of wick separation at any point in the test series was not known.

B. Box-Fin Tests

Tests were performed on the full box and each of the two halves run with the wick on the bottom of the chamber. In general the results of these tests indicated that there is an interaction between box halves when run together and there is a strong effect of fluid inventory and angle of inclination on limiting heat flux. One box half gave poorly defined results due to deterioration in performance caused by foreign matter clogging some of the pores. Tests on the full box in which a noncondensable gas was present indicated that the water vapor and the gas mixed.

1. Complete Box-Fin Tests

As shown in Table 2, Tests Nos. 21-48 were conducted to determine the operating characteristics of the complete box fin, including the limiting heat flux, effects of inventory, and effect of the pressure of a noncondensable gas.

A typical temperature distribution is presented in Figure 21, which shows the variation of measured fin temperature with length for the top and bottom box halves on Test No. 29. The two thermocouple readings appearing closest to

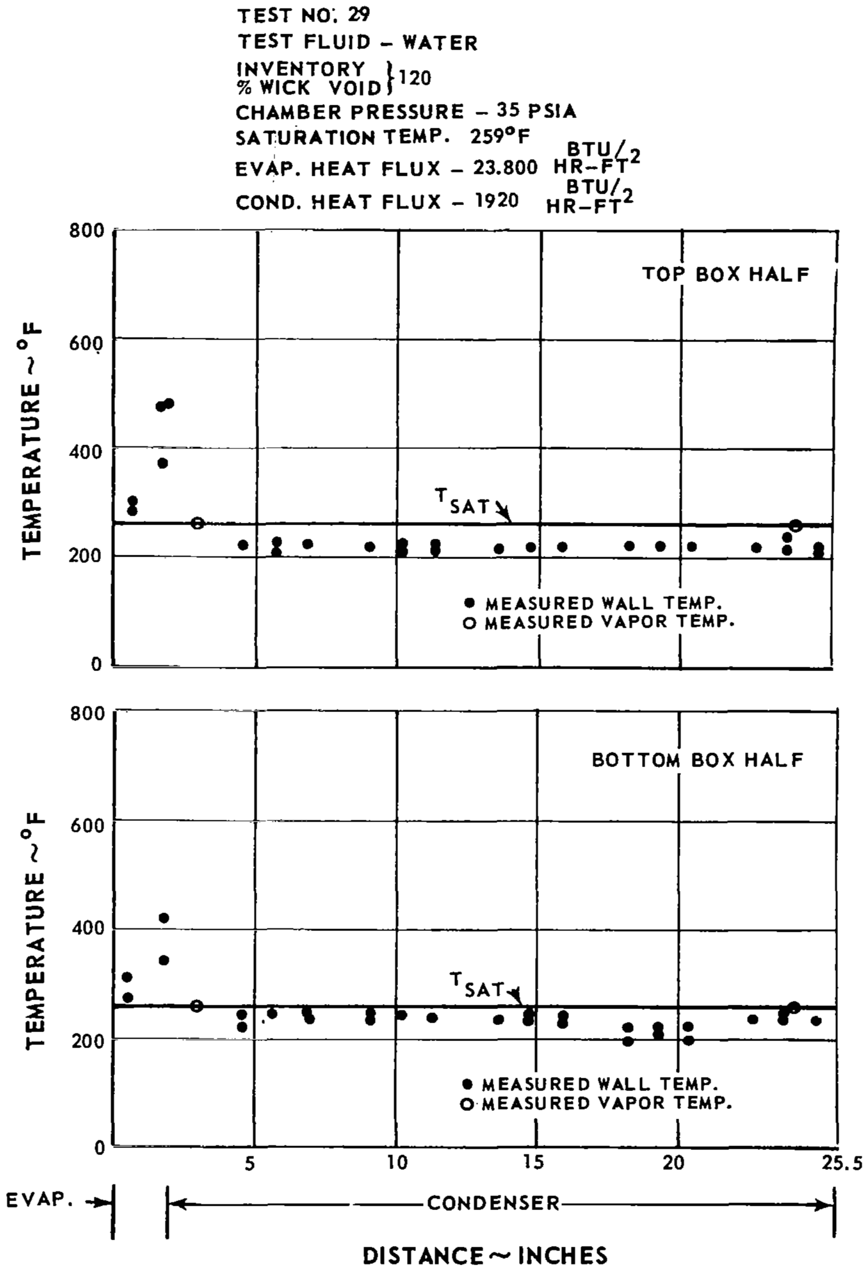

Figure 21 Typical Temperature Distribution for Box Fin with H13 Wick

the origin in the curves are generally lower than the other evaporator-region thermocouple readings due to conduction of heat to the flange of the box. The heater arrangement and evaporator thermocouple locations are shown in Figure 22.

A limiting heat flux occurred at a value of heat flux between those of Tests Nos. 26 and 27 in the bottom box half but not in the top box half. This is

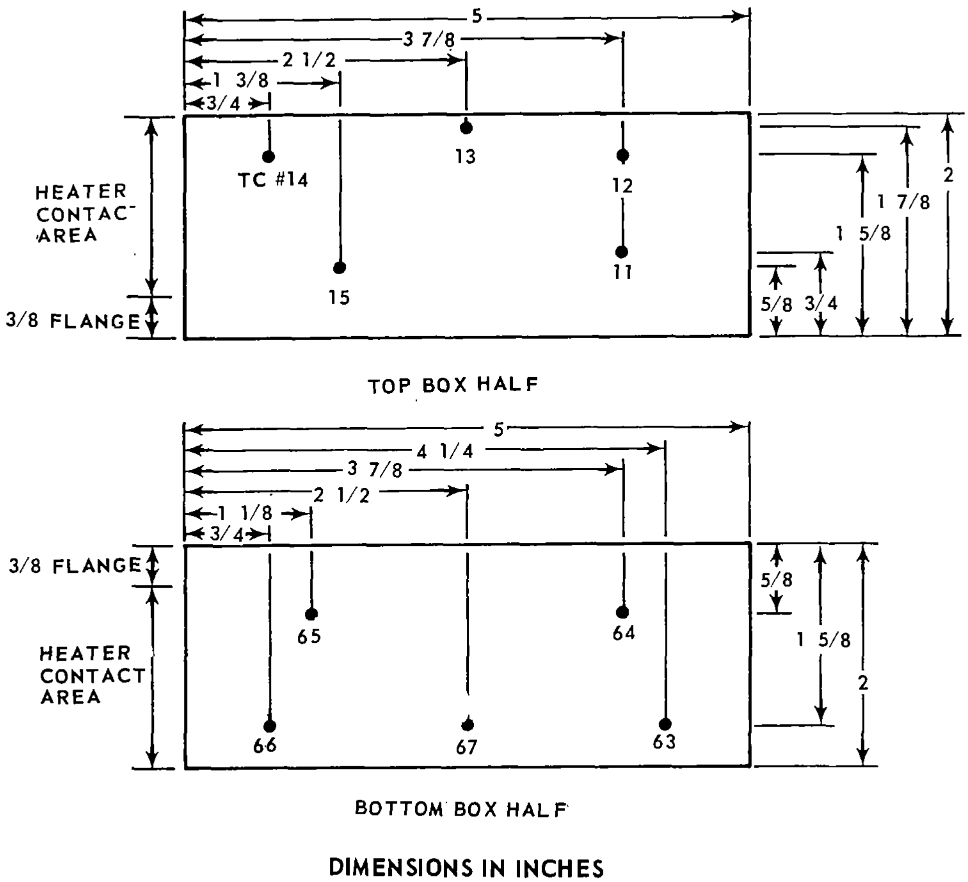

Figure 22 Thermocouple Locations on Box-Fin Evaporator

illustrated in Figure 23 which shows the variation of evaporator heat flux with wall superheat for the thermocouples in the evaporator section. The end of the bottom wick farthest from the condenser exhibits a sharp rise in temperature for a small change in heat flux, representative of drying out in the evaporator. In this series of tests, the sharp bend in the graph or the limiting heat flux was reached at an evaporator heat flux of between 27,000 and 29,900 Btu/hr ft^2, corrected for heat loss. The large variations between thermocouple temperatures is probably due to variations in contacts of either the heater or the wick to the evaporator wall in which the thermocouples are embedded.

In order to check repeatability and verify initial results, Tests Nos. 28-32 were made with all variables similar to those in Tests Nos. 21-27. A

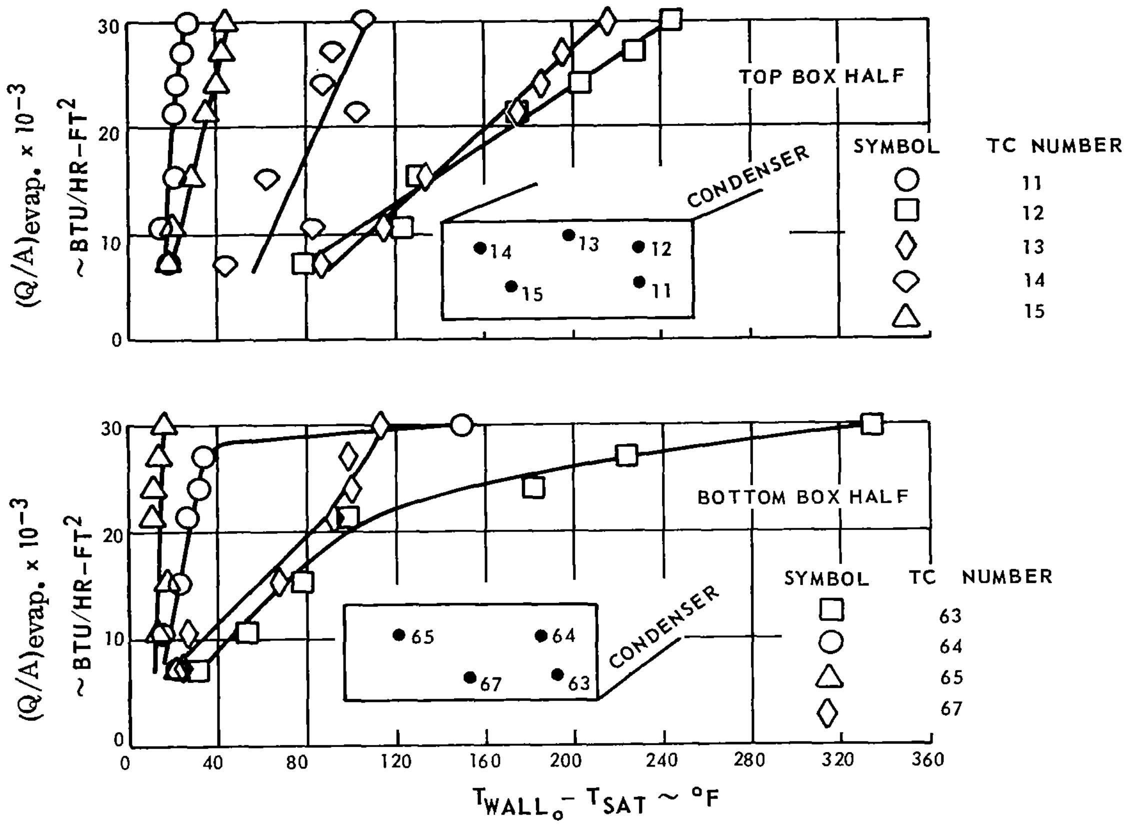

Figure 23 Evaporator Heat Flux vs ΔT_{sat} for Box Fin in Horizontal Position at 120% Inventory. Tests Nos.21 - 27

limiting heat flux occurred between 23,800 and 28,300 Btu/hr ft^2 for the lower box half and a limiting heat flux was not reached for the top box half as shown in Figure 24. This result tends to show good repeatability between tests. This repeatability is further corroborated by comparing the evaporator thermocouple measurements for the two test series.

In order to determine the effect of inventory, tests were made at 100 percent, 120 percent and 150 percent inventory (Tests Nos. 33-28). The results are

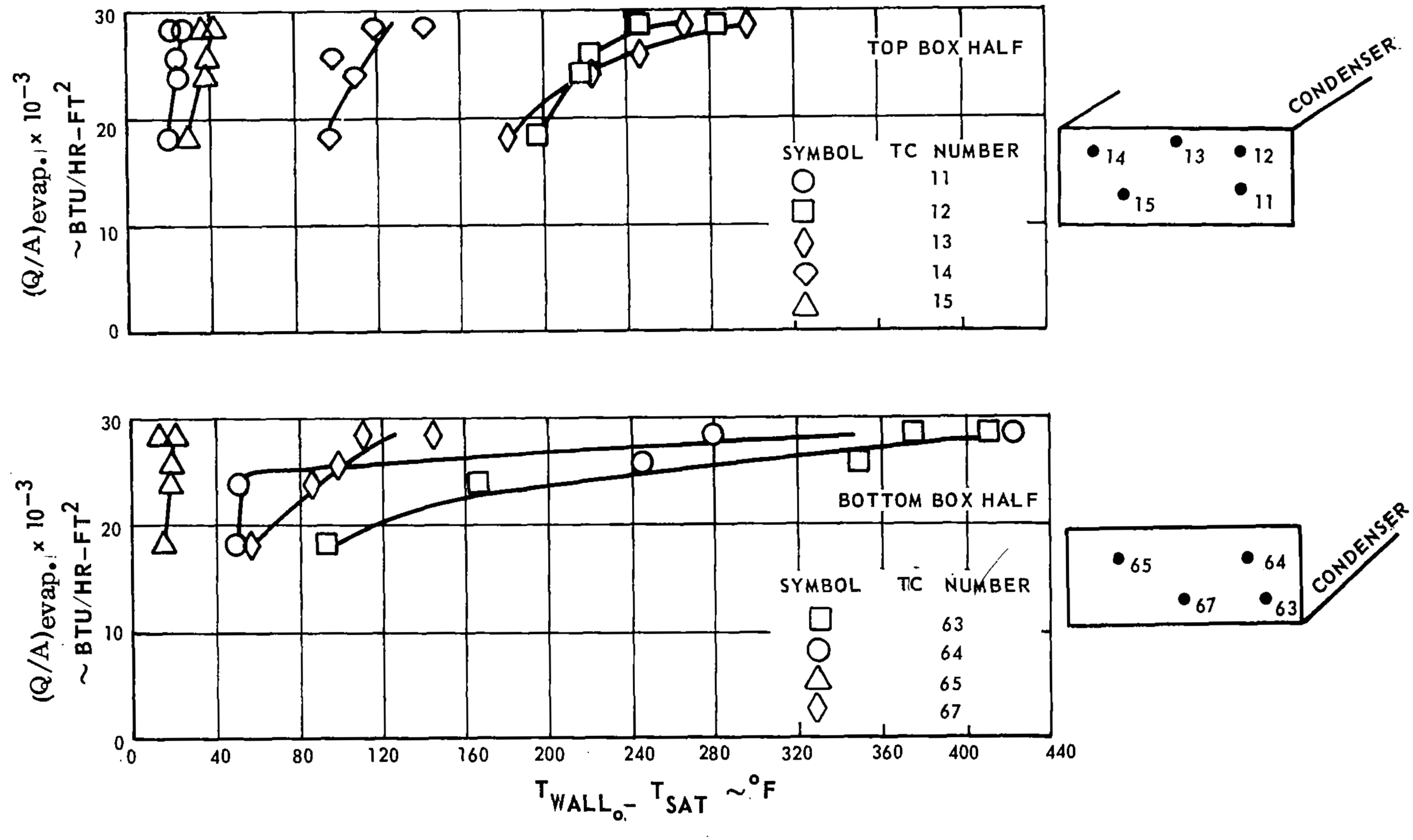

Figure 24 Evaporator Heat Flux vs ΔT_{sat} for Box Fin in Horizontal Position at 120% Inventory. Tests Nos. 28-32

shown in Figure 25, which is a graph of evaporator heat flux versus wall superheat for the evaporator thermocouples located farthest from the condenser for both the top and bottom box halves. A comparison of the curves indicates that limiting heat flux increased with increasing inventory. A summary of these limiting heat fluxes is presented in the table below:

		Limiting Heat Flux - Btu/hr ft^2	
Test No.	Inventory, %	Top Box Half	Bottom Box Half
33-36	100	23,000-25,000	18,000-20,000
37-39	120	>28,800	19,000-23,000
40-44	150	> 38,000	22,000-26,000

The following table summarizes the experimental values of limiting heat flux for the full box fin tests as well as the predicted values of limiting heat flux for the conditions of these tests.

Test No.	Inventory (% Wick Open Volume)	Measured Limiting Heat Flux, Btu/hr ft^2 Top Box Half	Measured Limiting Heat Flux, Btu/hr ft^2 Bottom Box Half	Predicted Limiting Heat Flux, Btu/hr ft^2 Top Box Half	Predicted Limiting Heat Flux, Btu/hr ft^2 Bottom Box Half
21-27	120	>29,900	27,000-29,900	$6.05x10^5$	$3.4x10^5$
28-32	120	>28,300	23,800-28,300	$6.05x10^5$	$3.4x10^5$
33-36	100	23,000-25,000	18,000-20,000	$6.05x10^5$	$3.4x10^5$
37-39	120	>28,800	19,000-23,000	$6.05x10^5$	$3.4x10^5$
40-44	150	>38,000	22,000-26,000	$6.05x10^5$	$3.4x10^5$

The predicted values of limiting heat flux are based on values of ℓ_m obtained from a test using the H13 planar wick and K_1 obtained in Tasks 1 and 2. In all cases a limiting heat flux was reached well below the predicted value. This result could be explained by the effective equilibrium wick rise height being less than the value used in the analysis, by the wick friction factor being higher, or by a combination of these effects. Also, the predicted value is based on an analysis which assumed the same model in the evaporator section as in the condenser section. This assumption requires that evaporation occur at the liquid-vapor interface at the surface of the wick rather than at nucleation

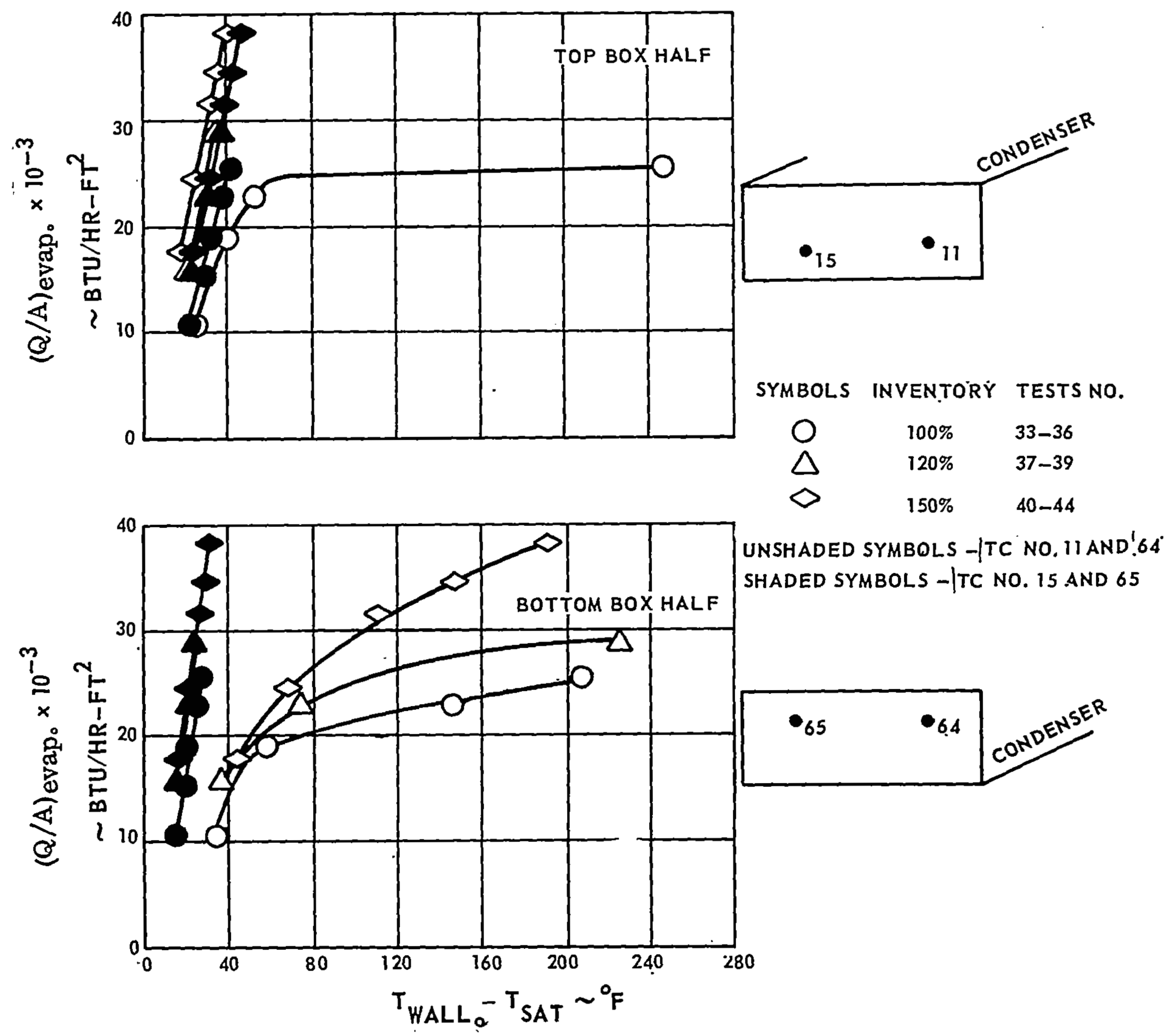

Figure 25 Evaporator Heat Flux vs ΔT_{sat} for Box Fin in Horizontal Position with Different Inventories

sites within the wick. Therefore, even if the correct effective values of equilibrium wick rise height and wick friction factor were used in the predictions, a limiting heat flux would be reached at a lower-than-predicted value due to a higher-than-estimated frictional pressure drop caused by partial blockage to liquid flow in the evaporator by water vapor. Later in this report other evidence is presented which indicates that the effective $_m$ is lower than that measured in Task 1 and that the wick friction factor in the evaporator section is influenced by boiling interaction.

Another factor of significance is that the model used in the analysis presented in the Topical Report on Tasks 1 and 2 does not consider the case of a liquid inventory greater than 100 percent. The data plainly shows that there is a definite effect of liquid inventory. However, the theory presented in Report NASA CR-812 does not account for the effects of inventory. With the liquid inventory greater than 100 percent the frictional pressure drop could be less than predicted in the analysis due to flow of the excess liquid on top of the wick in the horizontal sections.

In all of the preceding box-fin tests it was observed that cooling water in the top box half received more heat than that in the bottom box half. It appears that this difference was primarily due to a much higher thermal resistance on the coolant side for the bottom box half. Apparently trapped air in the cooling channels covered part of the wick backup plate for the bottom box half, even though an attempt was made to purge each channel of air by causing the maximum possible coolant flow through each cooling channel during the tests. Since the condenser heat flux was higher for the top half than the bottom half, the condensation rate was higher. The evaporator heat flux was identical for both box halves and therefore the evaporation rate was identical. Therefore, excess liquid that condensed on the top box half dripped or flowed to the bottom box half.

Tests Nos. 45-48 were run with nitrogen gas present in the chamber. The objective of this series was to determine the operating characteristics of a vapor-chamber fin with a noncondensable gas present in the chamber. In this test series the coolant flow and inlet temperature were held constant while the heat load was varied. Figure 26 shows a typical temperature distribution from one of the tests. This temperature distribution shows that the condenser section was essentially isothermal. In tests including a noncondensable gas performed by other investigators[1], as well as in earlier tests at Pratt & Whitney Aircraft,

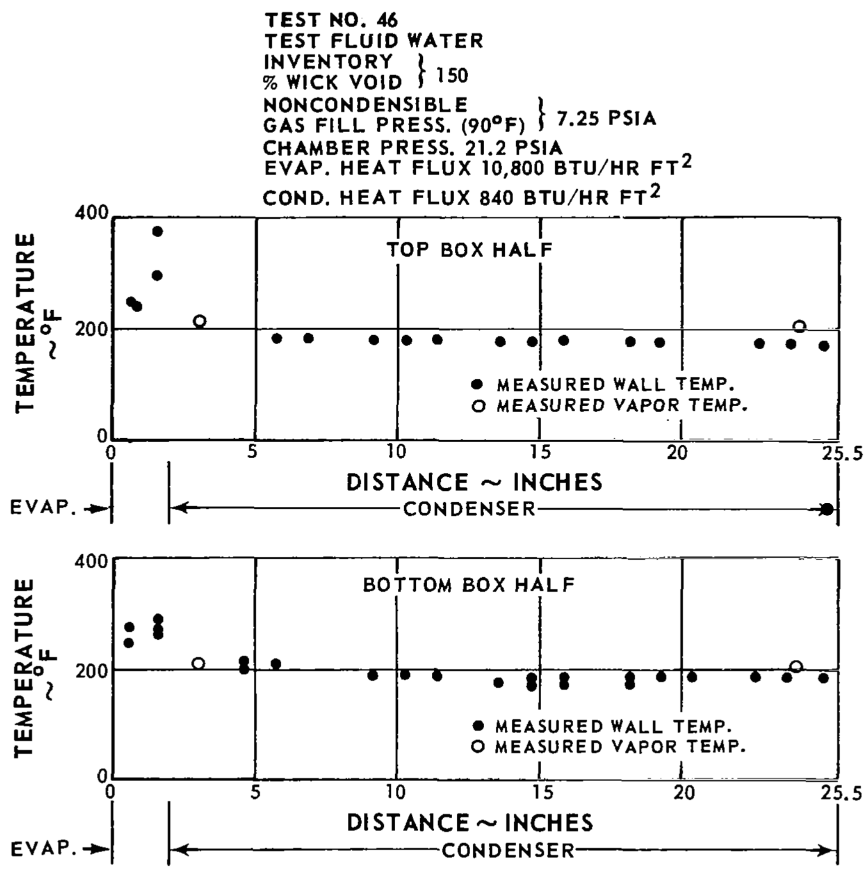

Figure 26 Typical Temperature Distribution for Box Fin with Noncondensable Gas

the condenser section temperature distribution showed two distinct regions (see sketch below), indicating that the working fluid vapor and the noncondensable gas did not mix.

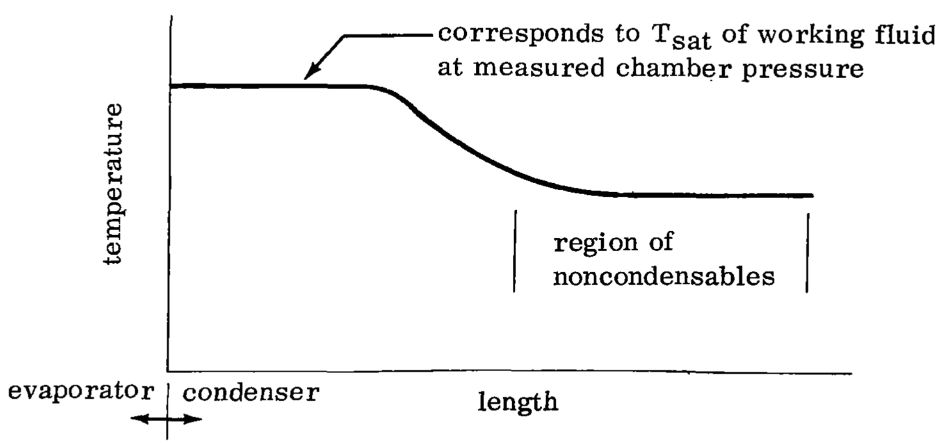

Since Tests Nos. 45 to 48 did not show this same type of temperature distribution, the vapor and the noncondensable gas probably mixed. Theorectical predictions of the variation of chamber pressure with heat load at constant coolant temperature for both complete mixing and no mixing were made. The derivation of the equations for these predictions is presented in Appendix 3. Figure 27 shows the theoretical lines for both cases at the conditions of the noncondensable gas test series. The measured data for this test series is also shown in this figure. As can be seen, the test data falls very near the theoretical line for the mixing case. It was therefore concluded that for the conditions tested mixing did occur.

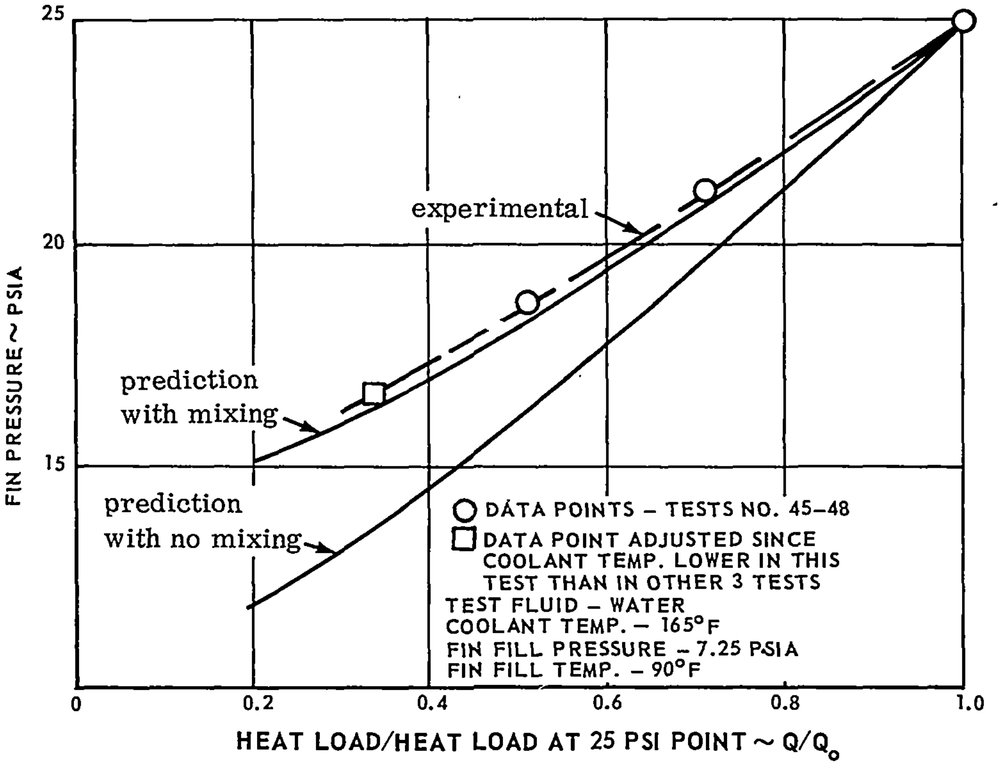

Figure 27 Predicted and Experimental Results of Tests with Noncondensable Gas Present

Natural convection and diffusion provide the impetus for mixing. Since diffusional effects are small, the mixing zone would be small and the two fluids would stay essentially unmixed if free convection were eliminated. The main factors which aid natural convection are large differences in molecular weight of the two fluids, large passage cross-sectional area, and large temperature gradients. The test conditions of this study which contributed to mixing were the large cross-sectional area of the full box and the relatively large

Since Tests Nos. 45 to 48 did not show this same type of temperatur
the vapor and the noncondensable gas probably mixed. Theorectical
of the variation of chamber pressure with heat load at constant coola
for both complete mixing and no mixing were made. The derivation
equations for these predictions is presented in Appendix 3. Figure
the theoretical lines for both cases at the conditions of the noncondei
test series. The measured data for this test series is also shown ir
figure. As can be seen, the test data falls very near the theoretical
the mixing case. It was therefore concluded that for the conditions t
mixing did occur.

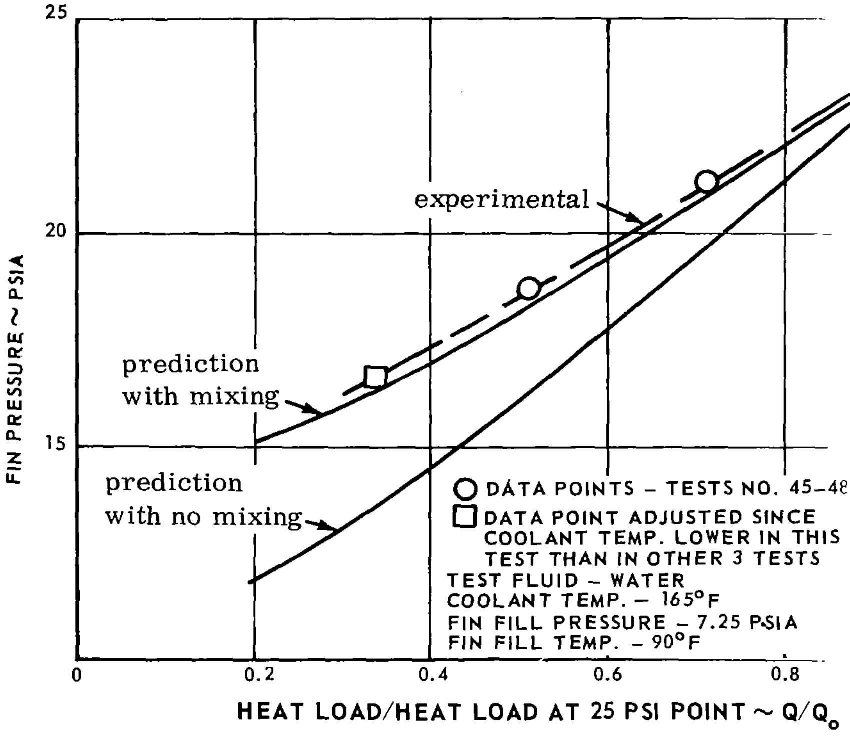

Figure 27 Predicted and Experimental Results of Tests with Nonco
Gas Present

Natural convection and diffusion provide the impetus for mixing. Si
diffusional effects are small, the mixing zone would be small and tl
fluids would stay essentially unmixed if free convection were elimii
main factors which aid natural convection are large differences in i
weight of the two fluids, large passage cross-sectional area, and la
ature gradients. The test conditions of this study which contribute
were the large cross-sectional area of the full box and the relativel

difference in the molecular weights of the two fluids; namely 28 for the nitrogen and 18 for the water.

2. Bottom Box-Half Fin Tests

a. Original Bottom Box Tested with Wick Below Chamber

As shown in Table 2, Tests Nos. 49-100 were made to determine the effect of inventory on performance, the variation of limiting heat flux with both condensing length and fin orientation. The effect of inventory is shown in the table below where the average wall superheats for the two upper thermocouples and the average for the two lower thermocouples in the evaporator section and evaporator heat flux for Tests Nos. 50, 51, and 54 are presented. A comparison of these values shows that a much higher degree of wall superheat is required as the inventory is reduced from 150 percent to 120 percent to 100 percent. Thus, fin performance progressively increases as inventory increases from 100 percent to 150 percent.

Test No.	Inventory (% Wick Void)	Evaporator Heat Flux, Btu/hr ft^2	$(T_{wall_o} - T_{sat})$ Thermocouple Location Measured from Condenser, inches: 3/8	1-3/8
50	100	2810	122	89
51	120	3900	86	39
54	150	10700	46	32

A graph of evaporator heat flux versus degree of wall superheat for Tests Nos. 53-63 is shown in Figure 28. This curve indicates that a limiting heat flux occurred at an evaporator heat flux of between 46,700 and 50,800 Btu/hr ft^2. This capillary failure point is considerably higher than any of those observed in the bottom box half for the full box at the same zero degrees angle of inclination (see table on page 45). It should be noted that the effective percentage inventory for the bottom half in a full box case is greater than the designated percentage inventory since the top half cannot hold excess inventory. Thus for a 120 percent inventory case in a full box test, the bottom box half has an effective inventory of 140 percent or greater. The limiting heat flux for the bottom half of the full box at 120 percent inventory was about half that of the same box half when run separately at 150 percent inventory. The limited data available on critical heat flux for the two cases prevents further analysis of the differences.

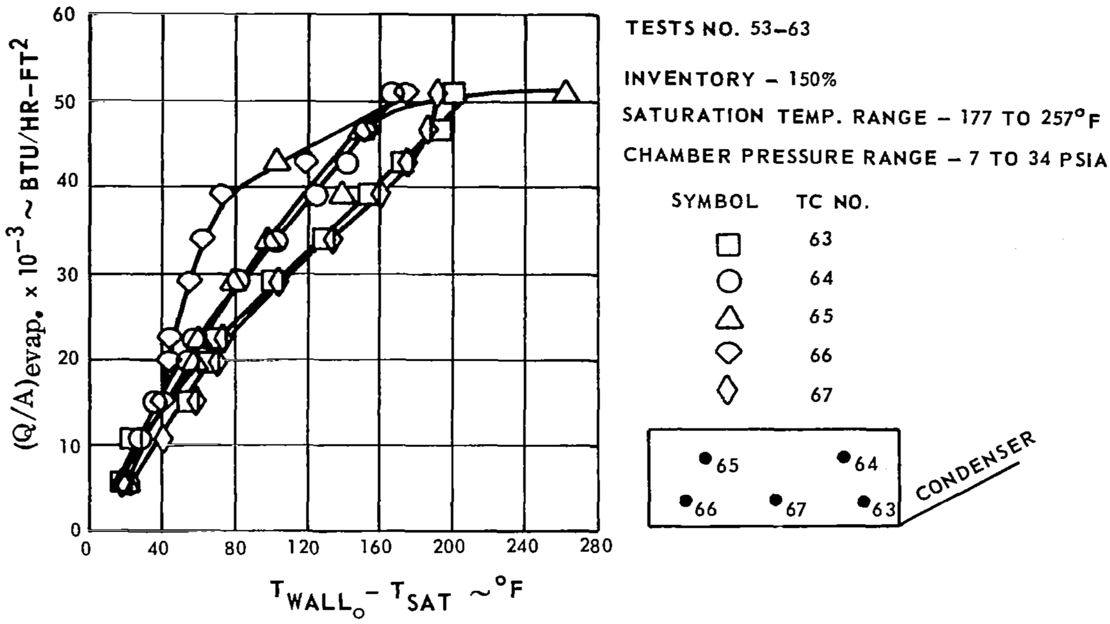

Figure 28 Evaporator Heat Flux vs ΔT_{sat} for Bottom Box Half in Horizontal Position. Test Fluid Water

b. Original Top Box Half Tested with Wick Below Chamber

In the series of tests on this configuration, Tests Nos. 101-131 (with the exception of Tests 117-121), the method of testing was somewhat different from that of all other tests. For this configuration the heat flux was set at various constant levels and the angle of inclination of the wick varied with the evaporator section of the wick elevated with respect to the condenser section. Thus for angles greater than zero, the excess inventory could not flow by gravity towards the evaporator region as might have occurred in the planar fin in the horizontal orientation, but would collect at the end opposite the evaporator. Thus all liquid would have to flow into the evaporator because of capillary forces. Tests Nos. 117-121 were conducted by the usual method of varying heat flux for a specific angle, in this case, zero degrees to horizontal. No limiting heat flux was observed in this zero-angle series as can be seen in Figure 29. For all other test series, plots of angle of inclination versus wall superheat (ΔT_{sat}) for each thermocouple in the evaporator section indicated between which angles ΔT_{sat} increased abruptly for the specific heat flux. The abrupt change in ΔT_{sat} at the high end of the evaporator section was considered to be due to insufficient capillary pumping and is termed a capillary failure.

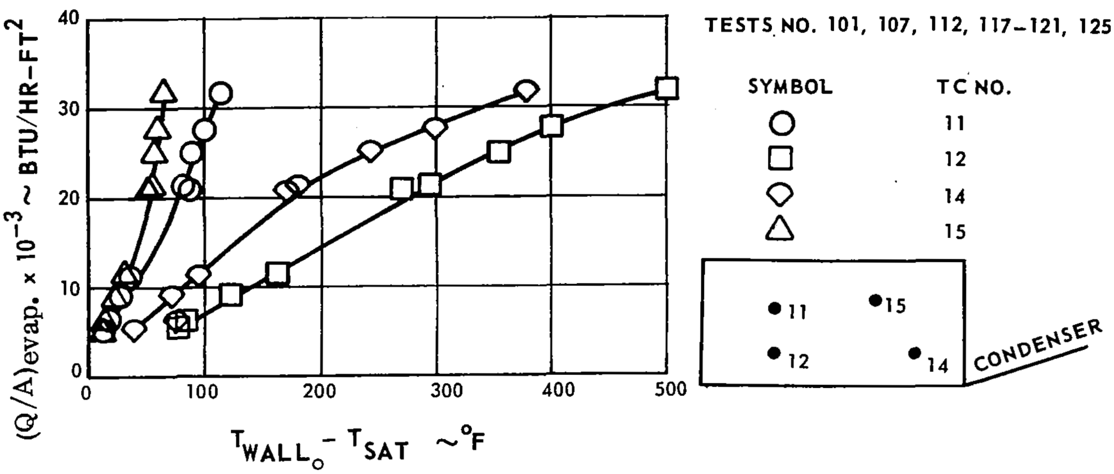

Figure 29 Evaporator Heat Flux vs ΔT_{sat} for Half-Box Tests in Horizontal Position at 150% Inventory

The table below indicates the figure numbers for the graphs of the angle of inclination versus ΔT_{sat}, the nominal heat flux level, the range of angle where capillary failure occurred and the predicted failure angle for each of the test series.

Nominal Heat Flux	Test No.	Test Failure Angle, Degrees	Predicted Failure Angle, Degrees	Figure No.
4,640	101-106	2 1/2 - 3 3/4	7.4	30
5,900	107-111	2 1/2 - 3 3/4	7.3	31
11,200	112-116	1 1/4 - 2 1/2	7.2	32
31,300	121-124	>1 1/2	6.6	33
8,950	125-131	3 - 4	7.3	34

It should be noted that in Tests Nos. 125-131 the observed failure angle was near those of Tests Nos. 107-111 and 112-116 which indicated that wick properties did not change significantly with time.

The above table indicates that the predicted angle of inclination where capillary failure should occur was considerably higher than the experimentally observed

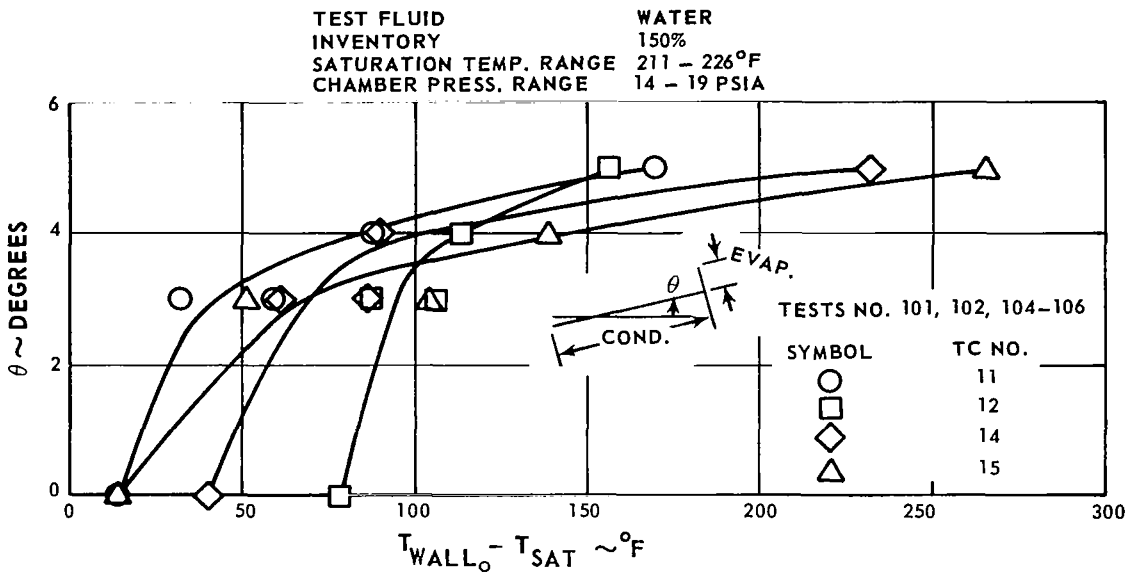

Figure 30 Angle of Inclination vs ΔT_{sat} for Half-Box Tests. Nominal Evaporator Heat Flux 4, 640 Btu/hr ft^2

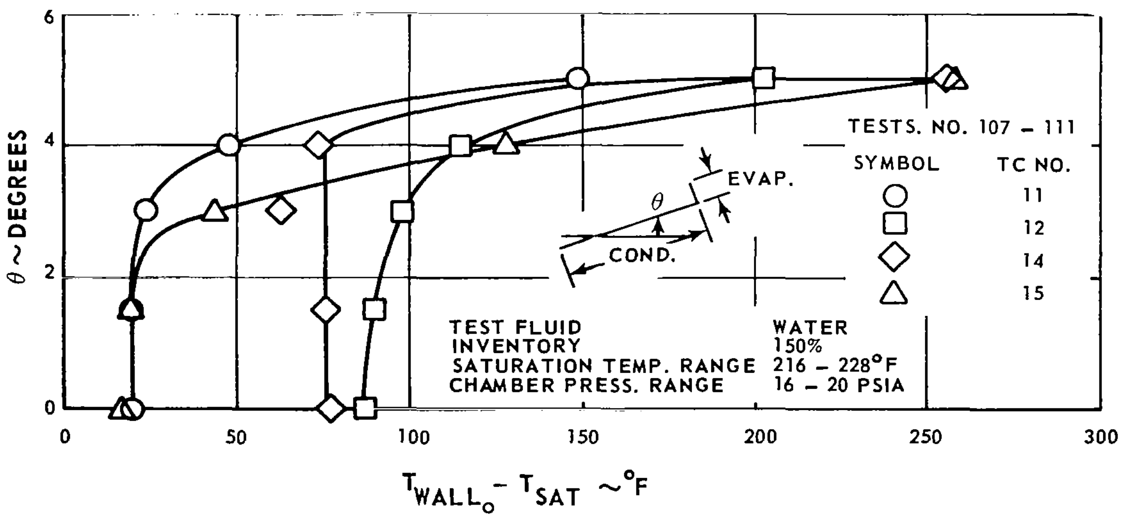

Figure 31 Angle of Inclination vs ΔT_{sat} for Half-Box Tests. Nominal Evaporator Heat Flux 5, 900 Btu/hr ft^2

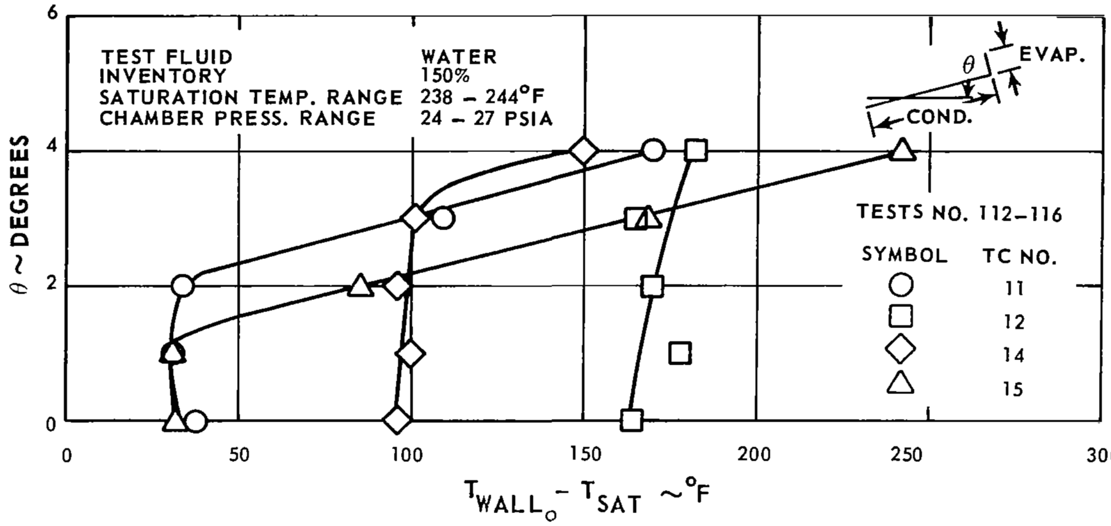

Figure 32 Angle of Inclination vs ΔT_{sat} for Half-Box Tests. Nominal Evaporator Heat Flux 11,200 Btu/hr ft^2

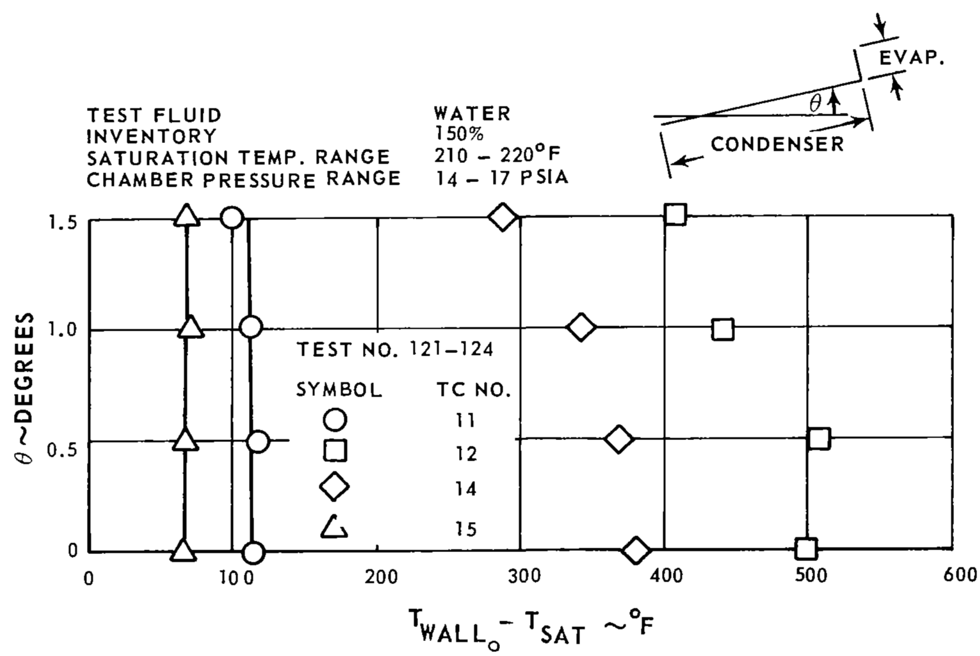

Figure 33 Angle of Inclination vs ΔT_{sat} for Half-Box Tests. Nominal Evaporator Heat Flux 31,300 Btu/hr ft^2

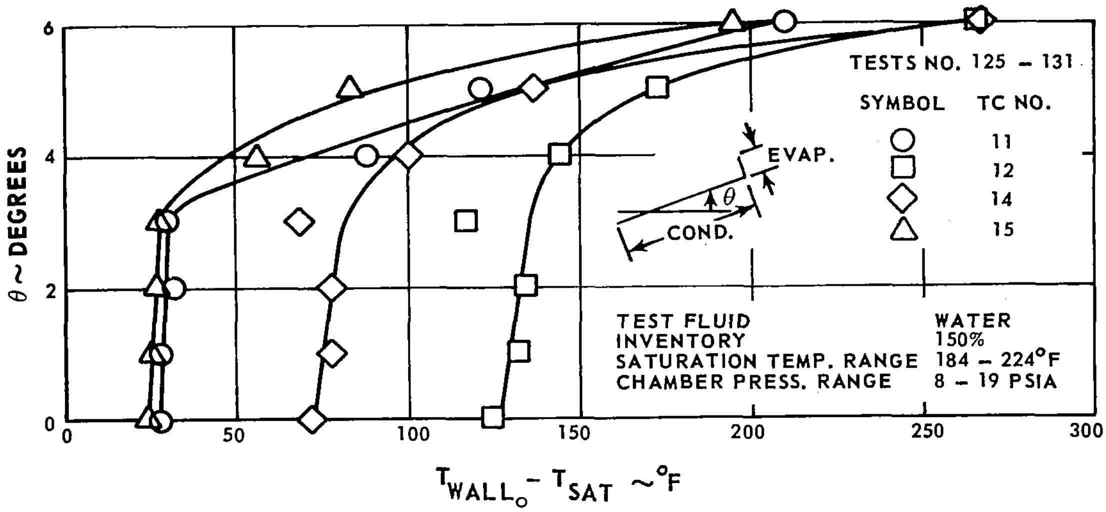

Figure 34 Angle of Inclination vs ΔT_{sat} for Half-Box Tests. Nominal Evaporator Heat Flux 8,950 Btu/hr ft^2

capillary failure angles. One hypothesis that can resolve this discrepancy is that the effective ℓ_m is less than the value used in the prediction. Figure 35 shows the measured range of values of capillary failure angle versus evaporator heat flux, together with the predicted quantities based on the values of ℓ_m and K_1 measured in Task 1. Also shown in this figure is a predicted curve based on a value of ℓ_m(4.0 inches) selected so that the prediction agrees favorably with the experimental observations at the lower heat flux levels. The limiting heat flux obtained with the other box half at zero degrees inclination is also indicated in this figure. At the higher heat flux levels the lower predicted curve does not agree with the data. One possible explanation is that boiling interaction becomes more prevalent as the heat flux is increased. This results in an increased resistance to liquid flow through the evaporator section and thus effectively reduces the limiting heat flux.

A value of ℓ_m equal to 4.0 inches instead of the 6.3 inches determined by wicking rise test in Task 1 may be reasonable, since the latter value is dependent on the wicking ability of only the smaller pores. The pressure drop would be excessive in a wick if only the smaller pores were effective. Therefore, it seems reasonable that the effective value of ℓ_m would be less in an operating heat pipe than that obtained from a wicking rise test.

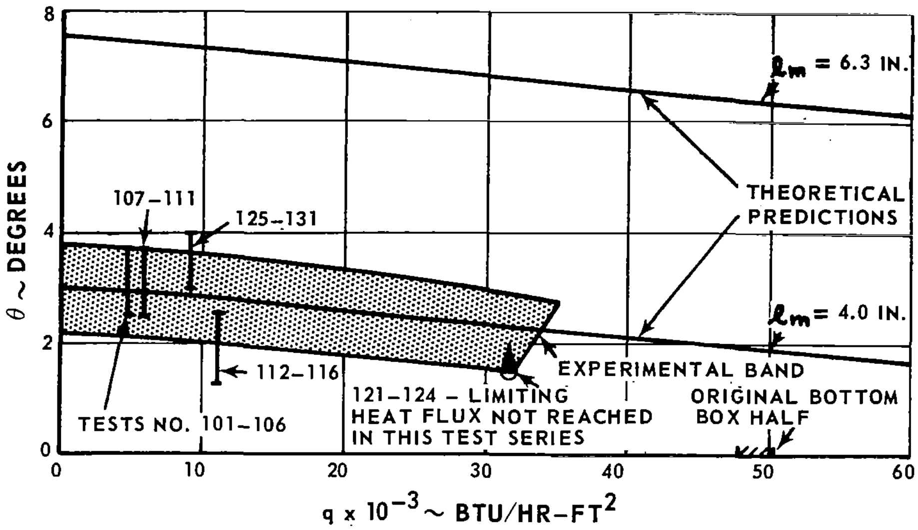

Figure 35 Fin Failure Angle vs Evaporator Heat Flux for Top Box Half

Figure 36 shows typical temperature distributions along the fin wall at angles of inclination of zero and 4 degrees for this configuration. In the 4-degree case the limiting heat flux was reached. The highest thermocouples in the evaporator section reflect having reached this limit by the dramatic increase in temperature shown between the zero and 4-degree cases.

3. <u>Evaporative Heat Transfer Characteristics of Box Fin</u>

Figure 37 shows curves of evaporator heat flux versus ΔT_{sat} for both halves when run separately and for the whole box. In all cases the wick was H13, a sintered stainless-steel fiber material, and the wicking fluid was water. In all of the tests the water inventory was 150 percent of the total wick void volume. This constant percentage inventory assures, for the cases of the two separate box-half tests and for the bottom box half in the full-box test, that the base of the evaporator section was situated in a pool of liquid.

A comparison between the two curves for the full-box tests indicates that the top wick ran cooler than the bottom wick at all heat flux levels. This was as expected since gravity aids the top wick performance and retards the bottom wick performance.

Both of the two halves when run separately with the wick located below the vapor chamber produced similar results. These results do not differ very much from the performance of the bottom box half when run in the full box

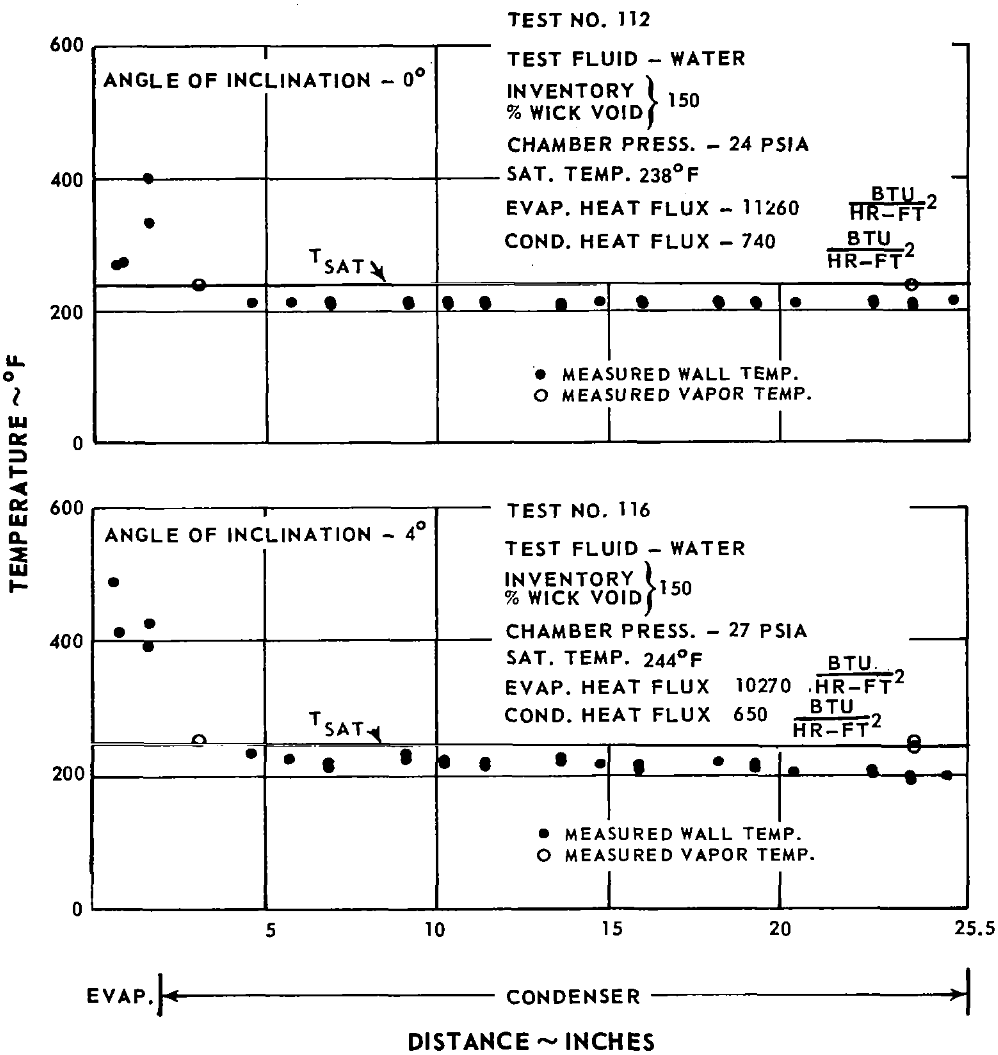

Figure 36 Typical Temperature Distributions for Half-Box Test at Two Angles of Inclination. Original Top Box Half

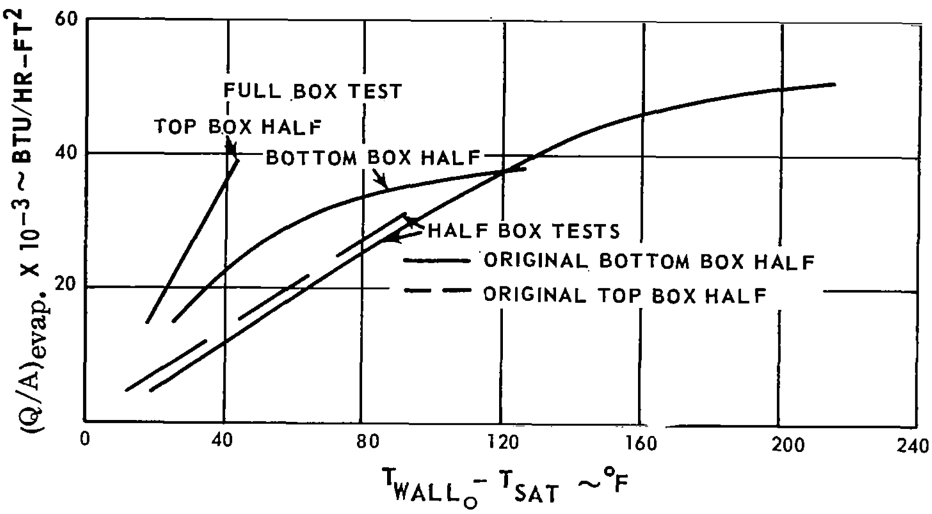

Figure 37 Evaporative Heat Transfer Characteristics of H13 Wick in Box Fin

configuration. The slightly better performance for the full box might be attributed to liquid flowing off the top wick which would allow the bottom wick to run cooler than if no wick were above it.

4. Condensing Heat Transfer Characteristics of Box Fin

The heat transfer conductance in the condenser section was calculated using the data of several test series for both full and box half tests and compared to analytically predicted values. One of the objectives was to determine the equivalent thermal conductivity of the porous metal wick filled with liquid. Two cases, one in which the metal and liquid conduct heat in parallel and the other in which these two conduct heat in series, were used to calculate the conductance. These two calculated values have been shown to result in the upper and lower limits of the effective wick thermal conductivity[7]. The methods of determining these limits are discussed in more detail in the referenced paper. Another objective was to determine if the convective heat transfer coefficient of the condensing vapor was high enough to offer negligible resistance to heat transfer. In order to accomplish the above objectives, calculations of the overall conductance between the backup plate-wick interface and the condensing vapor were compared to those experimentally determined.

a. Full Box Tests

Predicted and experimentally determined values of condenser conductance for the full box tests analyzed are presented in the table below.

		Condenser Heat Flux, Btu/hr ft^2		Condenser Heat Transfer Conductance, Btu/hr ft^2 °F					
				Experimental		Predicted			
Test No.	Fill Inventory, % Wick Void Vol. at 75°F	Top Half	Bottom Half	Top Half	Bottom Half	Top Half Series	Top Half Parallel	Bottom Half Series	Bottom Half Parallel
40	150	4450	890	276	53	57.1	240	25.6	38.9
42	↓	3920	855	301	57	↓	↓	↓	↓
43	↓	4280	990	229	49	↓	↓	↓	↓
44	↓	5170	1010	220	42	↓	↓	↓	↓

As can be seen from this table, the experimentally-determined values of conductance for both box halves are closer to the values predicted for the parallel conductance case of the wick-liquid composite than for the series conductance case. This is especially evident when the values for the top box half are compared. In some cases the experimental value of conductance exceeds the predicted upper limit (i.e. parallel case). This result is possibly due to the inaccuracies in determining the experimental heat loads for the two halves.

In order to obtain the experimental values of the overall heat conductance in the condenser region, the heat loads of each box half were required. To obtain these, the values of enthalpy rise of the coolant streams for each box half were used. Since the temperature differences between inlet and outlet of the coolant streams of the top and bottom halves were only 14°F and 3°F, respectively, and the possible error in this difference is about ±3°F, the results are questionable. However, a heat balance showed that the coolant enthalpy rise and electrical heat input minus estimated heat losses were approximately equal. The overall experimental heat conductance was determined by the following equation:

$$U_c = \frac{Q_c/A_c}{T_{sat} - T_{wls}} \qquad (8)$$

and

$$T_{wls} = \bar{T}_{measured} - \frac{Q_c/A_c}{k/t} \qquad (9)$$

where

U_c = condenser conductance

Q_c = condenser heat load

A_c = condenser area

T_{sat} = fluid saturation temperature

T_{wls} = wick-liquid-solid interface temperature

$\overline{T}_{measured}$ = average measured fin wall temperature

k = fin wall thermal conductivity

t = fin wall thickness

In calculating the theoretical values of overall conductance, the top wick was assumed to be 100 percent saturated and all excess inventory was assumed to be on the top of the bottom wick. Thus, the bottom half had the additional resistance of the free liquid in series with the wick-liquid composite resistance. Effects of liquid expansion due to temperature were included in determining the thickness of the free liquid above the bottom wick. The convective heat transfer coefficient of the vapor was always considered to be infinite.

Although the comparisons presented above were based on only estimated values, the effective thermal conductivity of the wick-liquid composite was concluded to be closer to the parallel-conductance case than the series-conductance case. Also, in the tests used in the comparison, the convective heat transfer resistance of the condensing vapor probably could be considered low relative to the other resistances.

b. Half Box Tests

The heat transferred in the condenser section in the box half tests was determined by subtracting an estimated heat loss based on measured temperatures from the heat input. Probable errors in thermocouple measurements ruled out using the heat transferred to the coolant since the average coolant temperature rise was only 4 to 5°F. Also, heat balances were poor in the tests used for comparison. Since the heat losses were estimated to vary between 15 and 44 percent, the calculated values of heat transfer conductance are only approximate. The condenser conductance was calculated using a procedure similar to that for the full box tests. However, for the cases in which the fin was inclined, the variation of the thickness of the free liquid layer above the wick with length was taken into account.

Tests in the series numbered 56 to 63 were selected for determining the bottom box half condenser conductance, since after this series the fin performance showed a marked deterioration. Tests Nos. 121 to 124 provided data for analysis of the box half that was the top in the full box tests since the predicted heat loss was lowest for this test series. Also, Tests Nos. 112 to 115 on the latter configuration were used to provide additional information.

Predicted and experimental values of condenser conductance for the box half tests analyzed are presented in the table below.

Test No.	Fill Inventory, % Wick Void Vol. at 75°F	Fin Angle, Deg-Measured From Horizontal	Condenser Heat Flux, Btu/hr ft^2	Condenser Heat Transfer Conductance, Btu/hr-ft^2 -°F		
				Experimental	Predicted Series	Predicted Parallel
56	150	0	1480	60	35.6	67.6
60			3090	49		
61			3420	96		
62			3750	92		
112		0	739	35	35.6	68
113		1	723	30	43.0	149
114		2	730	33	45.7	172
115		3	715	36	47.0	182
121		0	2490	24	35.8	69.4
122		1/2	2550	26	40.6	126
123		1	2500	27	43.2	152
124		1 1/2	2470	29	44.6	177

The experimental values of overall conductance for Tests Nos. 56, 60-62 are either close to or greater than the parallel wick-liquid conductance case which confirms the results of the full box tests. However, in the other tests, the experimental value is even lower than the series-conductance case (i.e. the lower limit). One possible explanation of this discrepancy in the latter tests is that noncondensable gases may have been present to a sufficient extent to cause a significant additional heat transfer resistance. A comparison of the pressure gauge readings and the saturation pressure corresponding to the measured vapor temperature at the condenser end indicates that considerably more noncondensable gases might have been present in Tests Nos. 112-115 and 121-124 than in Tests Nos. 56, 60-62 on the previously discussed full box tests. The presence of noncondensable gases would be indicated when the pressure gage registered a higher pressure than indicated by the saturation pressure corresponding to the measured vapor temperature. The convective heat transfer coefficient of the condensing vapor would be lower when noncondensable gas is present since the condensable vapor must diffuse through the noncondensable gas to reach the liquid-vapor interface and condense.

The results presented above for both the full box and half box tests indicate that the effective thermal conductivity of the wick-liquid composite is close to the value predicted when the wick and liquid conduct heat in parallel. The resistance due to convection of the condensing vapors is negligible except when noncondensable gases are present in sufficient quantity. Noncondensable gases can cause a significant reduction in the overall conductance, particularly when much mixing of noncondensable gas and condensable vapor occurs, as was found in the present study.

VI. CONCLUDING REMARKS

The principal results obtained under this investigation are presented below:

A comparison was made between the experimental limiting heat fluxes obtained in both the planar and the box vapor-chamber fin geometries with limiting heat fluxes predicted by a theory based on capillary pumping. The one limiting heat flux obtained in the planar configuration agreed favorably with the theory. The comparison of the data from the box configuration and the theory showed that at evaporator heat fluxes less than about 32,000 Btu/hr ft^2, the experimental limiting heat fluxes fell below the predicted fluxes, but the trend of the data was similar. By assuming a minimum effective pore radius for capillary pumping 56 percent larger than the value determined from a wicking rise test, an empirical modification of the theory was obtained which agreed with the data in both magnitude and trend. This required modification suggests that the method of obtaining minimum effective pore radii from wicking rise tests needs refinement. The limiting heat flux data at evaporator fluxes above 32,000 Btu/hr ft^2 were lower than the values of the flux predicted by the empirically modified theory. An interaction between the boiling and capillary pumping processes may have occurred which increased the frictional resistance to liquid flow and reduced the maximum evaporative heat flux. The data for the box geometry showed a definite effect of fluid inventory on limiting evaporative heat flux. Increased fluid inventory, in excess of the wick void volume, resulted in increased limiting evaporative heat fluxes. The capillary pumping theory did not account for this effect of inventory.

An evaluation of the overall condenser heat transfer coefficients in the box configuration indicated that, in some cases, an additional significant resistance to heat flow was present besides those attributable to the wall, wick, and liquid resistance. Estimates were made which showed that this additional resistance could have been due to noncondensable gases known to be present. In tests where a noncondensable gas (nitrogen) was intentionally introduced into the vapor chamber, the temperature profile indicated that the inert gas mixed with the steam. The mixing of the noncondensables and the water vapor was likely caused by natural circulation within the chamber and was enhanced by the relatively large cross-sectional area of the box geometry and by the difference in molecular weights of the inert gas and the steam. However, in zero gravity, mixing could occur only by molecular diffusion and would not be as great.

An analysis of overall condenser heat transfer coefficients indicated that the effective thermal conductivity of the wick-liquid composite was best approximated by assuming parallel conduction of heat through the metallic wick and through the liquid contained within the wick. This observation is limited, however, to the particular wick-liquid combinations of this investigation and could change with different wick porosity and structure, and with different thermal conductivities of the wick and liquid.

A major problem encountered in these experiments was the failure of the bond between the wick and its backup plate in the evaporator section. This failure resulted in extremely high thermal resistances which could be detrimental to the performance of any component employing vapor-chamber fins. However, in the case of vapor-chamber fins using working fluids with high liquid thermal conductivity, such as the liquid metals, good bonding of the wick to the backup plate may not be essential.

In view of the above remarks, the designer of a vapor-chamber fin radiator should include:

1. Use of excess inventory
2. Conservative estimate of minimum effective pore radius from wicking rise test.
3. Boiling interaction considerations in the estimation of the limiting pumping capability of the wick.
4. Adequate contact between wick and wall.
5. Evaluation of the condensing heat transfer coefficient with noncondensable gas present.
6. Use of a minimum vapor cross-sectional area where noncondensable gases are present in order to minimize mixing between the gas and vapor.
7. Use a noncondensable gas with a molecular weight near that of the vapor, to minimize mixing in cases when a noncondensable gas is desired.

REFERENCES

1. Grover, G. M., T. P. Cotter, and G. F. Erickson, Structures of Very High Thermal Conductance, J. Appl. Phys., Vol. 35, No. 6, p. 1990, June 1964

2. Deverall, J. E., and J. E. Kemme, High Thermal Conductance Devices Utilizing the Boiling of Lithium or Silver, Report No. LA-3211, Los Alamos Scientific Laboratory, Los Alamos, New Mexico, April 9, 1965

3. Deverall, J. E. and J. E. Kemme, Satellite Heat Pipe, Report No LA-3278-MS, Los Alamos Scientific Laboratory, Los Alamos, New Mexico, April 20, 1965

4. Haller, H. C., S. Lieblein, and B. G. Lindow, Analysis and Evaluation of a Vapor-Chamber Fin-Tube Radiator for High-Power Rankine Cycles, NASA TN D-2836, NASA Lewis Research Center, Cleveland, Ohio, June 1964

5. Kunz, H. R., L. S. Langston, B. H. Hilton, S. S. Wyde, and G. H. Nashick, Vapor-Chamber Fin Studies - Transport Properties and Boiling Characteristics of Wicks, NASA CR-812, June 1967

6. Advances in Energy-Conversion Engineering, Critiques, and Summaries of Papers at Intersociety Energy-Conversion Engineering Conference, American Society of Mechanical Engineers, pp 168-172, August 1967

7. Gorring, R. L. and S. W. Churchill, Thermal Conductivity of Heterogeneous Materials, Chemical Engineering Progress, Vol. 57, No. 7, pp 53-59, July 1961

APPENDIX 1

Nomenclature

A_s	condenser area
g	local acceleration
g_o	proportionality constant in Newton's second law
H	fin height
h_{VL}	latent heat of vaporization
K_1	wick friction factor
ℓ_m	maximum height to which a liquid will rise in a vertical wick sample
L_c	consenser length of box fin model
L_{fill}	length of box fin occupied by noncondensable gas at fill conditions
L_{nc}	length of the condenser section of box fin model occupied by noncondensable gas assuming no mixing of noncondensable and condensable
L_t	length of condensable section plus length of noncondensable section in box fin assuming no mixing of noncondensable and condensable
M_{nc}	mass of noncondensable gas
P_{fill}	pressure to which an evacuated fin is filled with noncondensable gas
P_{fin}	fin pressure
P_{nc}	pressure of noncondensable gas
Q	heat flow rate
Q_o	heat flow rate at some reference condition
Q/A cond. max.	maximum condenser heat rejection rate per unit area due to capillary pump limitation
Q/A evap. max.	maximum evaporator heat rejection rate per unit area due to capillary pump limitation
R_{nc}	gas constant of noncondensable gas
$T_{coolant}$	fin coolant temperature
T_{fill}	temperature of noncondenable gas in fin at fill conditions
T_{nc}	noncondensable gas temperature
T_{sat}	saturation temperature of fin fluid
T_{wi}	calculated temperature of backup plate surface adjacent to wick
$Twall_o$	measured wall temperature - thermocouple location about 50 mils from liquid - wick - solid interface
U	thermal conductance between vapor in fin and coolant
V	fin vapor chamber volume
W	condenser width
x_A	length of adiabatic section of vapor-chamber fin
x_C	length of condenser section of vapor-chamber fin
x_E	length of evaporator section of vapor-chamber fin

Nomenclature

x_T	total length of condenser, evaporator and adiabatic section of vapor-chamber fin
x_{Rmin}	distance from condenser-evaporator junction to point in evaporator where radius of curvature of liquid-vapor interface is a minimum

Greek Letter Symbols

ΔT_{sat}	difference between fluid saturation temperature and measured wall temperature
δ	liquid-wick thickness
θ	angle fin makes with horizontal, positive when evaporator section is at elevated end and negative when evaporator section is at lower end
μ	absolute viscosity
ρ	mass density
σ	liquid-vapor surface tension

Subscripts

1	indicating Condition 1
2	indicating Condition 2
L	liquid
WR	pertaining to conditions of wicking rise tests

APPENDIX 2

Tables

TABLE 2

TEST PROGRAM

Test No.	Fin Model	Test Fluid	Fluid Inventory (% Wick Void Volume)	Angle of Inclination deg.	Non-Cond. Fill Press., psia	Active Condenser Length Inches	Evaporator Length Inches	***Nominal Heat Flux (Btu/Hr ft^2) Evaporator	Condenser	Fluid Saturation Temp., °F	Fin Press., psia	Test Objective and Comments
1	Planar - H6	Distilled Water	100	0	0	11.6	6.2	12400	5850	282	51	To determine limiting heat flux with wick horizontal. Test series terminated due to chamber leak.
2								15100	7130	308	75	
3								14500	6700	334	109	To determine limiting heat flux with wick horizontal. A possible limit was observed at an evaporator heat flux between 23500 and 26700 Btu/hr ft^2.
4								17400	8350	333	108	
5								19800	9780	342	121	
6								23300	11200	348	131	
7								23500	11300	355	144	
8								26700	12800	355	144	
9								5340	2040	226	19	To determine fin performance at a low pressure
10								7360	3310	234	22	
11				15°				4490	2310	181	1	To determine limiting heat flux with wick inclined. Indications were that the test value of heat flux exceeded the limiting value.
12				0				5860	2370	289	57	To determine fin performance at intermediate pressure.
13								8080	3550	288	56	
14								10900	4960	298	65	
15								12800	6020	297	64	
16				5°				3950	2110	181	8	Same as test No. 11
17				0				12400	5650	337	114	To repeat suspected failure point observed in test series numbered 3 to 8. High temperatures (800°F) were observed in the evaporator section indicating deterioration of bond between wick and backup plate. Testing terminated.
18								14800	6840	348	132	
19								17300	8210	347	130	
20								19800	9490	352	138	
21	Box-H13	Distilled Water	120	0°	0	23.5 Each Half	2 Each Half	7180	570	142	3	To determine operating characteristics of complete box fin, including limiting heat flux. Possible limiting heat flux occurred at an evaporator heat flux of about 27,000 to 29,900 Btu/hr ft^2 for the bottom box half - no limit observed for top box half
22								10500	810	235	23	
23								15300	1220	216	16	
24								21300	1720	227	20	
25								24000	1950	238	24	
26								27000	2200	242	26	
27								29900	2440	252	31	
28								18100	1440	242	28	To verify results of above series. Limit observed at an evaporator heat flux of about 23800 to 28300 Btu/hr ft^2 for the bottom box half - no limit observed for top box half
29								23800	1920	259	35	
30								28300	2300	266	39	
31								25600	2080	248	29	
32								28200	2300	256	33	

TABLE 2 (Cont'd)

Test No.	Fin Model	Test Fluid	Fluid Inventory (% Wick Void Volume)	Angle of Inclination deg.	Non-Cond. Fill Press., psia	Active Condenser Length Inches	Evaporator Length Inches	***Nominal Heat Flux (Btu/Hr ft^2) Evaporator	Condenser	Fluid Saturation Temp., °F	Fin Press., psia	Test Objective and Comments
33	Box-H13	Distilled Water	100	0°	0	23.5 Each Half	2 Each Half	10600	820	223	18	To determine effects of inventory on limiting heat flux. Indications were that limiting heat flux increased with increasing inventory.
34								18900	1520	228	20	
35								22800	1850	229	20	
36								25500	2080	238	24	
37			120					15600	1250	208	14	
38								22800	1860	224	19	
39								28800	2360	230	21	
40			150					31600	2600	232	22	
41								17800	1440	212	15	
42								24500	2000	228	20	
43								34600	2860	231	21	
44								38300	3170	232	22	
45					7.25			14900	1190		25	To determine effect of presence of noncondensable gas on fin operating characteristics. Indications were that the water vapor and noncondensable gas (nitrogen) mixed.
46								10800	840		21	
47								7930	600		19	
48								5460	403		15	
49	Bottom Box Half-H13		100		0	23.5	2	1350	~0	163	5	To determine the effect of inventory on fin performance. These tests and tests at 150% inventory indicate that fin performance was best at 150% and poorest at 100% inventory.
50								2810	76	196	11	
51			120					3900	210	169	6	
52								7160	460	185	8	
53			150					5650	340	177	7	To determine limiting heat flux as a function of both condensing length and fin orientation. A possible limiting heat flux occurred in Tests Nos. 53-63 at an evaporator heat flux between 46,700 and 50,800 Btu/hr ft^2. No limiting heat flux was observed in Tests 64-93. Test results indicated a deteriroation in fin performance.
54								10700	710	227	20	
55								15000	1050	243	25	
56								19800	1480	231	21	
57								22400	1690	235	23	
58								28900	2240	240	25	
59								33800	2650	242	26	
60								39000	3090	244	27	
61								42800	3420	238	24	
62								46700	3750	241	25	
63								50800	4080	257	34	
64						14.1*		11890	1690	223	18	
65								15970	2260	232	22	
66								23230	3300	239	25	
67								8404	1190	219	17	
68								5900	836	207	13	
69						9.1*		5900	1250	205	13	
70								7520	1600	220	17	
71								9340	1990	231	21	
72								10810	2300	233	22	
73								13570	2880	235	23	
74								15970	3400	234	22	
75								17890	3800	238	24	

TABLE 2 (Cont'd)

Test No.	Fin Model	Test Fluid	Fluid Inventory (% Wick Void Volume)	Angle of Inclination deg.	Non-Cond. Fill Press., psia	Active Condenser Length Inches	Evaporator Length Inches	*** Nominal Heat Flux (Btu/Hr ft^2) Evaporator	Condenser	Fluid Saturation Temp., °F	Fin Press., psia	Test Objective and Comments
76	Bottom Box	Distilled	150	0°	0	9.4*	2	5900	1250	200	12	
77	Half-H13	Water						7520	1600	221	17	
78								8850	1890	231	21	
79								10800	2300	233	22	
80								13000	2760	237	24	
81								15300	3260	239	25	
82				3°		23.5		4470	380	188	9	
83								5500	470	193	10	
84								7080	602	199	11	Note for Tests Nos. 76-93 on preceding page
85								8850	753	204	13	
86				1°				3780	322	193	10	
87								5110	435	200	12	
88								7080	602	214	15	
89								9340	794	215	16	
90				0°				1980	2 0	199	11	
91								3310	110	200	12	
92								4270	190	207	13	
93								7180	410	221	18	
94		Freon 113		-14.5				5740	489	193	49	To determine limiting heat flux using a fluid with properties different from water - no distinct change in slope of the Q/A vs Δ Tsat curves was noted in this test series.
95								7940	675	193	49	
96								9290	790	197	54	
97								12980	1100	212	64	
98				0				1660	0	210	62	
99								2980	55	222	72	
100								3530	95	228	78	
101	Top Box	Distilled						4640	202	226	19	
102	Half-H13	Water		3						226	19	
103**	Tested in			6						220	17	To determine angle at which a limiting heat flux occurs with heat flux held constant.
104	Bottom			3						211	14	
105	Box Half			4						216	16	$Q/A)_{evap}$ = 4640 Btu/hr ft^2 possible failure at 2 1/2-3 3/4°
106	Orientation			5						211	14	
107				0				5900	301	223	18	
108				1 1/2						228	20	$Q/A)_{evap}$ = 5900 Btu/hr ft^2 possible failure at 2 1/2-3 3/4°
109				3						223	18	
110				4						222	18	
111				5						216	16	$Q/A)_{evap}$ = 11200 Btu/hr ft^2 possible failure at 1 1/4-2 1/2°
112				0				11200	727	238	24	
113				1						242	26	
114				2						242	26	
115				3						243	26	
116				4						244	27	

TABLE 2 (Cont'd)

Test No.	Fin Model	Test Fluid	Fluid Inventory (% Wick Void Volume)	Angle of Inclination deg.	Non-Cond. Fill Press., psia*	Active Condenser Length Inches	Evaporator Length Inches	***Nominal Heat Flux (Btu/Hr ft²) Evaporator	Condenser	Fluid Saturation Temp., °F	Fin Press., psia	Test Objective and Comments
117	↓	↓	↓	0	↓	↓	↓	20700	1570	215	16	To determine limiting heat flux failure as a function of evaporator heat flux with fin horizontal. No limit observed-test series terminated due to temp. limitation of rig.
118	↓	↓	↓	↓	↓	↓	↓	21100	1590	224	19	
119	↓	↓	↓	↓	↓	↓	↓	24900	1930	217	16	
120	↓	↓	↓	↓	↓	↓	↓	27500	2150	217	16	
121	Top Box Half-H13 Tested in Bottom Half Box Half Orientation	Distilled Water	150	0	0	23.5	2	31500	2490	220	17	To determine limiting heat flux as a function of angle at a relatively high evaporator heat flux. No failure observed. Test series terminated due to coolant pump failure.
122				1/2				32200	2550	216	16	
123				1				31500	2500	212	15	
124				1 1/2				31100	2470	210	14	
125	↓	↓	↓	0	↓	↓	↓	8950	579	218	17	To determine capillary pump failure point as a function of angle with heat flux constant and to check repeatability by comparing to Tests No. 101-116. A possible limit occurred between 3° and 4° and repeatability was satisfactory.
126	↓	↓	↓	1	↓	↓	↓	↓	↓	222	18	
127	↓	↓	↓	2	↓	↓	↓	↓	↓	222	18	
128	↓	↓	↓	3	↓	↓	↓	↓	↓	224	19	
129	↓	↓	↓	4	↓	↓	↓	↓	↓	198	11	
130	↓	↓	↓	5	↓	↓	↓	↓	↓	191	10	
131	↓	↓	↓	6	↓	↓	↓	↓	↓	184	8	
132	Planar - M2	↓	100	0	↓	17.8	6.2	3060	1070	195	10	To determine limiting heat flux for M2 planar fin - a hot spot developed in the evaporator region during this test series - No limiting heat flux was observed.
133	↓	↓	↓	↓	↓	↓	↓	4530	1580	207	13	
134	↓	↓	↓	↓	↓	↓	↓	7600	2650	234	22	
135	↓	↓	↓	↓	↓	↓	↓	13000	4530	275	45	
136	↓	↓	↓	↓	↓	↓	↓	17800	6200	288	56	In the next test attempted, excessively high temperatures were observed throughout the evaporator region - visual inspection revealed complete separation of wick and backup plate in evaporator section.

*Adiabatic section located between evaporator and condenser

**Transient point indicating capillary pump failure

***Values of heat flux are nominal for Tests Nos. 16, 64-89, 94-97 and 132-136 in that heat losses have not been substracted and for Tests Nos. 101-116 and 125-131 in that the values given are representative of an average of the test series values corrected for heat loss. The values given for all other tests have been corrected for heat loss.

TABLE 3 - Test Data
A. Modified Planar Fin - H6 Wick

Test No.	Fin Angle, Degrees	Inventory % Wick Void at 75°F	Power Input		Pressure, psig			Coolant Flow, lb/hr Channel Number						Temperature Measurements, °F (Thermocouple Numbers Noted Below)															
														Coolant Channel												Vapor Region			
			Volts	Amps	Gage	Transducer								Inlet						Outlet						Evaporator End		Condenser End	
					1	1	2	1	2	3	4	5	6	1	2	3	4	5	6	1	2	3	4	5	6	43	44	45	46
1	0	100	2.44	425	-	38	39	72	74	76	71	85	78	96	96	96	96	96	97	106	100	100	102	104	103	290	-	282	282
2			2.70	470	-	64	62	80	82	85	84	95	87	100	100	100	100	100	100	108	106	106	104	107	106	312	-	308	308
3			2.70	450	-	95	95	80	82	85	84	95	87	-	100	100	-	100	100	107	106	104	106	106	104	336	-	334	334
4			2.9	500	-	98	99	151	149	156	149	170	154	72	72	72	-	72	72	77	77	77	76	77	76	336	-	332	334
5			3.1	532	-	110	109	176	172	179	172	192	178	56	56	56	-	56	56	60	60	60	61	60	60	359	-	342	343
6			3.3	580	-	122	121	594	576	582	564	586	580	46	46	46	-	46	45	48	48	47	47	46	47	369	-	349	347
7			3.3	585	-	123	123	602	583	588	571	594	588	46	46	46	-	46	45	48	47	48	48	46	47	375	-	360	350
8			3.5	600	Transient - No steady-state data recorded									-	-	-	-	-	-	-	-	-	-	-	-	-	-	-	-
9			1.55	300	-	-	-	30	32	32	30	36	35	92	92	92	92	92	92	98	98	98	98	98	100	240	-	226	226
10			1.80	350	-	-	-	30	32	32	30	36	35	92	92	92	92	92	94	98	98	98	102	106	98	236	-	234	234
11	15		1.60	300	-	-	-	0	0	0	0	0	0	96	98	91	86	85	81	188	100	90	82	81	80	315	320	101	101
12	0		1.62	310	42	-	-	42	45	46	42	52	49	186	190	191	195	190	188	191	194	195	192	194	190	288	274	274	274
13			1.90	360	44	-	-	42	45	46	42	52	49	143	148	146	145	146	146	154	154	156	153	154	154	290	276	287	287
14			2.2	415	50	-	-	142	140	148	140	163	147	110	111	112	112	-	112	115	116	116	114	116	116	295	282	292	293
15			2.4	448	49	-	-	142	140	148	140	163	147	74	75	76	76	76	76	78	78	80	78	79	80	292	278	292	292
16	5		1.3	230	-	-	-	98	97	102	97	113	103	205	205	205	204	203	204	206	205	204	203	203	204	346	310	181	181
17	0		2.4	450	99	-	-	<42	<45	<46	<42	<52	<49	158	160	160	158	158	162	172	171	170	172	170	172	336	316	335	335
18			2.6	485	117	-	-	55	58	59	54	66	63	128	129	126	128	132	126	140	136	140	138	136	138	350	330	346	346
19			2.8	525	115	-	-	55	58	59	54	66	63	106	106	106	106	108	107	118	116	121	116	116	122	351	329	345	344
20			3.0	558	123	-	-	72	74	76	71	85	78	74	75	76	76	76	77	88	84	83	88	88	90	360	334	350	350

TABLE 3 - Test Data

A. *Modified Planar Fin - H6 Wick (Cont'd)*

Test No.	Temperature Measurements, °F (Thermocouple Numbers Noted Below)																																					
	Evaporator Section																Condenser Section																					
	1	2	3	4	5	6	7	8	9	10	11	12	13	14	15	16	18	19	20	21	22	23	24	25	26	27	28	29	30	31	33	34	35	36	37	41	42
1	344	376	374	344	400	440	414	432	408	424	390	350	346	300	296	312	194	176	176	173	166	168	168	182	172	168	164	168	167	164	182	174	178	168	180	188	202
2	384	426	418	384	450	494	464	486	456	476	432	395	386	338	326	346	210	194	194	188	184	174	174	200	186	184	180	184	188	182	206	192	195	188	100	212	232
3	412	457	456	432	478	503	466	458	493	484	450	-	438	370	362	363	254	262	248	233	234	252	227	236	224	228	-	220	224	248	248	226	236	267	234	288	296
4	432	480	490	454	500	540	498	654	530	522	480	-	458	376	368	374	246	244	236	222	220	232	214	212	211	208	-	202	200	216	224	203	220	242	219	266	284
5	454	508	530	478	528	568	520	690	562	556	512	-	486	386	378	390	265	250	260	248	230	236	234	237	237	246	-	240	210	220	234	212	227	250	227	258	284
6	473	535	566	510	577	621	567	763	603	589	539	-	503	395	389	402	266	250	264	257	233	238	235	229	242	242	-	238	209	225	231	212	230	250	225	235	280
7	478	540	574	513	593	631	577	776	610	594	545	-	506	399	392	404	267	255	265	262	238	241	238	229	245	246	-	242	212	226	230	217	232	250	228	238	280
8	Transient - No steady-state data recorded																																					
9	262	302	280	282	318	326	306	352	318	287	286	324	248	243	240	246	200	204	192	188	195	188	188	198	186	184	180	180	183	186	196	186	-	186	190	214	218
10	288	332	304	306	346	362	334	390	346	316	316	368	270	246	250	250	210	212	200	190	202	191	194	202	192	192	190	190	190	196	202	190	-	190	194	222	224
11	504	493	487	575	626	558	617	562	635	621	526	551	476	377	410	381	252	230	230	185	163	167	170	163	160	137	132	127	120	117	116	116	-	110	108	105	106
12	326	358	356	354	400	400	400	448	412	378	362	312	312	294	298	300	278	284	284	274	278	274	274	268	264	256	264	254	254	273	256	254	-	258	265	274	278
13	343	388	383	378	434	426	414	503	449	410	392	331	327	306	304	306	275	285	256	246	263	250	250	237	240	236	245	234	236	256	240	235	-	241	244	252	270
14	364	425	416	408	480	476	456	567	495	448	431	360	345	318	315	316	267	270	236	222	253	239	226	210	214	212	226	210	214	236	218	215	-	218	223	226	256
15	376	446	434	424	504	506	482	604	521	472	454	378	354	322	318	318	258	263	220	200	240	220	204	196	193	192	208	88	194	216	194	194	-	198	203	214	244
16	438	428	424	474	503	462	496	464	504	494	438	424	390	334	349	333	249	231	226	212	210	-	210	208	208	202	202	198	193	195	196	192	-	193	197	192	192
17	418	512	506	490	640	652	673	687	688	618	552	436	396	366	362	360	296	296	278	276	276	-	276	278	278	280	278	280	286	280	310	289	-	284	290	304	307
18	446	550	558	520	678	703	716	734	727	653	593	468	424	386	380	377	278	304	290	290	288	-	280	258	282	288	290	288	294	286	314	298	-	282	280	290	302
19	460	578	582	540	703	740	744	767	748	676	625	476	434	393	386	382	270	267	280	279	282	-	276	243	274	283	282	283	278	270	300	284	-	272	270	278	290
20	486	622	622	570	742	790	790	800+	786	718	668	504	458	408	400	394	280	296	280	275	282	-	274	230	272	280	280	280	292	270	290	290	-	263	262	268	280

TABLE 3 - Test Data
B. Full Box Fin - H13 Wick

Test No.	Fin Angle, Degrees	Inventory % Wick Void At 75°F	Power Input		Pressure Gage, psig		Coolant Flow, lb/hr Channel Number										Temperature Measurements, °F (Thermocouple Numbers Noted Below)																										
																	Coolant Channel																				Vapor Region					
																	Inlet										Outlet										Evaporator End			Condenser End		
			Volts	Amps	1	2	1	2	3	4	5	6	7	8	9	10	1	2	3	4	5	6	7	8	9	10	1	2	3	4	5	6	7	8	9	10	56	59	60	58	61	62
21	0	120	3.4	100	-	-23 *	0	0	0	0	0	0	0	0	0	0	80	80	-	-	71	122	120	81	-	101	79	75	73	72	-	127	82	80	104	102	144	134	142	137	133	133
22			4.2	121	9.5	8.25	0	0	0	0	0	0	0	0	0	0	120	122	-	-	110	187	214	164	-	212	122	91	104	92	-	214	214	212	212	213	235	216	235	233	234	234
23			4.9	145	0	1	<42	<45	<46	<42	<52	<49	<46	<41	<41	<41	144	143	-	-	157	156	151	147	-	157	150	156	137	153	-	182	181	177	174	171	217	211	218	215	215	215
24			5.8	170	6	5											149	149	-	-	153	145	151	152	-	143	150	146	131	155	-	179	172	180	171	167	227	225	228	224	224	224
25			6.2	180	10.5	9.7											144	144	-	-	148	143	150	180	-	143	148	142	131	151	-	184	175	178	174	170	238	240	239	235	236	236
26			6.6	190	12	10.2											138	137	-	-	142	175	142	179	-	140	144	142	136	140	-	175	172	212	165	164	242	248	243	239	240	239
27			7.0	200	18	16											140	140	-	-	144	146	146	190	-	144	148	146	130	142	-	183	176	212	168	168	250	263	253	250	250	250
28			2.8	305	14	12.8	42	45	46	42	52	49	46	41	41	41	160	164	165	163	163	160	158	158	155	-	162	162	163	163	163	160	158	166	166	166	242	242	240	238	238	238
29			3.2	350	22	21.5	72	65	76	88	85	78	77	55	79	86	163	162	163	163	162	164	166	164	164	-	166	162	164	168	162	174	172	170	168	168	260	260	258	256	256	256
30			3.59	385	24	22	115	114	120	114	133	120	119	115	112	112	177	177	177	177	176	177	176	176	176	-	178	177	177	178	175	181	180	180	177	177	262	270	266	267	257	258
31			3.4	360	16	14.2	67	59	67	59	72	70	68	63	62	-	136	136	138	136	136	134	134	133	132	-	138	138	138	136	137	144	142	140	140	210	248	250	246	244	242	242
32			3.55	380	20.5	18.2	59	66	68	59	76	70	64	63	62	-	126	127	128	126	126	128	129	128	126	-	130	131	130	127	128	140	139	136	136	190	256	258	256	252	252	252
33		100	2.2	225	4.0	4.5	42	-	46	42	52	49	53	41	41	47	-	169	169	-	-	170	172	170	168	168	169	169	170	170	169	180	178	177	176	176	224	-	224	222	222	222
34			2.9	295	6.0	6.5	115	114	111	114	124	129	127	123	133	117	-	-	152	-	-	152	153	152	152	152	152	152	153	152	152	156	156	155	154	154	230	-	228	226	226	226
35			3.2	325	7.0	7.2	125	123	129	123	144	129	127	118	120	112	-	-	144	-	-	144	144	143	144	144	144	144	144	144	144	148	147	146	146	146	232	-	231	228	228	228
36			3.4	345	10	10.8	115	123	129	123	138	129	127	118	116	117	-	-	146	-	-	146	146	146	146	145	146	147	147	146	146	150	150	149	148	148	240	-	240	236	236	236
37		120	2.6	270	0	0	42	45	46	42	52	49	46	41	41	41	170	173	174	172	172	174	174	172	172	169	171	174	175	174	174	184	184	183	181	178	208	208	208	208	208	207
38			3.1	325	5.0	4.4	42	45	46	42	52	49	46	41	41	41	175	178	178	176	176	177	177	175	176	174	176	180	180	178	178	190	191	190	188	185	224	225	225	224	224	224
39			3.5	360	8.0	6.5	72	78	85	62	85	70	85	70	70	52	179	180	181	179	180	180	181	180	180	180	180	183	183	181	181	190	190	189	188	185	230	231	231	230	230	230
40		150	3.7	375	9.0	6.5	42	45	46	42	52	49	46	41	41	41	163	166	167	165	165	168	168	167	168	164	166	170	170	168	168	186	186	184	182	180	232	233	233	232	232	232
41			2.8	285	0	1.2	42	45	46	42	52	49	46	41	41	41	176	180	182	178	178	178	180	179	176	175	175	180	180	178	177	187	187	186	183	180	212	212	212	212	212	211
42			3.3	330	6	5	55	58	59	54	66	63	59	55	55	52	176	176	176	176	176	178	178	176	178	176	178	178	179	179	178	190	189	189	189	185	227	228	228	228	228	227
43			3.9	390	8	7.2											164	166	166	164	164	166	166	166	165	164	166	168	168	168	168	180	180	178	176	174	231	232	232	231	232	230
44			4.1	410	9	7.6											158	158	159	158	158	158	157	157	157	156	160	161	162	162	160	174	174	172	170	168	232	232	232	232	232	232
45			2.7	270	10	10.5	42	45	46	42	52	49	46	41	41	41	160	162	164	162	163	165	164	162	161	159	161	163	165	164	165	177	173	172	171	169	** 226/232	220	220	220	218	-
46			2.3	230	6.5	6.5											159	160	162	160	160	165	165	163	163	161	160	161	163	161	162	176	173	171	170	167	** 215/220	208	210	209	207	-
47			2.0	195	4	4											162	164	165	164	164	169	169	167	166	164	162	165	166	165	165	175	173	170	169	166	** 203/207	198	201	197	196	-
48			1.7	165	0	0.5											151	155	155	154	150	160	161	155	156	153	153	154	154	149	151	166	160	160	161	161	** 188/194	182	183	180	180	-

*Indicates Reading in Inches of Mercury

**Fluctuating Between These Limits

TABLE 3 - Test Data
B. Full Box Fin - H13 Wick (Cont'd)

Test No.	Temperature Measurements, °F (Thermocouple Numbers Noted Below)																															
	Top Box Half																															
	Evaporator Section					Condenser Section																										
	11	12	13	14	15	17	18	19	20	21	22	23	24	25	26	27	28	29	31	32	33	34	35	36	37	39	40	41	42	43	44	45
21	161	221	229	186	162	139	139	133	-	137	136	134	136	134	134	133	132	130	130	130	128	126	123	-	122	121	118	115	116	116	114	112
22	250	358	350	318	256	224	223	216	-	225	224	223	220	222	222	222	220	214	220	220	219	220	220	-	218	220	220	220	220	220	218	217
23	237	346	347	279	245	199	189	191	-	194	192	193	190	192	187	193	205	205	206	206	203	183	189	-	187	187	178	182	179	180	178	181
24	248	402	402	330	262	198	184	190	-	193	188	188	184	187	180	190	210	210	210	210	208	183	186	-	184	184	172	177	173	176	174	178
25	260	442	424	326	278	204	190	196	-	200	190	193	190	193	185	195	219	219	219	219	217	190	191	-	189	188	178	180	176	180	177	182
26	267	470	438	334	285	200	182	193	-	195	188	192	191	192	186	194	220	219	220	220	218	178	185	-	184	186	176	179	174	178	176	181
27	279	496	468	358	296	208	190	201	-	202	194	196	195	198	190	200	224	221	223	222	220	181	190	-	188	190	180	184	180	182	180	186
28	262	440	426	340	272	216	218	206	-	220	212	216	218	216	210	214	206	208	220	206	206	206	206	-	208	209	204	205	202	212	202	203
29	285	481	484	370	298	222	224	214	-	224	220	220	224	220	220	218	219	218	219	218	220	220	220	-	220	219	218	219	217	232	216	218
30	288	551	566	410	303	222	223	218	-	224	208	220	226	221	214	220	221	221	221	222	222	218	221	-	223	222	217	219	216	233	216	220
31	273	472	496	348	288	208	188	214	-	202	185	212	218	210	192	208	196	202	200	196	200	192	200	-	200	200	213	216	214	214	214	214
32	284	504	526	376	300	210	180	220	-	207	190	218	218	218	186	213	200	208	205	200	203	196	204	-	203	204	236	230	236	244	238	234
33	248	318	-	282	245	212	210	-	208	209	208	209	212	210	207	212	208	207	206	206	205	206	206	-	206	205	200	203	200	202	199	200
34	268	374	-	312	260	208	205	-	201	204	200	205	209	206	198	209	200	202	200	198	198	200	201	-	200	200	192	197	193	196	190	191
35	282	486	-	322	267	206	203	-	198	200	198	202	208	204	196	207	197	199	198	194	196	197	199	-	198	196	188	194	188	192	185	186
36	484	600	-	310	280	213	208	-	204	206	205	208	214	210	202	214	204	205	204	200	201	204	205	-	204	202	194	200	194	199	190	192
37	230	302	-	251	231	-	194	-	193	194	193	194	196	195	194	197	190	-	192	191	194	190	190	-	190	190	183	187	186	188	186	-
38	254	316	-	273	254	-	202	-	203	203	203	203	203	206	205	203	208	-	202	201	204	200	200	-	200	200	191	196	194	198	194	-
39	264	338	-	272	267	-	205	-	206	205	205	205	208	207	205	210	202	-	204	204	207	203	202	200	202	200	193	198	197	201	197	-
40	264	396	-	281	272	-	204	-	202	202	202	202	205	204	200	206	196	-	199	199	200	198	196	196	196	196	187	187	192	190	192	-
41	230	310	-	266	237	-	196	-	196	196	196	196	198	198	195	198	194	-	194	194	196	193	192	192	192	193	186	189	188	190	189	-
42	253	362	-	286	260	-	204	-	204	204	204	204	205	205	203	206	200	-	202	201	204	200	200	200	200	200	192	196	195	198	196	-
43	266	416	-	278	274	-	200	-	200	198	199	198	200	200	198	200	194	-	194	195	196	194	193	191	193	192	183	189	187	191	188	-
44	274	438	-	282	279	-	197	-	196	194	194	194	198	197	194	200	188	-	190	190	192	190	188	186	188	188	177	184	180	186	182	-
45	410	492	-	332	258	-	188	-	185	191	183	190	188	190	184	188	182	188	182	179	183	177	182	180	183	182	175	179	175	176	173	-
46	240	376	-	293	246	-	184	-	182	186	179	183	183	183	180	183	177	181	179	177	180	175	179	177	178	178	173	175	173	174	171	-
47	227	279	-	256	230	-	180	-	178	181	176	179	179	179	176	178	174	177	176	174	176	172	174	173	174	174	170	172	170	170	169	-
48	214	249	-	234	216	-	170	-	171	172	170	171	171	170	169	169	167	168	168	167	165	165	165	164	168	165	160	164	160	160	158	-

TABLE 3 - Test Data
B. Full Box Fin - H13 Wick (Cont'd.)

Test No.	Temperature Measurements, °F (Thermocouple Numbers Noted Below)																																	
	Bottom Box Half																																	
	Evaporator Section					Condenser Section																												
	63	64	65	66	67	68	69	70	71	72	73	74	75	76	77	78	79	80	81	82	83	84	85	86	87	88	89	90	91	92	93	94	95	97
21	173	163	163	-	167	140	128	137	130	134	124	126	120	121	118	120	116	116	110	115	115	115	108	112	110	112	110	111	109	110	104	110	107	103
22	288	250	248	-	262	234	228	232	230	232	227	228	226	229	226	227	226	226	226	226	227	226	224	226	224	227	224	225	222	224	220	222	224	216
23	294	238	233	-	284	216	204	215	213	216	199	212	206	210	206	208	206	206	204	206	207	206	156	206	204	207	204	205	202	197	191	196	193	187
24	326	254	238	-	320	224	206	222	220	222	203	218	214	218	214	215	213	214	211	214	215	214	163	213	211	214	210	211	208	197	190	197	194	187
25	420	270	250	-	339	236	213	233	230	232	210	229	223	230	224	226	222	224	218	226	225	224	164	226	220	225	220	223	218	212	200	208	204	197
26	466	276	256	-	342	240	216	236	234	235	214	234	229	234	227	230	226	229	220	229	229	229	164	228	224	224	224	226	220	214	200	208	205	195
27	586	402	268	-	366	250	224	246	240	246	223	242	234	242	236	240	234	238	226	238	238	238	168	237	232	239	233	234	228	215	209	218	214	209
28	336	292	258	-	300	216	226	227	228	224	226	224	226	228	226	222	224	220	-	220	224	222	222	216	222	222	222	208	221	221	221	221	226	221
29	426	311	278	-	346	228	244	242	246	240	244	240	244	246	244	240	242	238	-	238	242	233	238	200	222	216	220	200	220	234	238	239	243	239
30	678	690	280	-	412	233	238	240	245	238	240	237	240	242	239	232	239	234	-	234	239	228	233	194	208	203	204	196	209	222	222	227	225	223
31	598	494	268	-	348	236	236	224	228	208	220	191	221	114	220	187	212	189	-	189	211	190	209	218	222	228	224	221	224	220	222	220	236	220
32	632	536	278	-	368	246	244	236	238	220	230	206	230	223	230	190	220	192	-	194	220	198	214	226	230	236	233	230	232	228	228	226	234	227
33	256	257	238	246	255	221	220	220	219	218	-	217	216	218	216	216	216	215	-	215	217	215	216	214	216	217	216	214	216	214	216	214	217	215
34	283	286	248	261	280	222	222	220	221	217	-	212	218	220	218	214	218	198	-	200	217	203	216	211	216	218	217	213	216	193	216	200	215	217
35	296	375	254	269	292	222	222	216	220	214	-	215	217	218	218	211	216	193	-	196	216	196	216	201	216	216	216	211	216	188	216	192	210	216
36	312	445	265	280	304	228	230	222	238	232	-	210	224	225	225	218	224	199	-	200	222	201	224	206	224	224	224	218	224	194	223	197	214	224
37	267	244	223	244	268	-	200	200	202	-	-	198	200	204	203	203	204	194	-	195	200	197	204	194	202	202	204	200	203	194	198	196	202	202
38	296	298	244	270	300	-	214	214	215	-	-	210	212	216	216	212	219	207	-	208	212	210	219	210	212	215	217	212	218	208	212	210	213	218
39	320	455	254	286	307	-	217	203	215	-	-	203	216	217	218	202	223	199	-	202	213	201	223	208	215	216	220	211	223	205	215	207	217	223
40	330	343	258	294	322	-	214	214	211	-	-	204	206	207	208	207	214	206	-	207	209	209	218	212	213	215	215	215	220	212	214	213	214	220
41	274	256	228	252	277	-	200	198	197	-	-	192	196	196	196	193	200	193	-	194	198	195	202	198	200	200	200	200	204	198	200	200	200	203
42	306	296	249	277	307	208	210	204	208	-	-	202	207	207	208	204	214	202	-	204	208	204	217	204	212	212	213	208	220	206	212	208	212	218
43	337	378	260	298	334	208	210	204	205	-	-	194	203	202	204	196	210	196	-	198	204	200	216	204	210	210	211	208	218	205	210	207	211	218
44	346	423	263	304	342	207	208	202	203	-	-	190	200	200	200	193	208	191	-	194	202	196	214	200	208	208	209	205	217	204	209	206	210	216
45	297	325	258	277	289	225	218	222	219	-	-	203	203	202	201	197	199	185	-	186	196	189	200	190	200	201	203	199	202	194	195	196	197	197
46	285	277	246	262	269	215	204	210	206	-	-	192	191	191	189	186	187	176	-	177	184	178	188	179	187	186	190	186	190	182	185	185	187	186
47	258	257	235	248	252	200	197	195	195	-	-	177	182	181	181	178	180	173	-	173	177	174	181	174	179	180	181	179	182	176	180	178	180	180
48	247	235	218	232	233	190	180	188	184	-	-	164	168	167	167	163	168	161	-	160	163	160	160	160	165	165	165	163	165	164	166	160	165	166

TABLE 3 - Test Data

C. Box Half Tests - Bottom Half of Full Box Fin

Test No.	Fin Angle, Degrees	Inventory, % Wick Void	Power Input Volts	Power Input Amps	Pressure Gage, psig 1	Pressure Gage, psig 2	Coolant Flow, lb/hr Channel Number 1	2	3	4	5	Temperature Measurements, °F (Thermocouple Numbers Noted Below) Coolant Channel Inlet 2	3	4	5	Coolant Channel Outlet 1	2	3	4	5	Vapor Region Evaporator End 59	Vapor Region Condenser End 61	62
49	0	100	1.0	50	-	-18.5*	374	383	379	389	378	189	189	189	189	188	189	189	188	188	162	163	163
50			1.5	75	-	-7*	366	377	370	378	371	209	209	209	209	209	209	209	209	209	200	198	194
51		120	1.6	70	-	-17*	42	45	46	42	52	164	165	161	163	159	162	162	160	162	170	171	166
52			2.2	115	-	-11*	0	0	0	0	0	121	126	124	120	120	115	117	120	120	222	185	184
53		150	1.6	85	-	-13*	0	0	0	0	0	119	123	123	117	123	117	112	111	137	180	177	177
54			2.2	115	4.0	5.5	42	45	46	42	52	168	169	168	168	167	169	170	169	170	230	227	227
55			2.6	135	11	12.5	55	58	59	54	66	166	166	165	165	165	168	167	167	167	247	243	243
56			2.9	155	6	7.5	98	97	102	97	113	150	151	150	150	150	153	152	152	152	234	231	231
57			3.05	165	7	8.3	98	97	102	97	113	147	147	146	146	147	149	149	148	148	237	234	235
58			3.5	185	9	9.5	98	97	102	97	113	119	121	122	118	119	123	119	122	122	241	240	240
59			3.8	200	9	10	98	97	102	97	113	100	100	100	100	100	105	105	105	105	246	242	241
60			4.05	215	9	10.5	98	97	102	97	113	86	86	86	86	90	90	90	90	90	250	244	243
61			4.3	225	7.5	8.5	98	97	102	97	113	100	100	100	100	104	106	104	105	105	248	238	237
62			4.5	235	8	9.5	98	97	102	97	113	85	85	85	85	90	90	90	90	90	257	241	241
63			4.7	245	No other steady-state data recorded																	257	257
90			1.2	55	-	-4*	42	45	46	42	52	199	199	195	196	194	201	198	198	198	204	199	199
91			1.5	70	-	-2.5*	42	45	46	42	52	196	197	194	194	192	194	196	192	193	215	200	200
92			1.9	85	-	0	42	45	46	42	52	186	186	186	185	185	187	187	185	185	235	207	207
93			2.2	100	-	3	42	45	46	42	52	196	197	194	194	195	197	197	194	194	255	221	221
98			1.4	72	44	-	45	51	59	53	47	-	209	208	204	204	210	206	206	204	214	210	209
99			1.8	90	46.5	-	49	51	59	53	47	-	206	206	204	207	206	204	206	204	228	222	222
100			2.0	95	47	-	49	51	59	53	47	-	204	204	198	200	203	201	202	198	234	228	228

*Indicates Readings In Inches Mercury

TABLE 3 - Test Data

C. Box Half Tests - Bottom Half of Full Box Fin (Cont'd)

Test No.	Temperature Measurements, °F (Thermocouple Numbers Noted Below)																															
	Evaporator Section					Condenser Section*																										
	63	64	65	66	67	68	69	70	71	72	73	74	75	76	77	78	79	80	82	83	85	86	87	88	89	90	91	92	93	94	95	97
49	182	198	184	-	198	164	164	166	166	164	164	165	165	166	166	166	165	166	166	166	166	167	166	167	166	167	166	168	172	167	168	174
50	283	343	292	-	287	196	197	197	197	196	196	196	197	197	197	196	197	196	196	197	197	196	198	197	199	196	199	197	199	197	199	199
51	207	265	246	-	208	169	166	168	167	168	168	168	166	167	166	168	166	167	167	166	165	164	164	164	164	164	163	163	164	162	163	163
52	397	532	495	-	374	187	183	186	183	185	186	185	181	183	181	185	181	185	185	182	180	183	179	182	180	182	179	181	179	181	180	179
53	194	198	197	-	196	178	178	177	178	177	177	175	177	178	177	174	177	176	176	176	175	173	174	176	175	172	174	172	173	171	173	172
54	250	255	290	-	268	224	225	224	225	222	222	214	222	223	222	208	222	218	218	222	221	206	221	222	222	204	221	201	221	201	219	220
55	298	280	357	284	302	239	240	238	239	236	234	216	236	237	237	208	235	229	228	237	235	209	236	235	237	208	236	206	236	206	232	233
56	298	286	290	276	300	228	229	227	228	223	222	178	224	220	224	172	223	172	174	218	222	174	222	214	223	177	222	176	221	170	201	218
57	306	293	296	280	307	231	231	230	230	226	226	176	226	221	226	171	226	170	173	219	225	178	226	216	226	180	226	176	226	170	202	220
58	342	322	320	296	345	233	234	230	232	227	225	166	228	216	228	156	234	160	164	216	226	166	228	202	228	166	228	162	228	160	195	221
59	372	346	342	306	377	233	224	229	232	222	222	157	228	209	227	146	226	148	154	206	226	156	227	196	227	154	226	150	224	142	186	219
60	399	370	384	318	406	223	235	190	230	195	197	148	230	198	228	134	226	142	148	198	226	148	228	192	228	148	226	141	224	133	183	218
61	411	380	342	358	414	156	230	154	218	146	146	153	224	192	223	140	220	148	155	190	220	158	222	190	222	158	220	158	220	152	186	212
62	436	395	393	394	429	151	233	154	220	145	145	141	238	191	227	137	224	145	151	189	223	153	226	191	225	154	223	154	222	149	187	221
63	459	425	521	433	450	No other steady-state data recorded																										
90	216	228	225	-	225	-	200	198	199	197	-	200	199	199	199	199	199	199	198	198	198	196	198	197	197	196	197	196	197	196	196	196
91	264	301	253	-	225	-	200	197	199	198	-	197	199	198	199	197	199	197	197	198	199	196	198	197	198	197	197	196	197	195	196	196
92	355	429	353	-	311	-	205	204	205	204	-	203	204	204	204	202	204	202	202	203	203	204	204	205	205	204	203	204	205	204	203	202
93	389	489	396	-	273	-	218	214	215	213	-	213	215	214	215	212	215	211	211	214	214	212	214	214	214	212	214	209	213	210	213	213
98	333	370	354	342	342	227	225	218	218	213	-	213	-	210	208	-	-	-	207	205	-	-	-	205	204	-	-	-	-	204	204	-
99	430	482	472	442	436	247	236	222	225	212	-	212	-	206	206	-	-	-	205	206	-	-	-	205	204	-	-	-	-	203	204	-
100	470	526	516	482	472	252	234	220	221	212	-	212	-	208	208	-	-	-	203	204	-	-	-	204	204	-	-	-	-	202	204	-

*Condenser section temperatures are higher on coolant inlet side (see Figure 2) than on coolant outlet side due to 1° lateral tilt of fin. This resulted in the liquid layer above the wick being thicker on the coolant inlet side than on the coolant outlet side.

TABLE 3 - Test Data

D. Box Half Tests - Top Half of Full Box Fin Tested in Bottom Box Half Orientation

Test No.	Fin Angle, Degrees	Inventory, % Wick Void at 75°F	Power Input Volts	Power Input Amps	Pressure Gage, psig	Coolant Flow, lb/hr Channel Number					Temperature Measurements, °F (Thermocouple Numbers Noted Below) Inlet					Outlet					Vapor Region Evaporator End		Vapor Region Condenser End
					2	6	7	8	9	10	6	7	8	9	10	6	7	8	9	10	56	100	58
101	0	150	2.0	75	5.4	63	58	59	54	66	160	160	160	158	158	162	160	162	160	159	226	-	226
102	3		2.02	75	5.4	55	58	59	54	66	179	180	180	180	179	183	182	183	182	180	232	-	226
103	6		2.0	75	Evaporator region thermocouples indicated fin failed between 3 and 6 degrees - no steady-state point reached																		
104	3		2.0	75	5.0	55	58	59	54	66	185	186	187	186	186	185	186	187	186	185	222	221	211
105	4		2.0	75	6.7	55	58	57	54	66	185	186	186	185	185	186	188	188	187	185	233	235	216
106	5		2.0	75	4.5	55	58	59	54	66	183	184	185	183	183	184	185	185	184	183	230	239	207
107	0		2.2	80	4.3						182	183	183	182	182	184	185	185	185	184	225	224	223
108	1 1/2		2.2	80	6.5						188	190	191	189	190	191	192	193	192	191	230	230	228
109	3		2.2	80	4.0						182	183	183	182	182	184	185	185	185	187	227	227	223
110	4		2.2	80	3.8						185	186	187	185	185	188	188	189	188	186	228	230	222
111	5				2.5	No other steady-state data recorded															230	-	216
112	0		2.9	105	8.6	55	58	59	54	66	162	162	162	161	161	166	168	167	166	165	240	240	238
113	1		2.9	105	11.5						163	164	164	163	162	168	169	169	168	166	247	245	242
114	2		2.9	105	11.7						158	159	160	158	158	164	164	164	163	161	248	248	242
115	3		2.9	105	12.2						167	168	168	168	168	172	172	172	172	170	253	252	243
116	4		2.9	105	13.4						167	168	168	168	167	174	174	174	173	170	255	256	244
117	0		3.8	135	2.5	184	179	183	178	195	61	61	61	61	61	66	65	64	62	62	221	219	215
118			4.0	140	5.5	184	179	183	178	195	61	61	61	61	61	66	65	64	62	61	229	227	224
119			4.4	150	3.2	268	260	266	259	273	-	60	60	60	60	-	64	64	62	61	221	219	217
120			4.6	160	4.0						60	60	60	60	60	64	64	62	62	62	220	219	217
121			5.0	170	4.0						60	60	60	60	60	64	64	63	63	64	222	220	220
122	1/2		5.05	170	2.5						60	60	60	60	60	66	65	62	63	62	222	218	216
123	1		5.0	165	2.0	227	219	226	217	234	60	60	60	60	60	66	64	64	62	62	222	215	212
124	1 1/2		5.0	160	1.1	227	219	226	217	234	60	60	60	60	60	66	64	63	62	62	222	218	210

*Indicates Readings In Inches of Mercury

TABLE 3 - Test Data

D. Box Half Tests - Top Half of Full Box Fin Tested in Bottom Box Half Orientation (Cont'd)

Test No.	Temperature Measurements, °F (Thermocouple Numbers Noted Below)																														
	Evaporator Section				Condenser Section																										
	11	12	14	15	17	18	19	20	21	22	23	24	25	26	27	28	29	30	31	32	33	34	35	36	37	39	40	41	42	43	44
101	240	304	266	240	218	206	-	207	207	210	222	222	223	210	222	212	222	211	216	211	222	220	222	222	220	220	220	218	218	220	216
102	258	313	287	277	220	216	-	213	210	224	224	224	222	214	210	223	223	220	218	218	213	220	220	220	212	205	214	210	208	206	202
103	Evaporator region thermocouples indicated fin failed between 3 and 6 degrees																														
104	270	317	297	315	207	204	-	201	199	202	200	200	198	199	195	200	196	199	198	198	193	198	196	197	193	191	194	191	192	192	192
105	303	329	305	354	215	210	-	207	204	209	208	207	204	204	200	204	203	204	204	203	200	203	201	201	198	195	199	195	196	196	195
106	380	367	443	476	209	205	-	202	198	203	201	200	197	199	193	200	196	197	197	197	191	197	193	194	191	188	193	188	190	189	189
107	243	310	300	240	212	214	149	217	215	213	209	215	210	218	213	213	207	216	213	218	213	212	208	212	208	206	211	207	209	211	211
108	248	318	304	248	220	219	172	218	220	219	218	219	216	218	218	218	215	220	218	219	218	218	216	217	214	211	216	213	214	214	212
109	247	321	286	267	216	214	166	212	213	214	213	214	211	212	210	214	210	214	212	212	207	213	211	211	209	204	209	205	205	205	203
110	270	337	296	350	216	213	-	211	210	214	213	212	210	206	213	210	213	212	210	210	205	212	210	210	207	203	207	203	203	202	201
111	365	419	472	474	No other steady-state data recorded																										
112	276	402	334	270	213	216	-	216	212	215	210	215	210	216	208	214	207	214	214	215	209	214	210	214	210	210	214	208	212	214	214
113	273	420	342	273	220	220	-	218	216	219	217	219	216	217	213	218	214	218	216	216	212	218	214	216	212	209	213	207	210	210	210
114	276	412	338	327	223	220	-	218	214	221	219	220	216	218	210	220	217	218	216	216	209	219	215	216	212	207	210	204	204	202	202
115	352	408	344	412	230	225	-	220	214	228	224	222	220	219	211	226	220	220	217	216	210	220	218	218	212	212	210	204	204	202	201
116	414	426	394	486	237	228	-	222	217	234	228	226	224	222	214	232	225	222	220	220	212	224	224	222	216	208	212	206	204	201	200
117	304	487	386	270	97	157	-	156	131	143	89	111	111	142	101	135	121	139	146	147	99	190	169	198	187	191	201	199	201	204	201
118	307	521	407	280	99	163	-	161	129	150	90	117	111	149	96	142	116	147	145	154	101	196	170	204	192	197	209	206	208	212	207
119	307	573	462	276	97	125	-	128	136	122	85	109	84	120	81	113	80	112	99	112	81	85	85	149	118	114	163	183	183	191	194
120	318	620	518	278	88	130	-	140	90	128	86	111	84	122	78	112	76	110	94	110	80	112	80	110	94	124	172	158	166	106	154
121	336	723	600	286	88	132	-	146	86	134	84	108	82	132	80	120	78	118	100	118	82	116	80	102	86	108	118	90	108	96	122
122	333	725	585	284	96	155	-	158	92	148	90	118	86	132	84	118	78	113	94	110	78	108	76	94	80	92	106	82	97	86	106
123	324	654	552	282	100	164	-	160	98	158	94	120	90	150	84	140	80	131	100	123	80	116	78	96	80	75	110	84	98	88	110
124	308	616	496	276	98	162	-	158	96	158	92	124	92	144	88	132	82	120	96	114	78	112	76	94	78	72	104	80	92	82	102

TABLE 3 - Test Data

D. Box Half Tests - Top Half of Full Box Fin Tested in Bottom Box Half Orientation (Cont'd)

Test No.	Fin Angle, Degrees	Inventory, % Wick Void	Power Input		Pressure	Coolant Flow, lb/hr Channel Number					Temperature Measurements, °F (Thermocouple Numbers Noted Below)													
											Inlet					Outlet					Vapor Region		
			Volts	Amps	Gage, psig																Evaporator End		Condenser End
					2	6	7	8	9	10	6	7	8	9	10	6	7	8	9	10	56	100	58
125	0		2.9	85	2.5	98	97	102	97	113	137	138	138	138	138	141	138	138	139	140	222	221	218
126	1		2.9	85	3.8						140	140	140	140	140	144	140	141	142	142	227	225	222
127	2		2.9	85	3.8						139	140	140	140	140	144	140	140	142	141	230	229	222
128	3		2.9	85	2.0						138	138	138	138	138	143	139	140	140	140	228	226	224
129	4		2.9	85	-5.5*						136	136	136	136	136	140	138	138	138	137	211	211	198
130	5		2.9	85	-7.2*						139	139	139	139	139	144	141	141	141	140	209	205	191
131	6		2.9	85	-9.1*						137	138	138	138	137	142	139	140	139	138	209	204	184

*Indicates Readings In Inches of Mercury

TABLE 3 - Test Data

D. Box Half Tests - Top Half of Full Box Fin Tested in Bottom Box Half Orientation (Cont'd)

Test No.	Temperature Measurements, °F (Thermocouple Numbers Noted Below)																														
	Evaporator Section				Condenser Section																										
	11	12	14	15	17	18	19	20	21	22	23	24	25	26	27	28	29	30	31	32	33	34	35	36	37	39	40	41	42	43	44
125	246	342	290	242	180	195	-	194	180	211	210	214	212	212	212	212	210	212	213	210	206	208	182	208	180	172	191	168	188	186	200
126	250	354	300	247	190	199	-	197	183	215	213	218	216	217	215	215	214	216	216	214	209	213	187	212	180	164	194	174	190	185	200
127	254	356	300	249	192	199	-	196	179	216	217	220	218	218	217	217	215	216	217	215	209	213	187	209	175	162	192	171	186	180	193
128	254	341	293	252	191	196	-	191	174	211	211	214	213	213	211	212	209	211	210	209	181	207	180	198	168	156	184	166	178	170	181
129	286	342	298	254	180	184	-	184	178	164	197	195	196	192	188	162	194	193	186	176	152	184	163	171	153	148	169	153	161	154	158
130	312	364	328	274	178	182	-	177	161	193	191	190	186	178	158	187	181	182	177	169	152	174	154	164	151	148	164	151	157	150	154
131	394	450	451	379	179	181	-	176	161	189	186	184	176	170	153	180	174	172	168	162	149	166	151	158	147	149	157	146	150	146	149

TABLE 3 - Test Data

E. Planar Fin - M2 Wick

Test No.	Fin Angle, Degrees	Inventory, % Wick Void	Power Input		Pressure Gage, psig		Coolant Flow, lb/hr Channel Number									
			Volts	Amps	1	2	1	2	3	4	5	6	7	8	9	10
132	0	100	1.2	193	-	-6.5*	55	58	59	54	85	63	59	55	55	52
133			1.4	245	-	0	55	58	59	54	84	63	59	55	55	52
134			1.8	320	9	8.3	55	58	59	54	85	63	59	48	55	52
135			2.4	410	30	-	49	51	53	48	82	56	53	48	55	52
136			2.9	465	40	-	55	58	59	54	85	63	59	55	55	52

Test No.	Temperature Measurements, °F (Thermocouple Numbers Noted Below) — Coolant Channel																			
	Inlet										Outlet									
	1	2	3	4	5	6	7	8	9	10	1	2	3	4	5	6*	7	8	9	10
132	-	188	189	-	189	187	187	187	190	188	186	188	189	188	189	192	188	188	190	188
133	-	193	194	-	193	196	193	192	196	194	192	193	194	193	194	193	194	193	194	195
134	-	202	202	-	202	200	202	198	202	200	202	204	204	204	204	204	204	202	204	204
135	-	208	208	-	207	202	202	200	202	200	214	214	212	212	210	204	208	206	206	206
136	-	178	178	-	178	174	176	174	176	174	184	186	184	184	182	186	184	184	182	182

Test No.	Vapor Region				
	Evaporator End		Condenser End		
	66	67	68	69	70
132	198	198	145	151	195
133	211	211	153	158	207
134	236	236	170	174	234
135	276	276	204	208	275
136	292	286	228	238	288

*Indicates Readings In Inches of Mercury

TABLE 3 - Test Data
E. Planar Fin - M2 Wick (Cont'd.)

Test No.	Temperature Measurements, °F (Thermocouple Numbers Noted Below)																																						
	Condenser Section																																						
	1	2	3	4	5	6	7	8	9	11	12	13	14	15	16	17	19	22	23	24	25	26	27	28	29	30	31	32	33	34	35	36	37	38	39	40	41	42
132	205	190	148	190	191	192	191	190	191	192	192	191	192	191	190	190	187	192	192	192	191	192	190	192	190	191	192	191	190	191	190	190	189	189	190	76	150	190
133	221	198	158	198	200	200	200	196	220	200	200	200	200	200	198	200	201	200	200	200	197	199	194	199	197	198	199	199	196	198	198	199	198	198	200	77	162	199
134	252	214	176	216	218	218	216	203	216	218	218	216	216	216	212	214	218	216	216	216	210	214	210	214	210	213	214	214	208	212	212	214	212	213	216	82	174	216
135	307	226	174	238	232	230	252	148	228	244	258	233	229	232	229	245	238	237	238	238	225	236	228	231	229	245	263	266	228	252	236	268	230	244	256	82	196	252
136	328	226	204	236	228	230	254	184	228	228	256	224	224	220	210	226	228	224	222	228	202	212	210	221	214	218	230	222	204	218	218	231	218	228	228	82	218	230

Evaporator Section																				
43	44	45	46	47	48	49	50	51	52	53	54	55	56	57	58	62	63	64	65	67
205	201	206	205	199	202	202	204	211	206	217	200	201	207	201	216	207	202	202	217	201
221	215	223	221	210	217	216	225	229	226	240	214	216	225	216	244	222	218	217	241	216
252	244	256	252	238	246	296	254	264	258	280	240	244	258	242	286	254	246	244	280	244
307	292	314	286	280	290	294	312	324	314	325	282	294	300	287	338	310	298	290	354	292
328	308	338	318	288	310	308	340	356	348	354	296	318	318	306	444	342	322	308	448	314

APPENDIX 3

Derivation of Noncondensable Gas Theory

The cases considered for the box fin are those of uniform mixing of working fluid and noncondensable gas, and no mixing of working fluid and noncondensable gas. In the actual tests run, the noncondenable gas volumes were determined from the pressure and temperature in the chamber after it was filled with the noncondensable gas.

Case A - No Mixing of Noncondensable Gas and Condensable Working Fluid

In the case where the noncondensable gas and the working fluid vapor do not mix, the two fluids are assumed to exist in two distinct regions with the noncondensable gas collecting at the end of the chamber opposite the evaporator section. The pressures of the noncondensable gas and the vapor at the interface of these two regions must be equal. Since frictional pressure losses are small in the vapor-chamber passage, the pressure is assumed to be uniform throughout the chamber. Thus, during fin operation, the chamber total pressure is the saturation pressure of the condensing fluid. The equilibrium chamber pressure is such that the saturation temperature of the condensing fluid at that pressure provides the necessary temperature driving potential between the chamber and the coolant in order to reject the heat input. The volume that the noncondensable gas occupies, or the wick area which the noncondensable gas covers is also a function of the chamber pressure. Only a fraction of the wick surface area is left for condensation of the working fluid vapor.

The derivation presented below relates both the axial length of the region containing the noncondensable gas and the chamber total pressure as a function of the total heat load and the coolant temperature.

The following assumptions were made in the derivations for this case:

1) No mixing of noncondensable and condensable fluids

2) Uniform fin pressure

3) Negligible heat transferred along the fin wall into the noncondensable section compared to heat transferred across the wick in the condensable section

4) Noncondensable gas temperature is the same as working-fluid saturation temperature

5) Heat transfer is uniform and constant with heat load

6) The coolant temperature is uniform

The sketch below indicates the location of the evaporation, condensation and non-condensable gas section of the box fin used in the analysis for Case A.

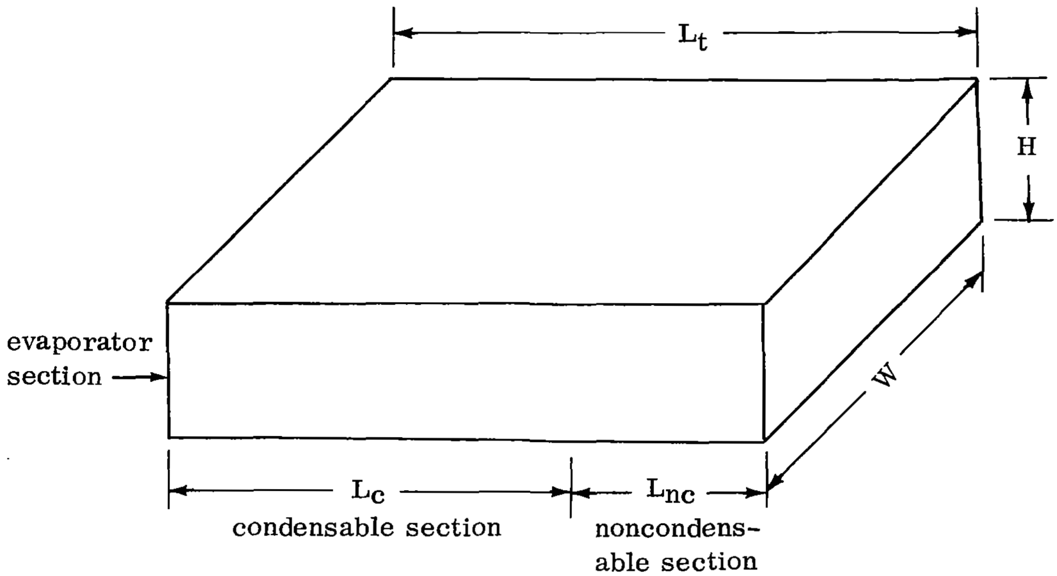

Using Assumptions 1, 2, 3, 5 and 6 above, the following equations may be written

$$Q = UA_s\,(T_{sat} - T_{coolant}) = UWL_c\,(T_{sat} - T_{coolant}) \tag{10}$$

Using the equation of state applied to the noncondensable gas and Assumptions 1 and 2

$$P_{nc} = \left(\frac{MRT}{V}\right)_{nc} = \frac{M_{nc}R_{nc}T_{nc}}{L_{nc}WH} \tag{11a}$$

$$P_{fill} = \frac{M_{nc}R_{nc}T_{fill}}{L_{fill}WH} \tag{11b}$$

by Assumption 2

$$P_{nc} = P_{fin}$$

Thus

$$\frac{P_{fin}}{P_{fill}} = \frac{T_{nc}}{T_{fill}} \cdot \frac{L_{fill}}{L_{nc}} \tag{12}$$

Solving for the length of the noncondensable section yields

$$L_{nc} = \frac{T_{nc}}{T_{fill}} \frac{P_{fill}}{P_{fin}} L_{fill} \tag{13}$$

Using Equation 10 and Assumption 5 the ratio of the heat transferred at two fin operating conditions may be written as

$$\frac{Q_1}{Q_2} = \frac{L_{c1} (T_{sat\ 1} - T_{coolant\ 1})}{L_{c2} (T_{sat\ 2} - T_{coolant\ 2})} \tag{14}$$

As can be seen in the sketch of the fin shown above

$$L_c = L_t - L_{nc} \tag{15a}$$

At filling the noncondensable gas occupies the entire chamber. Thus

$$L_{fill} = L_t \tag{15b}$$

By using Assumption 4

$$T_{nc} = T_{sat} \tag{16}$$

Therefore, using Equations (15), (16) and (13) the length of the condensable section is

$$L_c = \left(1 - \frac{T_{sat}}{T_{fill}} \frac{P_{fill}}{P_{fin}}\right) L_t \tag{17a}$$

and

$$L_{nc} = \left(\frac{T_{sat}}{T_{fill}} \frac{P_{fill}}{P_{fin}}\right) L_t \tag{17b}$$

Substituting Equation (17) into Equation (14) yields

$$\frac{Q_1}{Q_2} = \frac{\left(1 - \frac{T_{sat\ 1}}{T_{fill}} \frac{P_{fill}}{P_{fin\ 1}}\right)\left(T_{sat\ 1} - T_{coolant\ 1}\right)}{\left(1 - \frac{T_{sat\ 2}}{T_{fill}} \frac{P_{fill}}{P_{fin\ 2}}\right)\left(T_{sat\ 2} - T_{coolant\ 2}\right)} \tag{18}$$

Since $P_{fin} = P_{sat}$ and T_{sat} and P_{sat} are directly related for pure fluids, Equation (18) can be used to predict the chamber pressure change between any two operating conditions when there is no mixing of noncondensable and condensable. Equation (18) was used to predict the fin pressure as a function of heat load ratio at the condition of the noncondensable gas tests, as shown in Figure 27. By using Equations (17b) and (18) the length of the fin occupied by noncondensable gas can be related to heat load ratio at various conditions. Figure 38 shows this relationship for the same conditions as those used for Figure 27.

Case B - Uniform Mixing of Noncondensable Gas and Condensable Working Fluid

The following assumption was made for the case where uniform mixing is considered.

1) Same as Assumptions (2), (5) and (6) of Case A, and uniform mixing of noncondensable and condensable fluids.

With the above assumptions plus the knowledge that the condensing area is always the total wick area, the ratio of heat transferred at two operating conditions may be written as

$$\frac{Q_1}{Q_2} = \frac{T_{sat\ 1} - T_{coolant\ 1}}{T_{sat\ 2} - T_{coolant\ 2}} \tag{19}$$

Using the ideal gas law, the partial pressure of the noncondensable is determined by

$$P_{nc} = P_{fill} \frac{T_{nc}}{T_{fill}} \tag{20}$$

Since the noncondensable gas temperature is at the saturation temperature

$$P_{nc} = P_{fill} \frac{T_{sat}}{T_{fill}} \tag{20a}$$

By Dalton's law of partial pressure

$$P_{fin} = P_{nc} + P_{sat} \tag{21}$$

where P_{sat} is the saturation pressure of the working fluid corresponding to T_{sat}. Substituting P_{nc} from Equation (21) into Equation (20a) yields

$$P_{fin} = P_{sat} + P_{fin} \frac{T_{sat}}{T_{fill}} \tag{22}$$

Since P_{sat} and T_{sat} are directly related for pure fluids, Equations (19) and (22) can be used to predict the fin operating characteristics when there is complete mixing of noncondensable and condensable fluids. These equations were used to predict the fin pressure as a function of heat load ratio at the conditions of the noncondensable gas tests, and the results are shown in Figure 27.

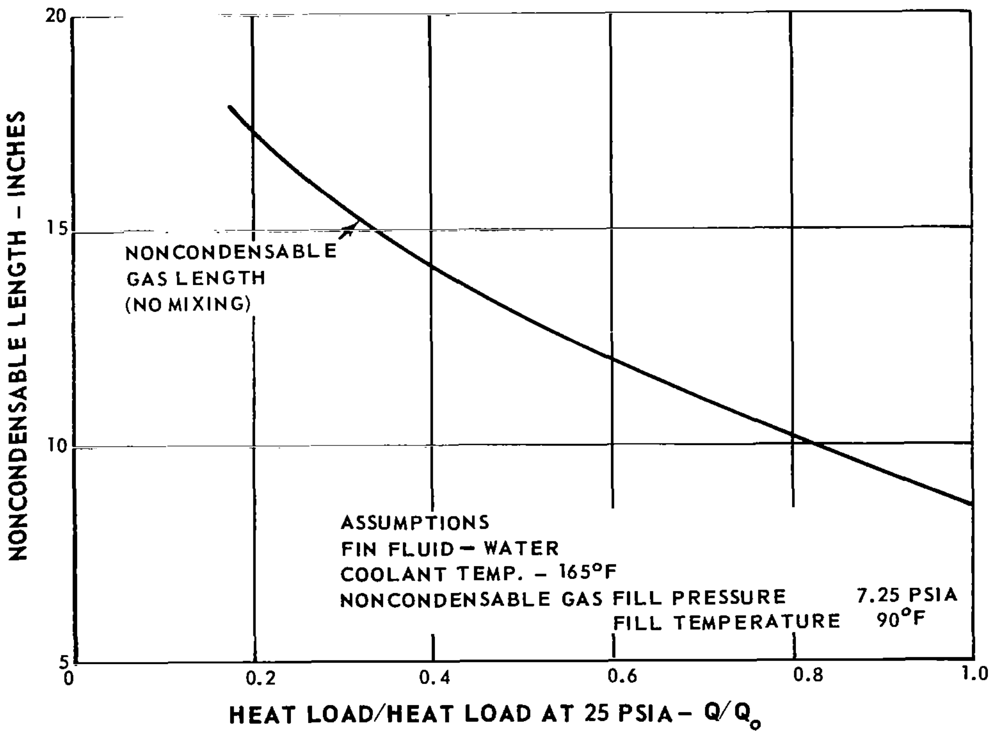

Figure 38 Predicted Variation of Noncondensable Gas Length with Heat Load for Box-Fin Model